Practical Analysis Tools for Structures Subjected to Flow-Induced and Non-Stationary Random Loads

Karen Mary Louise Scott

Dissertation submitted to the Faculty of the

Virginia Polytechnic Institute and State University

in partial fulfillment of the requirements for the degree of

Doctor of Philosophy

in

Aerospace Engineering

Rakesh K. Kapania, Chair

Mayuresh J. Patil

Michael K. Philen

Joseph A. Schetz

June 20, 2011

Blacksburg, Virginia

Keywords: Flow-induced vibration, random vibration, non-stationary forcing,

Karhunen-Loeve expansion, polynomial chaos

Practical Analysis Tools for Structures Subjected to Flow-Induced and Non-Stationary Random Loads

Karen Mary Louise Scott

(ABSTRACT)

There is a need to investigate and improve upon existing methods to predict response of sensors due to flow-induced vibrations in a pipe flow. The aim was to develop a tool which would enable an engineer to quickly evaluate the suitability of a particular design for a certain pipe flow application, without sacrificing fidelity. The primary methods, found in guides published by the American Society of Mechanical Engineers (ASME), of simple response prediction of sensors were found to be lacking in several key areas, which prompted development of the tool described herein. A particular limitation of the existing guidelines deals with complex stochastic stationary and non-stationary modeling and required much further study, therefore providing direction for the second portion of this body of work.

A tool for response prediction of fluid-induced vibrations of sensors was developed which allowed for analysis of low aspect ratio sensors. Results from the tool were compared to experimental lift and drag data, recorded for a range of flow velocities. The model was found to perform well over the majority of the velocity range showing superiority in prediction of response as compared to ASME guidelines. The tool was then applied to a design problem given by an industrial partner, showing several of their designs to be inadequate for the proposed flow regime. This immediate identification of unsuitable designs no doubt saved

significant time in the product development process.

Work to investigate stochastic modeling in structural dynamics was undertaken to understand the reasons for the limitations found in fluid-structure interaction models. A particular weakness, non-stationary forcing, was found to be the most lacking in terms of use in the design stage of structures. A method was developed using the Karhunen Loeve expansion as its base to close the gap between prohibitively simple (stationary only) models and those which require too much computation time. Models were developed from SDOF through continuous systems and shown to perform well at each stage. Further work is needed in this area to bring this work full circle such that the lessons learned can improve design level turbulent response calculations.

Dedication

To my parents, Gwen and Ian.

Acknowledgments

Through my life, I have encountered many individuals and groups who have had a profound influence on both my academic and personal development. I am indebted to all of you for the knowledge and guidance you have imparted to me.

I am dedicating this work to my parents Gwen and Ian Scott who have shaped the person I am today. Their love, support and guidance have been invaluable through all stages of my life and it fills me with joy to share this achievement with them. Of course, I cannot forget my brother Edward, Aunt Sadie and Uncle Jimmy. They complete the core family unit in which I was brought up and each of them have given me strength and inspiration throughout my life.

I must thank those who have had direct influence on my work. First, my advisor Dr. Rakesh K. Kapania for giving me the opportunity to work with him first on an SBIR project with Luna Innovations which kick started my own work and aided in development of my first Journal paper. He has provided encouragement and guidance throughout my time at Virginia Tech and has had patience with me where others may have not. Second, to Dr.

Sameer B. Mulani for helping me shape my work beyond the SBIR. He is not only a colleague but a friend and must have the patience of a Saint for the numerous times spent explaining concepts in different ways so that I might understand. Thanks also should be extended to Mr. Thomas McQuigg for assistance in performing the experiments found in this dissertation.

I would like to express my deepest gratitude to my friend, the late Dr. Ronald Slingerland of the Technical University of Delft. I met Ronald during an IAESTE internship at TU Delft in 2004. Ronald encouraged me to pursue further studies and maintained contact with me from my time at TU Delft through the beginning of my Doctoral studies at Virginia Tech until his tragic death in October 2007. Although he started as my advisor, Ronald became a dear friend and he has been sorely missed.

Finally, to my husband William who was there when I needed him most. Graduate school at Virginia Tech brought us together, and now with the closing of this chapter of our lives, I look forward to a bright future together.

Contents

List of Figures

List of Tables

Nomenclature

$\mathbf{C}$	Covariance double integral
$\mathbf{D}$	Matrix of participation factor of basis functions
$\mathbf{N}$	Matrix of integral of basis functions
A	Area of cross-section, m^2
A_L	Lift amplification factor
C_D	Mean drag coefficient
C'_D	Fluctuating drag coefficient
C'_L	Fluctuating lift coefficient
C_n	Reduced damping coefficient
C_R	Turbulent forcing coefficient
d_{ji}	Constants

E Modulus of elasticity, Pa

$E[\,]$ Expectation of a process

f_s Vortex shedding frequency, Hz

G Shear modulus, Pa

G_f Single sided power spectral density, $(N/m)^2/Hz$

h_j User-defined basis functions

I Moment of inertia, m^4

J_{nn} Joint acceptance

L_e Correlation length, m

m_j Response of system due to basis function excitation

M_n Generalized mass

m_t Total mass per unit length, kg/m

p_i Deterministic responses of a system due to forcing by the eigenvectors of the covariance eigenvalue problem

$R_{X_iX_j}$ Covariance of response

R_{XX} Auto-covariance of the displacement

S_t Strouhal number

S_y	Joint acceptance
y_n	Displacement amplitude of n^{th} mode, m
X	Random variable set x_1, x_2,...x_n
Y	Random variable set y_1, y_2,...y_n
β	Slope due to shear deformation
α	Slope due to bending
λ	Eigenvalues of the covariance function
μ	Mean value of a process
ω_n	Natural frequency of vibration, rad^{-1}
ϕ	Eigenvectors of the covariance function
Φ	Normalized power spectral density
ϕ_n	n^{th} mode shape
ρ	Density, kg/m^3
$\mathbf{\Lambda}$	Diagonal matrix of eigenvalues
ξ	Set of random variables
ξ_n	Modal damping coefficient
$\sigma_x(t)$	Standard deviation of the displacement

Chapter 1

Introduction

1.1 Motivation

The primary topic for discussion in this dissertation is the development of practical design tools for certain applications in fluid structure interaction and random vibration. While these subjects may seem significantly different from one another, they are in fact inherently linked. Interest in fluid structure interaction problems was spurred by the introduction of a SBIR project to Luna Innovations and Virginia Tech from NASA Stennis relating to real-time sensing of temperatures in cryogenic rocket fuel lines. This required the sensor to not only have extremely low response times but also be able to survive in the cryogenic fuel line environment. Previous sensors used by NASA were found to have either inadequate response time, be subject to serious fatigue problems or a combination thereof. Luna Innovations

believed that their expertise in fiber optic sensing technology could solve at least one of these problems though they lacked an appropriate housing for the sensor and relevant analysis methods to study suitability of housing designs. Virginia Tech was tasked with development of an analysis tool to aid designers at Luna to check suitability of their designs for a variety of cryogenic fuel line applications. Sensors in such fuel lines are prone to vortex induced vibrations and turbulence induced vibrations. Modeling such phenomena ranges from simple single degree of freedom models to bi-directional fluid-structure interaction numerical studies.

For the purposes of developing a design tool, it is advantageous to not only maintain simplicity such that a non-expert can interpret results, but also include enough complexity in the modeling that the essential system response is captured. These requirements are somewhat conflicting, so a happy medium must be met. As this is an important problem in industry, the American Society of Mechanical Engineers conducted a brief literature review and from that constructed a recommended analysis method for sensors subject to fluid induced vibrations. At a first pass, this appeared adequate for use in a design tool for the industrial partner. However, it was found the accuracy of this method was called into question following an industrial accident in Japan when a sensor failed due to fatigue as a result of fluid induced vibrations at a fatigue life much less than expected. It was postulated that this may also have been what was occurring with sensors utilized by NASA which had failed. As a result, it was deemed necessary to investigate the ASME methods, find the technical faults and form a much improved method for vibration response prediction of sensors in a pipe flow environment.

While working on fluid structure interaction problems, it was noticed that a significant amount of work in this area depends on stochastic modeling. This sent post SBIR work into further investigation of stochastic modeling capabilities available. Although stationary processes are well described and studied in the literature [4, 5, 6], non-stationary processes are not as well understood, primarily due to past limitations of computational power. The ASME method relies upon solutions to a simple stationary random vibration solution problem. Solutions exist for non-stationary random vibrations but only for extremely simple cases [7, 8]. When considering larger, more complex structures, researchers typically resort to expensive Monte Carlo type simulations. A gap exists for efficient analysis of medium complexity structures which does not require the end user engineer to be an expert in stochastic modeling. With this in mind, it follows that a tool be developed for analysis of such structures from simple SDOF through continuous systems and be capable of running on standard desktop computers with minimal model setup time, such that it could be used early in the design process.

1.2 Objectives

The primary objective of this study is development of practical design tools to deal with specific problems in flow-induced vibration and non-stationary random vibration analyses. The objectives identified for each topic are listed:

In the topic of fluid structure interaction the objectives are:

- Investigate current design methodologies and guides for sensor design in fluid structure interaction environments
- Investigate the performance of the models developed through experimentation
- Apply the models to a real industrial problem
- Create deliverable analysis tool to transfer to the sponsor

In the area of non-stationary random vibration, the objectives follow a similar theme as before:

- Investigate current methods of evaluating non-stationary random vibration
- Develop a tool which captures the fundamentals of response and which does not need significant model setup time
- Apply this tool to MDOF problems and test this tool against exact theoretical solutions
- Extend the proposed method to consider basic continuous systems

1.3 Dissertation Outline

To ensure research efforts for this dissertation followed a logical path, a literature search was performed for both topics discussed in this dissertation. While a plethora of literature is available, Chapter 2 highlights those studies of most importance to this work. Following the

establishment of a firm research base, technical work could begin, the details of which are found in Chapters 3 and 4.

Chapter 3 continues the discussion of fluid induced vibrations started in Chapter 2. Work in this topic was split into three regions and tackled in consecutive fashion. The first key idea in this Chapter was finding those areas in existing models which could be improved upon and would be most useful later in development of the design tool. On identification of these areas, improvements to the models were sought and then algorithms developed for swift calculation of sensor response. This led into the experimental portion of the work where a suitable experiment was designed, conducted and the data analyzed. Comparison of these results to those produced by the algorithms developed showed good agreement. Comparison of experimental data with results produced by the current ASME guidelines showed significant discrepancy, highlighting the benefit of the updates given in this work.

Work undertaken to explore the capabilities of stochastic modeling in structural vibration is presented in Chapter 4. A method was developed utilizing the Karhunen Loeve expansion. The models developed followed logical progression in complexity from SDOF to MDOF and finally continuous systems. At each step, the results produced by the model developed were compared with theoretical solutions that were available. For MDOF systems the derivation was shown and confirmed for simple 2 DOF cases before being tested against a well-known 10 DOF model first presented by Roberts [3]. Finally, the method was applied to a tall chimney found in Muller [9] and once again shown to provide good agreement with theoretical results, with minimal computation time spent.

1.3 Dissertation Outline

Finally this dissertation comes to a conclusion in Chapter 5 presenting the important findings of this work, highlighting their publication in both AIAA Conference Proceedings and AIAA Journals, and final thoughts presented on future paths the work presented herein could take.

Chapter 2

Literature Survey

2.1 Flow Induced Vibration

2.1.1 Vortex Induced Vibration

Fluid structure interactions (FSI), in particular, the vibration of a circular cylinder in a fluid flow have been investigated for more than a century[10]. The problem of FSI is an important one and has resulted in hundreds of papers being published through the years. Such interest in FIV can be attributed to its many applications such as the flow around cooling tower stacks, over wires, around periscopes and of course around sensors. While such a wealth of literature is available in this area, only the key studies in the field will be highlighted in the course of this section.

2.1 Flow Induced Vibration

From a fluid mechanics point of view, the phenomena of interest for flow around bluff bodies are vortex shedding and free stream turbulence. Flow around bluff bodies depends highly on the Reynolds number of interest. At extremely low Reynolds numbers (less than 5), the flow around a circular cylinder remains attached to the body. A slight increase in Reynolds number sees vortices forming in the cylinder wake but the flow still remains attached. However, beyond a Reynolds number of approximately 40 [11], the vortices are shed from the cylinder and as Reynolds number increases, this shedding occurs in a periodic fashion. Periodic vortex shedding is known as the Karman vortex street and results in alternating forces being placed on the cylinder in both transverse and in-line directions. At a Reynolds number beyond $3x10^5$ vortex shedding breaks down into a fully turbulent wake but vortex shedding resumes again following a Reynolds number of approximately $3.5x10^6$. This behavior over these Reynolds numbers ranges is represented in Figure 2.1 created by Farell [1].

These vortex streets exist for many different types of bluff bodies, some of which were studied by Delany and Sorensen in 1953 [12]. The Reynolds numbers considered ranged from 10000 to 2300000 and found steady drag coefficients for a variety of shapes from a simple circular cylinder, through elliptical cross-sections as well as some diamond shapes. In terms of a sensor housing application, it is desirable to use a cross-section that causes minimal disturbance to the flow and also which can be analyzed effectively. For these reasons it is desirable to concentrate on circular and elliptical cross-sections. The key findings from Delany and Sorensen's study showed the mean drag coefficient for a circular cylinder and for an elliptical cross-section with a 2:1 fineness ratio to be 1 and 0.6 respectively at a Reynolds

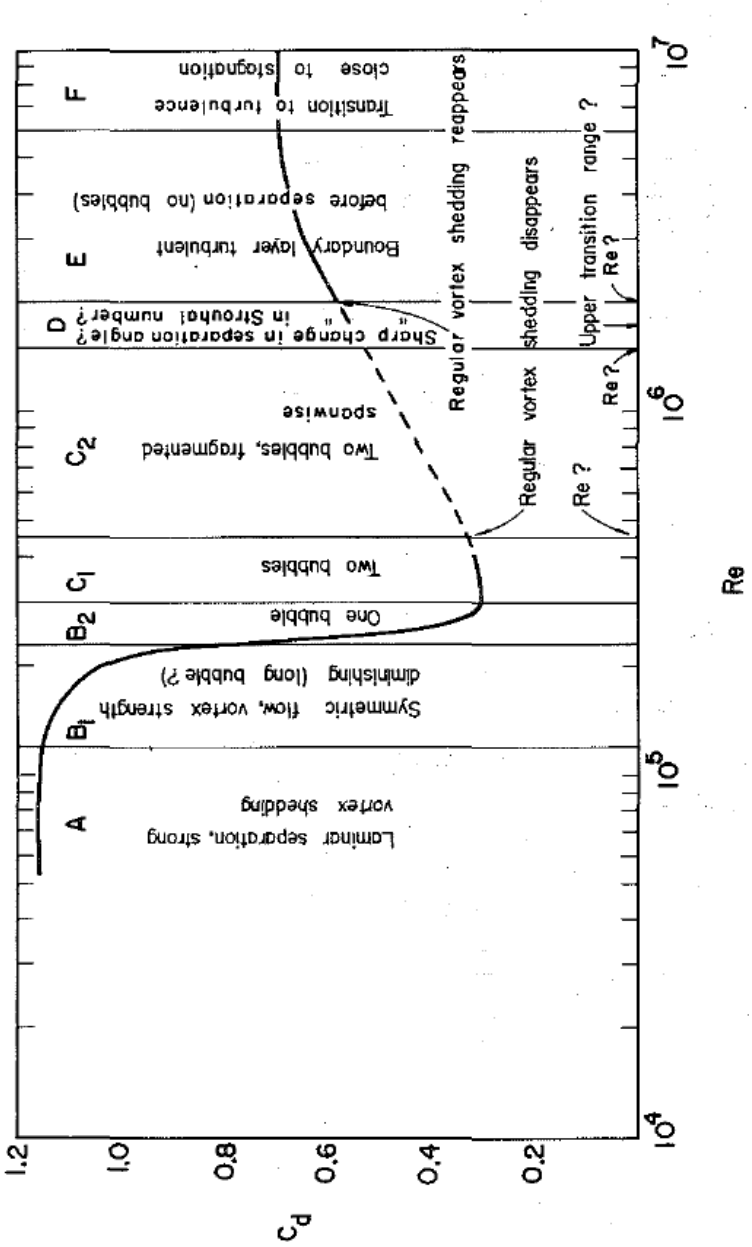

Figure 2.1: Variation in drag coefficient with Reynolds number, showing differing flow regimes [Fair Use] [1]

number of 100000. However, this study did not touch upon the alternating forces which arise on the bluff bodies due to vortex shedding.

The frequency of vortex induced vibrations is characterized by the Strouhal number. Strouhal number is defined as $St = f_s D/U$ where f_s, U and D are the vortex shedding frequency, free stream velocity and cylinder diameter respectively. For most subcritical Reynolds numbers, Strouhal number for cylinder remains around 0.2, a fact highlighted by Roshko in 1954 as part of a study on the shedding frequency of a variety of bluff body shapes [13] and illustrated in Figure 2.2 by Shin and Wambsganss in 1977 [2].

In 1961, Keefe published an extensively cited study on fluctuating forces on a stationary circular cylinder where forces on the cylinder were modeled simply as a harmonic oscillatory force, combined with a simple measure of correlation length in the forcing. Works such as Roshko and Keefe centered on subcritical Reynolds number ranges. Fung [14] claimed to be one of the first to explore excitation of cylinders in the supercritical Reynolds number range and his study was important in that it showed that at such high Reynolds numbers it is best to analyze the vortex shedding process statistically rather than following a traditional harmonic excitation approach, due to the inherently random nature of the vortex shedding in this regime. The ASME noted a much increased interest in this area and thus started sponsoring symposia on the topic of flow induced vibrations in the 1970s [15]. Since then, a variety of experimental results published and a range of analytic methods have been developed.

An excellent review of early experimental studies performed was published by Bearman [16]. For understanding on the physics of vortex shedding, Bearman directs readers to the

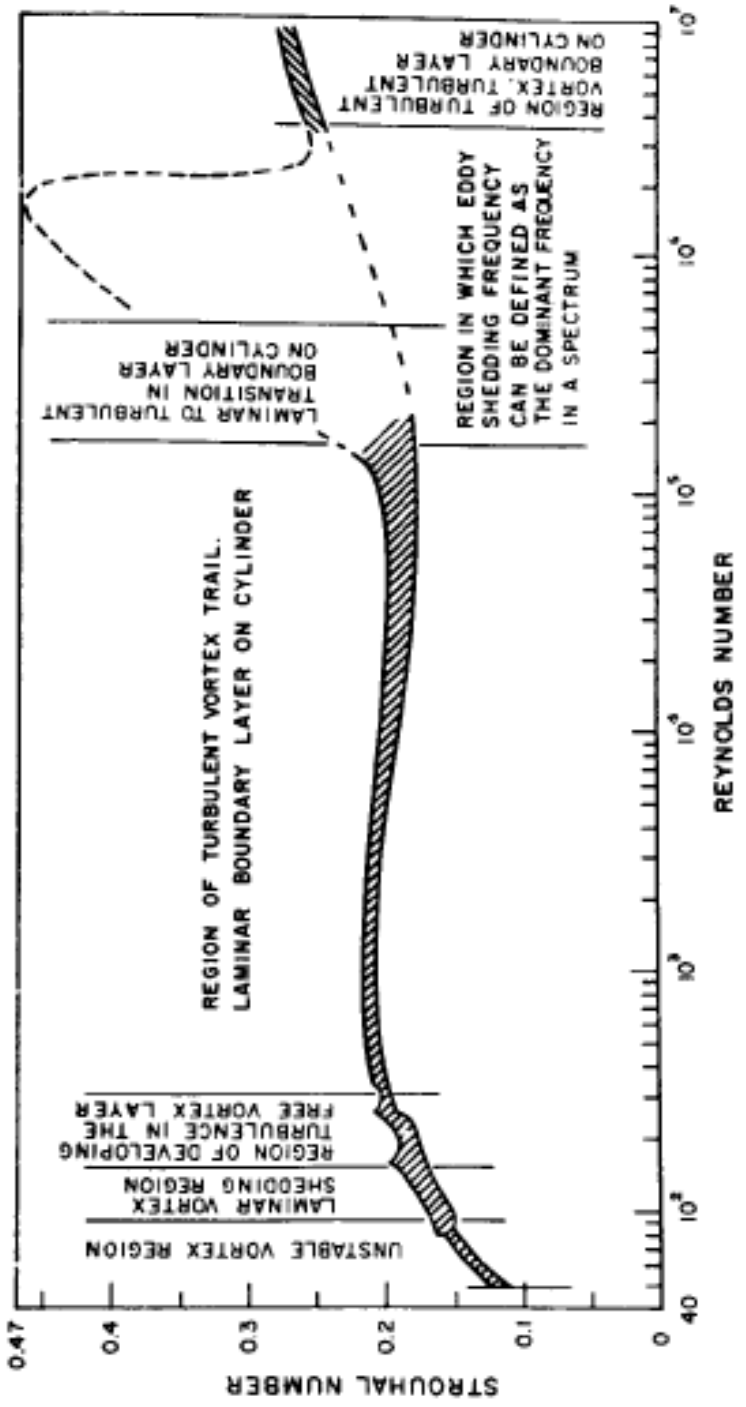

Figure 2.2: Variation of Strouhal number with Reynolds number [Fair Use] [2]

study performed by Gerrard [17] where Gerrard's primary observation explains that vortex shedding is primarily caused by the interaction of the two shear layers which exist in flows around bluff bodies. The bluff body itself promotes "feedback between the wake and the shedding of circulation at the separation points " [16, 17]. Bearman notes that much research in the 1970s and 1980s on vortex shedding concentrated on the influence of disturbances on the vortex shedding processes. These disturbances include body surface finish, aspect ratio and flow turbulence, all of which have differing effects in vortex induced vibration. Among the most cited publications of this era include a variety of studies by Sarpkaya [18, 19, 20, 21, 22]. Not only did Sarpkaya contribute extensively to modeling two dimensional bluff bodies by the discrete vortex technique, he also was instrumental in investigating the limitations of assumed two dimensionality of vortices shed by bodies. This lack of two dimensionality is found by investigating unsteady quantities such as "fluctuating surface pressure, sectional lift force or fluctuating lift force" and finding the spanwise correlation between them [16]. Sarpkaya showed that this correlation length parameter for a circular cylinder varies between 3 and 6 cylinder diameters for Reynolds numbers in the range 10^4 to 10^6 [20]. This fact is important in this work and will be discussed further later.

Vortex shedding will usually induce oscillations transverse to the fluid flow direction. For bodies free to oscillate, motion of the body can "take control of the instability mechanism that leads to vortex shedding [23]." This means the vortex shedding frequency and body's natural frequency coincide. When the frequencies approach one another and the vortex shedding frequency is captured by the body natural frequency, the body is said to be in lock-

in. Although vortex induced vibrations are self limiting, the body will experience fatigue problems if lock-in is experienced for long periods of time. It is therefore desirable to avoid a design which will experience lock-in. While it is intuitive to only consider body motion in the transverse direction, movement of the body parallel to the flow must not be neglected. Both mean and fluctuating drag components will exist for a body in a fluid flow. Each time a vortex is shed a small fluctuating drag is generated also. Since vortices are shed from both the top and bottom of the body, the frequency of vibration in-line with the flow is twice that of the transverse vortex shedding frequency. However a situation also exists where it is possible (in a heavy fluid) to observe vortices shed from the top and bottom of the cylinder concurrently. This behavior was reported by Wooton *et al.* in [24] and studied by King who showed two distinct regions of vortex shedding behavior [25]. This change of vortex shedding regime can be attributed to the increased two dimensionality of the flow which means correlation length previously discussed is now increased. An extensive discussion on how vortex shedding changes from one regime to the next can be found in Zdravkovich [26].

A variety of different types of models to predict the response as a result of vortex induced vibrations have been developed through the years. For a rigid cylinder, Bishop and Hassan used a van der Pol type oscillator to represent forces on the cylinder due to vortex shedding [27, 23]. This model is represented by coupled differential equations:

$$x_r^{''} + 2\zeta x_r^{'} + x_r = a\omega_0^2 C_L \tag{2.1}$$

$$C_L^{''} - \alpha\omega_0 C_L^{'} + \frac{\gamma}{\omega_0}\left(C_L^{'}\right)^3 + \omega_0^2 = b x_r^{'} \tag{2.2}$$

Here the time derivatives are taken with respect to dimensionless time $\tau = \omega_n t$, x_r is the dimensionless cylinder displacement, C_L is lift coefficient, ω_0 is the ratio of the vortex shedding frequency to cylinder natural frequency and ζ is cylinder damping. Parameter a is a known constant, α, γ and b are chosen to fit to experimental data.

Modifications were made to the model by Skop, Griffin, Iwan and Blevins [28] to include more dependence on physical system parameters. The basic model is based upon a rigid cylinder elastically mounted at either end, free to vibrate in only the transverse direction. Important assumptions of the Iwan-Belvins model are: inviscid flow, a well formed vortex street and two dimensional flow. The resulting model was found to perform well but required additional experimental knowledge of the specific system studied beyond that required in the previous model discussed in [27, 23]. It is clear that the fundamental issue with these types of models, is their dependence on quite specific experimental data. For a design problem, specific experimental data will be lacking at the initial stages therefore it would not be appropriate to include a model of this type in a design tool. It is true that following experimentation, these models will perform well but only with the availability of appropriate detailed experimental data [23].

Of greater interest to this study, from a practical standpoint, is the prediction of an elastic cylinder response due to vortex induced vibrations. Wake oscillator models such as those developed by Skop, Griffin, Iwan and Blevins, were extended to include the elasticity of the structure. For the Iwan-Blevins model [28, 29], strip theory is applied to the problem which assumes there is no spanwise coupling of the flow and also the structure is assumed

to exhibit classic normal modes. With this in mind, Iwan and Blevins modify their wake oscillator model and obtain an expression for the maximum modal displacement, $Y_{n_{max}}$, per diameter, D, presented in Eq. (2.3).

$$\frac{Y_{n_{max}}}{D} = \frac{a_4\sqrt{4/3}\gamma_n}{2\pi^3 S^2 \mu \zeta_n^T}\left[\frac{(a_1 - a_4)}{a_2} + \frac{a_4^2}{\pi^2 a_2 S \mu \zeta_n^T}\right]^{1/2} \tag{2.3}$$

Again, experimental data is relied upon in the parameters a_1, a_2 and a_4. However, one significant improvement seen here over previous models includes total damping of the structure, ζ_n^T which includes both structural damping, ζ_n and the damping due to the fluid which is significant for a heavy fluid such as water, LOX etc. Where experimental data is known, the model does perform well but again it is of limited use for a design application.

One of the first authors to offer a model which could be used by non-experts without extensive experimentation was Connors. Connors objective was to provide the framework for predicting vortex shedding from bluff bodies which could be used by those who are not flow induced vibration specialists. Connors begins by representing the vortex shedding as a sinusoidal process correlated over a certain spanwise length, akin to the representation given by Keefe [30]. This is applied to a rigid cylinder before being extended to elastic systems through modeling elastic cylinders as a series of rigid bars attached by rotatory springs. Connors results offered promising insight into prediction of vortex induced vibrations without thorough experimental knowledge and was incorporated into the early revisions of the ASME guidelines for designing for vortex induced vibration of thermowells and remains in

the ASME Boiler and Pressure Vessel Code N-1300[31].

2.1.2 Turbulence Modeling

While vortex shedding has been the primary concern thus far, it was mentioned in the previous section that other factors such as turbulence influence the response of a cylinder undergoing vortex induced vibrations. Turbulence is an inherently random process and thus the usual deterministic methods cannot be applied in this case. One of the pioneers in turbulent boundary layer research was Corcos. The Corcos model, despite hailing from the 1960's, is still widely used today and indeed still forms the basis for many further studies and analyses [32, 33]. Corcos represents turbulence in a stochastic fashion and assumes the processes are stationary and homogeneous. Corcos uses spectra to represent mean square pressure and cross-spectral density. In a later work, Au-Yang notes that random components of the dynamic pressure are defined by both the pressure power spectral density and a complex coherence function. Another important parameter is the RMS pressure coefficient which is defined as the product of dynamic pressure and a turbulence forcing coefficient, C_R, the value of which was reported by Corcos to be 0.007 for smooth cylinders. For practical cases however, this value was found to be much higher and is commonly accepted to be in the range of 0.1 to 0.2 [34]. The acceptance integral response method is widely accepted as the standard for these types of applications. Here $\bar{w}^2(x)$ is mean square response varying

with location x.

$$\bar{w}^2(x) = 2\pi^2 \sum_i \zeta_i f_i S_d(x, f_i) \tag{2.4}$$

Here S_d is the displacement power spectral density which is defined by mode shape function Ψ, transfer function H for the dynamic system and joint acceptance integral $\bar{J}$:

$$S_d(x, f) = \sum_i \Psi_i^2(x) \left|H_i(f)\right|^2 \bar{J}_{ii}(f) + 2 \sum_{i \neq j} \Psi_i(x)\Psi_j(x) Re\left[H_i^*(f) H_j(f)(\bar{J}_{ij}(f))\right] \tag{2.5}$$

The power spectral density of the pressure field, S_p, is introduced in the expression for the joint acceptance integral:

$$\bar{J}_{ij}(f) = \int_a \int_a \Psi_i(x_1)\Psi_j(x_2) S_p(x_1, x_2, f)/S_p(x_1, f) dx_1 dx_2 \tag{2.6}$$

This process was actually originally demonstrated by Powell [35] and used by Au-Yang [36], Chen and Wambsganns [37], Pettigrew and Gorman [38], and Axisa *et al.* [39]. In particular, Axisa *et al.* provide a more detailed explanation on arriving at the result. What gained particular attention in the literature was the development and solutions to the joint acceptance integrals to make them easy to solve and implement. Pettigrew and Gorman [38] and Axisa *et al.* [39] look at practical application of these solutions to flow induced vibration problems. Au-Yang summarizes the basic results in [40]. Here an important discovery is made which shows that for small correlation length (as compared with the length of the

beam considered), the joint acceptance integral reduces to $J_{11} = 2\lambda/L$ where λ is correlation length and L is the length of the beam. With all assumptions and simplifications in place, the mean square response of the cylinder in a fluid flow is:

$$y_2 = \sum_i \frac{LG_p(f_i)\psi_i^2(x)}{64\pi^3 M_i^2 f_i^3 \zeta_i} J_{ii} \tag{2.7}$$

Here G_p represents the single sided power spectral density and M_i the generalized mass. This is the form which has been incorporated into the ASME BPV design guidelines previously mentioned [31].

2.1.3 Application to Cryogenic Sensor Problem

In recent times, the subject of vortex induced vibrations gained particular attention as a result of a sodium leakage incident at a fast breeder reactor, Monju in 1995 caused by high cycle fatigue of a thermometer well subject to flow-induced vibration. Many studies followed [41, 42, 43, 44], primarily in Japan, to attempt to improve and validate the analysis methods cited in ASME N-1300 and these will be discussed later. The analysis method presented by ASME requires knowledge of the structural natural frequencies and mode shapes. These natural frequencies and mode shapes are primarily generated using exact solutions of Euler-Bernoulli beam theory. As is well known, this theory neglects both the shearing of a beam's cross-section and the contribution of rotatory inertia. The ASME code applies only to beams whose length is significantly greater than its depth, usually a 10:1 ratio. Existing

sensor designs tend to satisfy this requirement such that Euler-Bernoulli beam theory can be utilized in the generation of response prediction data with the ASME codes. However, such sensors as studied previously[41, 42, 43, 44] have the disadvantage that they are somewhat slender which is not an ideal characteristic when considering fatigue life. Fatigue failure is undesirable as more often than not the broken sensor can contribute to significant foreign object damage which can lead to significant environmental issues such as that experienced at Monju. The problem has been experienced extensively in cryogenic applications where foreign object damage leads to rocket failure.

With these considerations in mind, it is advantageous to design a sensor that is minimally intrusive to an internal flow whose fatigue life is extended whilst maintaining adequate measurement characteristics. The improvement of the analysis tools to deal with less slender, lower aspect ratio sensors in addition to sensors with a non circular cross-section is a useful step. Shortening the sensor means that shear and rotatory inertia effects now become very important and results generated via integration of EB theory with ASME guidelines [31] are less reliable for predictions. The mechanism through which the analysis can be improved is through utilization of Timoshenko beam theory which is implemented through an energy methods approach. Using this modification, the response prediction can be decomposed into bending and shear stress contributions and as sensor aspect ratio decreases it is observed that shear stress contributions become significant. Most sensors are circular in cross-section, however it can be beneficial to consider elliptical cross-sections since both the mean and amplitude of the sensor response may be reduced due to a more streamlined shape. Reducing

the stresses ultimately leads to extended fatigue life of such a sensor when compared to that with a circular cross-section.

2.2 Random Vibration

The importance of stochastic modeling in real world problems was highlighted in the previous section in the application of stochastic processes to estimation of structural response to turbulent forcing. The concept of probability and reliability have been around since the days of Pierre Simon and Marquis de Laplace [45]. Random processes are defined by their lack of pattern or regularity [46]. The mathematical formulations of real physical problems can be studied in the time or frequency domains, which are of course related to each other through the Fourier transformation. In many applications, an engineer will find the spectral or frequency domain description of a process very useful since it is directly physically interpreted as the process energy density distribution over frequency [47]. Stochastic processes are broken into two groups, stationary and non-stationary. Much exhaustive research has been performed on stationary systems applied in real world engineering contexts. Non-stationary systems were explored some time ago [47] but typically only very simple examples could be solved due to lack of computational power. Even for stationary systems, it is still often assumed that the process is Gaussian in order to achieve convenient, closed form analytic solutions. In reality, many of the systems encountered in engineering are in fact non-Gaussian and non-stationary, for example, material properties, turbulence and seismic loads [48].

2.2 Random Vibration

With the exponential improvements in computational power, interest in solving complex non-stationary random vibration problems has increased rapidly in recent years [49]. With the computational power available, it is possible to revisit the analysis of large systems [50] with many degrees of freedom through the Stochastic Finite Element Method (SFEM), an excellent review of which has been published by George Stefanou [48]. However, despite the available computational power, it is not practical or possible to build extremely complex models during initial design and hence tie up valuable computational resources, although efforts have been made to reduce the computational effort required of the method (e.g. studies by Brenner and Bucher, and Charmpis and Papadrakakis [50, 51]). Most studies in the SFEM area continue to focus on important problems where variation in material and geometric properties of the structure are of paramount importance (see Graham, Gurley and Masters [52], Graham and Deodatis [53] and Huyse and Maes [54]).

Representation of inputs to a stochastic system is the first step in solving non-deterministic problems. Inputs are placed into the following categories: mechanical, geometric and loading of the system [48]. For most applications, experimental data is required which is then used to construct probability distribution and correlation of the random process. However, such experimental data is often lacking, requiring assumptions to be made about the stochastic fields. This is the primary reason why real, non-Gaussian processes are modeled as Gaussian [55]. The SFEM centers largely around Gaussian systems, most commonly using the spectral representation method or (much less often) the Karhunen Loeve expansion for representation of the Gaussian process (e.g. see Deheuvels and Martynov [56]), although non-Gaussian

systems can be represented by spectral methods [57]. System response is obtained via time or frequency domain methods. For large MDOF systems, system response is often obtained through the use of polynomial chaos techniques or through Monte Carlo simulation [58, 48].

The most straightforward method on finding system response to a non-stationary random vibration input is solving the convolution integral [5]. While effective for simple cases, it becomes immediately apparent that adopting this method for large systems quickly becomes impractical [5]. The traditional method on solving system response through spectral density functions do not directly apply here. However, Priestley [59, 60] introduced the notion of evolutionary spectral density. Here the random function is represented by a stationary component and a modulated function. It is common to see this in conjunction with the Hilbert transform, also a form of modulation of a random stationary signal [61]. Then solution of the problem follows a similar structure to that of stationary excitation. Usage of Priestley's spectrum allows the statistics of the non-stationary function to maintain physical meaning. This method was noted by Shihab to have emerged as the most effective analytical method of dealing with non-stationary excitation [62]. Shihab further extended the method for use through state-space form. In the literature, the observation was made that calculation of non-stationary responses are often performed using normal white noise processes as excitation [63, 64, 65]. Ibrahim proposed a technique to evaluate the covariance function of the non-stationary response of linear systems excited by white noise using complex analysis for classic systems [64]. Dario Gasparini was instrumental in development of closed form analytic solutions to non-stationary random excitations [65]. In this case, Gasparini derived

expressions for evolutionary covariance matrices for evolutionary white noise. Methods such as those of Priestley and Gasparini, and variations thereof dominate the field and continue to be used for many years [7]. As mentioned previously, the recent availability of inexpensive computational resources have now caused research efforts in this area to be revived and branch into new areas, rather than concentrating on building extensions to these existing models. One such area is further the use of Polynomial Chaos technique and also the Karhunen-Loeve expansion [46, 7].

Schuëller, Pradlwarter and Schenk note that for stationary systems, it is easy to compute system response through frequency transfer functions operating on the spectral density function of the excitation. For large systems, the solution procedure is much more involved meaning that application of frequency domain methods to these systems is not practical. It is in this case that the response of large MDOF systems are obtained through use of the Lyapunov matrix differential equation and the excitation is modeled through modulated white noise [66]. However, it is also noted in [66] that the use of white noise in the excitation modeling leads to unrealistic response in a large finite element model. It is in this situation that application of the Karhunen-Loeve (KL) expansion can prove to be useful, providing a compact representation of the excitation processes as an expansion of orthogonal polynomials [46].

Representation of the random excitation through the KL expansion allows for existing efficient deterministic solvers to be used to obtain the system response. In addition, non-Gaussian excitation can be well represented since it is still possible to expand the process as series of orthogonal polynomials [66]. While some studies use the state space form to obtain

system response, this has the disadvantage that the dimensionality of the system is being increased thus increasing computation time [67, 66, 68]. Schuëller, Pradlwater and Schenk proposed the use of modal analysis to maintain system dimensionality and have shown an algorithm partially utilizing KL expansion is practical for the analysis of large DOF systems ($> 100,000$ DOFs) [58, 66]. The accuracy of the KL expansion depends highly upon the generation of accurate eigenvalues and eigenvectors when solving a Fredholm equation of the second kind. Simple closed form solutions of this expression are available only for the simplest of models therefore it is often solved numerically through a Galerkin, Rayleigh-Ritz or Collocation method [69]. Phoon, Huang and Quek noted that generation of the collocation matrix through these methods resulted in a very dense matrix which increases computational cost. They also noted that although it is often not required to proceed beyond the 10th eigenvalue, which contributes less than 1% to system response for a simple exponential covariance, this is not the case for processes with non-smooth covariance functions and long weakly correlated processes [69]. In an attempt to reduce density of the covariance matrix, these authors proposed a wavelet-Galerkin scheme to decrease compulational cost. Results from this study showed that use of the wavelet-Galerkin within the KL expansion did not show any clear advantage for strongly correlated systems, but do show promise for non-stationary and long processes at the expense of orthogonality of the KL eigenvectors.

Studies of large linear non-stationary FE models by Schuëller, Pradlwater and Schenk [66] do not follow such a wavelet like scheme as in [69, 70] but rather use basis functions defined over the entire domain. Selection of the basis functions is very important and is therefore

critical to the accuracy of the eigenvalues and eigenvectors obtained for the KL expansion as highlighted by Phoon [69]. Appropriate selection depends on the covariance function to be considered and therefore requires the engineer to have *a priori* knowledge of the functions suitable to represent a particular covariance function. Such a scheme is not suitable in a design setting and thus requires development of a generic method which may be applied with minimal prior knowledge of the system at hand.

Chapter 3

Flow Induced Vibration of Pressure and Temperature Sensors

3.1 Introduction

The work described in this Chapter relates to Phase II of an SBIR project awarded to Virginia Tech and Luna Innovations regarding the development of a temperature sensor for cryogenic applications. Phase I of this research primarily consisted of fiber optic sensing and data acquisition development by Luna Innovations. Design and modeling of the sensor housing was identified as Virginia Tech's main interest and in the early stages a variety of designs were considered by fellow student Scott Bland. Restrictions on the design were enforced by NASA, noting that the diameter of the sensor should not exceed 1/4 inch, only one hole

could be made in the pipe to mount the sensor and the sensor should be manufactured from cryogenic safe stainless steel. With these restrictions in mind, Mr. Bland considered sensor designs which extended to half pipe span with circular and elliptical cross-sections [71]. For the cryogenic fluids under consideration (LOX and LH2) at operating velocities, Bland found through simple analysis that the magnitude of normal stresses in LOX and LH2 were 185MPa and 315MPa respectively for circular cross-section cantilevered designs, with fatigue life in an LH2 environment estimated to be around 300 million cycles (49 hours) [71]. While this initial investigation proved useful, little detail was provided by Bland on the analysis methods used other than the fact that it relied upon advise set out in the ASME Boiler and Pressure Vessel code [31]. When moving to Phase II Luna Innovations requested greater transparency on the analysis method as well as experimental results to ensure reliability of the method. In addition Luna requested that Virginia Tech study shorter, lower aspect ratio sensor designs. This altered the analysis significantly since the ASME BPV code relies upon Euler-Bernoulli beam theory only and therefore does not consider shear stresses. Modifications to the ASME code were therefore required and the results of this study are presented in this chapter.

Thanks should be given to my colleague, Mr. Thomas McQuigg for assistance in performing the experiments and post processing the results which are found in this Chapter.

3.2 Euler-Bernoulli vs Timoshenko Beam Theory

3.2.1 Euler-Bernoulli Beam Theory

Euler-Bernoulli beam theory has been in existence since the late 1700s and its use became widespread in large scale applications with the building of the Eiffel Tower and Ferris Wheel [72]. The primary assumption of the theory states that for a slender beam (whose length:depth ratio is no less than 10:1), shear deformation effects and rotatory inertia can be neglected and thus these drop out from the governing equation of vibration. Thus the equation for transverse free vibration of an Euler-Bernoulli beam is:

$$\frac{\partial^2}{\partial x^2}\left(EI\frac{\partial^2 w}{\partial x^2}\right) + \rho_s A\frac{\partial^2 w}{\partial t^2} = 0 \tag{3.1}$$

Where w is transverse displacement of the beam and x varies along the length of the beam from 0 to L. Equation (3.1) can be simplified further if a beam of constant cross-section is assumed. For simple boundary conditions, an exact solution can be obtained through assumption of harmonic motion of the beam and application of appropriate boundary conditions. The boundary conditions for a cantilevered Euler-Bernoulli beam which will be used in this study are well known as $w = w' = 0$ at $x = 0$ and $w'' = w''' = 0$ at $x = L$.

While Euler-Bernoulli beam models are useful in many vibration applications, they are not without limitation. Typically, as the ratio of length to depth drops below 10:1, vibration amplitudes calculated using Euler-Bernoulli beam models start to show deviation from ex-

perimental results as the inertial and shear effects become significant. It should be noted that for high aspect ratio beams, where the Euler-Bernoulli model is favored due to its simplicity, shear and inertial effects cannot be ignored for the case of high frequency vibrations. In both this case and that of a lower aspect ratio beam, it is often favored to apply the Timoshenko beam model.

3.2.2 Timoshenko Beam Theory

Timoshenko beam theory includes both rotatory inertia and shear effects. Here, if the total response of the beam is defined as w then the total slope can be seen to be made up of both bending (α) and shear (β) contribution. Derivation of the equations of motion, setting $\beta = \alpha - w'$, then leads to the following two partial differential equations [73].

$$\begin{aligned} \frac{\partial}{\partial x}\left[\kappa GA\left(\alpha - \frac{\partial w}{\partial x}\right)\right] + \rho A\frac{\partial^2 w}{\partial t^2} = 0 \\ \kappa GA\left(\alpha - \frac{\partial w}{\partial x}\right) - \frac{\partial}{\partial x}\left(EI\frac{\partial \alpha}{\partial x}\right) + \rho I\frac{\partial^2 \alpha}{\partial t^2} = 0 \end{aligned} \tag{3.2}$$

In this case, the boundary conditions for a cantilevered beam are $w = \alpha = 0$ at $x = 0$ and $\alpha' = \beta = 0$ at $x = L$. Both Eqs.(3.1) and (3.2) can be solved using a variety of methods and exact solutions can be obtained for simple boundary conditions [73]. However, it is often not convenient to rely upon and hard code an exact solution since computation with non-ideal boundary conditions may be favored in the future. For this reason, it is desirable to write expressions for both the kinetic and strain energies of the system, as these are easily modified

for alternate configurations, and solve the system through the use of an approximate method.

3.2.3 Eigensolution via Rayleigh-Ritz

The Rayleigh-Ritz method assumes a solution to the system in the form of a linear combination of kinematically admissible trial functions [74]. For the Timoshenko case, the solution approximates both the transverse deflection and rotation and takes the form:

$$w^{(n)}(x,t) = \sum_{i=1}^{n} a_i(t)\,\Phi_i(x) \tag{3.3}$$

$$\alpha^{(n)}(x,t) = \sum_{i=1}^{n} b_i(t)\,\Psi_i(x) \tag{3.4}$$

a_i and b_i can be further broken down such that $a_i = C_i e^{j\omega_n t}$ and $b_i = D_i e^{j\omega_n t}$ (assuming a harmonic beam response for free undamped vibration). Using this we substitute equations (3.3) and (3.4) into the beam energy expressions, minimize the function and thus generate the classic eigenvalue problem (see Meirovitch [74]):

$$\left|\mathbf{K} - \omega^2 \mathbf{M}\right| = 0 \tag{3.5}$$

Solving this problem for n trial functions for both w and α, leads to generation of $2n$ eigenvalues (ω^2) and $2n$ eigenvectors whose components correspond to $C_i^{(n)}$ and $D_i^{(n)}$. Selection of trial functions Φ and Ψ depend on the boundary conditions for the problem at hand, though it is imperative that the functions form a complete set. It is necessary to only satisfy

the essential boundary conditions, though violation of the natural boundary conditions will lead to a slower convergence. With suitable trial functions in place, the system can often be solved producing excellent results with only a few trial functions [74]. This is particularly advantageous if wishing to design a control system to limit vibration.

For circular cross-sections, the differential equations for transverse displacements in both Euler-Bernoulli and Timoshenko beam theory are independent of x and y directions. Mode shapes and eigenvalues are identical in each of these transverse directions due to identical mass moments of inertia. Hence the torsional differential equation can be decoupled so warping does not occur. This simplification makes sensors with a circular cross-section an obvious choice. However, circular cross-sections suffer the disadvantage that they experience increased mean drag and fluctuating drag force as compared to slimmer sections. With this in mind, it may be advantageous to consider elliptical cross-sections which may improve fatigue life. An obvious disadvantage is during manufacture of non-circular sections, it may be more likely for asymmetry to form in the structure which now means that a set of coupled equations needs to be considered. Information regarding flexural-torsional coupling with Timoshenko's beam theory may be found in Bercin and Tanaka [75].

3.3 Fluid-Structure Interaction Analysis

Regardless of the method used to solve the beam vibration problem, natural frequencies and mode shapes of the beam can be obtained. These frequencies and mode shapes feed

into the design code for flow induced vibrations which is specified by ASME Boiler and Pressure Vessel Code Section III Division I Appendix N-1300 [31]. The code comprises of two main areas of analysis, vortex induced vibration and turbulence induced vibration. Using the methods outlined in this code, engineers can quickly obtain information regarding the response amplitude of a sensor in a given fluid flow. Using this information, the mean and RMS stresses calculated by the code can be used in a fatigue analysis.

3.3.1 Vortex Shedding

Vortices are shed from an in line sensor periodically, hence giving rise to an alternating lift force which is representative of a deterministic system. The frequency of this lift force is the vortex shedding frequency $f_s = S_t U/D$ where S_t is Strouhal number, a dimensionless parameter used to characterize oscillatory flow. The oscillating lift force can be expressed as:

$$F = C'_L JqDL\left[\sin\left(2\pi f_s t\right)\right] \tag{3.6}$$

Where C'_L is oscillating lift coefficient, J is correlation coefficient, q is dynamic pressure, U is average free stream velocity, D is cylinder diameter and L is cylinder length. C'_L, f_s and J are all functions of Reynolds number [31] and are usually determined experimentally. Often a conservative value of 1 for C'_L and J are chosen though this assumes the flow is fully correlated over the entire cylinder length. In fact, the correlation length (L_e) for stationary

cylinders is often around 3 to 7 diameters (where $J^2 = L_e/L$). However, caution should be used as Eq.(3.6) is only valid for the off-resonance condition. Several checks exist to determine if resonance (lock-in) can be avoided [31]:

1. Lift and drag direction lock-in are avoided if the reduced velocity for the fundamental vibration satisfies $U/f_1 D < 1$ where f_1 represents the fundamental natural frequency (Hz) of vibration of the structure.

2. Reduced damping for an n^{th} individual mode is large enough ($C_n > 64$) where C_n is:

$$C_n = \frac{4\pi\xi_n M_n}{\rho D^2 \int\limits_{Le} \phi_n^2(x)\, dx} \tag{3.7}$$

   Where ξ_n is modal damping coefficient, M_n is generalized mass, ρ is fluid density and L_e is the length of the region of the cylinder assumed to be subject to lock-in cross flow (approximately $3D$ [44]).

3. For a given vibration mode $U/f_n D < 3.3$ and $C_n > 1.2$ where f_n is the n^{th} natural frequency of vibration.

However, even if lock-in synchronization does not occur, the vortex induced response must be still be calculated. The ASME code uses a derivation by Blevins [11] which shows that the maximum displacement (y_n^*) for a particular mode is:

$$\frac{y_n^*}{D} = \frac{C_L J \phi_n^*}{16\pi^2 S_t^2 \left[m_t \xi_n / (\rho D^2)\right]} \tag{3.8}$$

Where ϕ_n^* is the maximum value of the n^{th} mode shape. This model assumes a uniform structure and a uniform flow field. This and subsequent models require that the modes be normalized such that the maximum value of a particular eigenvector is 1. An updated version of this equation which gives displacement in the lift direction for the n_{th} mode ($y_{L,n}$) as a function of position and allows for varying sensor diameter, $D(x)$, is [76]:

$$y_{L,n}(x) = \frac{\rho V^2 C_L' \int_{Le} D(x)\,\phi_n(x)\,dx}{2(2\pi f_n)^2 \int_0^L m_t(x)\,\phi_n^2(x)\,dx} A_L \phi_n(x) \tag{3.9}$$

Where the lift amplification factor, A_L is defined as:

$$A_L = \frac{1}{\sqrt{\left\{1 - \left(\frac{f_s}{f_n}\right)^2\right\}^2 + \left\{2(\xi_n + \zeta_n)\frac{f_s}{f_n}\right\}^2}} \tag{3.10}$$

$$\tag{3.11}$$

modal fluid damping ζ_n is :

$$\zeta_n = \frac{1}{4}\left(\rho D^2 \int_{Le} \phi_n^2(x)\,dx\right)\left(\frac{U}{2\pi f_n D}\right) \tag{3.12}$$

and m_t is total cylinder mass per unit length which includes displaced fluid mass. The physical displacement of the sensor is then simply obtained by the principle of modal superposition.

Equations (3.9) and (3.10) can easily be modified for fluctuations in the drag direction by replacing subscript L with D and f_s with $2f_s$ [76]. Blevins [11] suggests that C'_L and C'_D have values of 0.6 and 0.06 respectively. A value of 0.6 for lift coefficient is somewhat conservative, hence if this value is used in our calculations the correlation with experimental values will be poor. Since it is known that fluctuating lift coefficient is a function of displacement amplitude, it is possible to use an iterative scheme, by using an estimate of C'_L to start iterative procedures, to compare the calculated displacement amplitude with that given in a displacement amplitude versus fluctuating lift coefficient chart provided by Blevins [11]. One must note however that these equations and the iterative scheme which was implemented are limited in that they can only be used up to the point of resonance. In the lock-in region, prediction of response is possible using the full non-linear model as given by Blevins [11] but many experimental coefficients must be obtained to adjust the model for the particular vortex induced vibration environment being studied.

3.3.2 Turbulence Model

The ASME guidelines [31] present an analysis method to predict vibratory response of a sensor due to turbulence.

The development of this response equation stems from the simple relation for standard

deviation (assuming a zero-mean response):

$$y^2(x) = \int_{-\infty}^{\infty} S_y(x,\omega)\, d\omega \tag{3.13}$$

$S_y(x,\omega)$ is the power spectral density of the displacement due to a random pressure fluctuation and varies with power spectral density of the pressure (S_p) which is assumed to be stationary in nature. However, the expression for $S_y(x,\omega)$ remains rather complicated. To simplify the expression, the following assumptions are used (see Au-Yang for details [77, 40]).

1. Cross terms are negligible in the transfer function
2. Turbulence is homogeneous - usually not true in real life but it is a necessary simplifying step
3. The acceptance integral is a slowly varying function of ω close to the natural frequency, but this is usually only valid for systems with damping of 5% or less

Au-Yang showed that Eq.(3.13) becomes (for these restrictions):

$$y^2(x) = \sum_n \frac{LG_f(f_n)\,\phi_n^2(x)}{64\pi^3 M_n^2 f_n^3 \xi_n} J_{nn} \tag{3.14}$$

Here the single-sided power spectral density, $G(f)$ is:

$$G_f(f_n) = \Phi(f_n)\left(\frac{1}{2}\rho U^2 D\right)^2 \left(\frac{D}{U}\right) \tag{3.15}$$

Where normalized power spectral density, $\Phi(f)$ is:

$$\Phi\left(f_n\right) = \frac{4C_R^2}{1 + \left(\frac{2\pi f_n D}{U}\right)^2} \tag{3.16}$$

and J_{nn} and C_R are defined as joint acceptance integral and turbulent forcing coefficients respectively. J_{nn} can be quite a complex expression and hence the upper bound of 1 is often taken in calculations [77]. However, special cases for cross-flow over beams exist. The most widely accepted approximation is:

$$J \approx \frac{2L_e}{L} \tag{3.17}$$

which is valid up to $L_e/L \approx 0.06$ [40] for beams with arbitrary boundary conditions. Insensitivity to beam boundary conditions is explained in Au-Yang [40] by the definition of joint acceptance: "a measure of the integrated effect over the surface of the structure," which is therefore "not very sensitive to local changes in the slopes of the mode shapes due to differences in the boundary conditions." Justification for use of Eq. (3.17) for flow induced vibration of beams is given by both Au-Yang and Blevins [11, 40] and both recommend correlation length L_e to be between 3 and 5 diameters.

While Eq.(3.14) has been proven by many authors throughout the last 30 years, few have offered expansion or modification of the expression to help with applicability to real world problems. Dozaki, Morishita and Iwata [76] presented a slight modification to this formulation, Eq. (3.18) which included the contribution of fluid damping. While this is somewhat

limited in applications involving air, it is very important to include this effect for structures vibrating in fluids such as water, LOX etc. and other heavy fluids.

$$y(x) = \sum_{n} \sqrt{\frac{L_e G_f(f_n) J_{nn} \int_{L_e} \phi_n^2(x)\, dx}{64\pi^3 M_n^2 f_n^3 (\xi_n + \zeta_n)}} \phi_n \tag{3.18}$$

3.3.3 Implementation and Extraction of Shear Stresses

To successfully use the presented formulations the mode shapes of a freely vibrating structure are required. It is possible to insert the results for approximate mode shapes for w only into these equations and obtain, through extraction, the contribution of shear to the sensor's response. To approximate this, a constant distributed load is applied to the beam to be analyzed. For this we use the approximate mean drag coefficient experienced by the sensor (determined empirically as a function of the Reynolds number) and a boundary layer approximation to give a distribution profile for force. With this forcing and application of Ritz method, the coupled bending and shear expressions are solved and hence for each point along the beam, the percentage contribution of shear is known. This percentage contribution is applied to the results determined from the preceding analysis and hence mean and RMS shear stresses can be obtained. A derivation of the variance of the shear stresses, σ_{zx} as a function of the variance of the axial stress (bending), σ_{xx} for a beam.

Axial stress, σ_{xx} and shear stress, σ_{zx} in the beam using Timoshenko theory are given by

Eqs. (3.19) and (3.20), respectively

$$\sigma_{xx} = -E\,z\,\frac{\partial \alpha}{\partial x} \tag{3.19}$$

$$\sigma_{zx} = k\,G\left(\frac{\partial w}{\partial x} - \alpha\right) \tag{3.20}$$

where E and G are elastic modulus and shear modulus, respectively; α is rotation caused by the bending only and w is the transverse displacement of the beam. Equation (3.21) defines the ratio of bending stress, σ_{xx}, and shear stress, σ_{xz}.

$$\frac{\sigma_{xx}}{\sigma_{zx}} = \frac{-E\,z\,\frac{\partial \alpha}{\partial x}}{k\,G\,\left(\frac{\partial w}{\partial x} - \alpha\right)} \tag{3.21}$$

While solving for dynamic response or eigenvalue problem using Rayleigh-Ritz method, w and α are approximated by trial functions given in Eqs.(3.3-3.4).

If we substitute these trial functions into Eq. (3.21), we get

$$\frac{\sigma_{xx}}{\sigma_{zx}} = \frac{-E\,z}{k\,G}\,\frac{\left[\sum_{i=1}^{m} b_i\,\Psi_i'\,(x)\right]}{\left[\sum_{i=1}^{n} a_i\,\Phi_i'\,(x) - \sum_{i=1}^{m} b_i\,\Psi_i\,(x)\right]} \tag{3.22}$$

In Eq.(3.22), time dependability of the coefficients is not represented for the compact representation of the equation. At the particular height,$z = z_0$, and the location along the beam, $x = x_0$, we get a ratio of σ_{xx} and σ_{zx} as a constant if $\Phi_i(x)$ and $\Psi_i\,(x)$ are functions of x

only. Hence for a particular x, y, z location:

$$\frac{\sigma_{xx}}{\sigma_{zx}} = C_0 \tag{3.23}$$

Therefore, variance of the shear stress is given by Eq. (3.24)

$$Var(\sigma_{zx}) = \frac{\sigma_{xx}}{C_0^2} \tag{3.24}$$

3.3.4 Additions

In addition to the calculated RMS strains in the lift and drag directions, a model to account for the contribution of the mean strains induced by fluid flow has been included. Since mean lift coefficient is zero, only the drag direction need be considered. The mean strain in the drag direction has been accounted for through the use of a boundary layer model for fully developed turbulent pipe flows. This model can be found in Fox [78] and is:

$$U(r) = U_{cl}\left(1 - \frac{1-r}{R}\right)^{(1/n)} \tag{3.25}$$

$$n = -1.7 + 1.8\log Re \tag{3.26}$$

$$U_{cl} = U_{av}\frac{2n^2}{(n+1)(2n+1)} \tag{3.27}$$

Here U_{cl} is velocity at the center of the pipe, R is radius of the pipe, r is position from the center line to pipe wall and U_{av} is the average velocity of the fluid flow. Using the

probe Reynolds number, an appropriate steady drag coefficient is obtained utilizing the C_D versus Re figure found in Blevins [11]. Using this information, an expression for force at each desired location from 0 to L is obtained. Using the Rayleigh-Ritz expression developed earlier for the Timoshenko beam, but now applying this force and removing all expressions dependent on time (giving a static deflection expression) static deflections and hence strain can be calculated.

This expression is key in extracting the shear strains in the later analyses. It is known that for a given static deflection the total response slope is the sum of beam bending and shear contributions. For static deflections at a given x coordinate, the contribution of each to the total response can be considered a constant. Hence, if total response and bending contribution are calculated, shear contribution follows. The same logic can be applied to the dynamic analyses previously discussed. Although the expressions are derived for an Euler-Bernoulli beam, it is possible to use the mode shapes for total response in these formulations and use the shear and bending constants to decompose the predicted total response into shear and bending contributions.

3.4 Experimental Work

3.4.1 Experimental Setup

Experimental validation of the analytic models took place in the Baker Hydraulics Laboratory of the Civil and Environmental Engineering Department at Virginia Tech. The hydraulics lab is home to three sediment demonstration channels whose primary purpose is study of water body sedimentation and associated water flow. These facilities were chosen based on availability, as well as cost and simplicity of implementation compared to a cryogenic facility. The smallest of the three channels, 20 ft Engineering Laboratory Design, Inc. Sediment Demonstration Channel, was provided for the project's use.

3.4.2 Test Apparatus and Materials

From a holding tank, two gravity fed hydraulic pumps send water through a system of PVC pipes to the channel head, where it then runs back to the holding tank. Water from the two pumps combines after a short distance. The water can then be sent either through a 2 in pipe or a 6in. pipe or both, depending on the capacity requirements of the current test. This arrangement is controlled by the appropriate ball valves. One or two pumps may be used; however, the second pump is only used if the larger pipe is used. Volumetric flow rate can be monitored using the appropriate Venturi nozzles and the corresponding supplied water and mercury manometers.

Table 3.1: Probe sizing and material properties.

Property	Symbol	Value	Unit
Elastic modulus	E	1.5	GPa
Density	ρ_p	1240	kg/m^3
Mass per unit length	m_p	0.0279	kg/m
Outer diameter	OD	6.223	mm
Inner diameter	ID	3.175	mm
Moment of inertia	I	6.859 x 10^{-11}	m^4
Length	L	38.1	mm

The original channel was modified for this experiment by replacing a section of the 2 in pipe running underneath the channel with an experimental test section. The original section of white PVC, was replaced by an identical section of clear PVC. An aluminum bossing was then constructed for the purpose of supplying a mounting location for the faux temperature probe to be studied. For this experiment only the first hydraulic pump was used, and flow only traveled through the 2 in pipe with our test section installed. Since fluid flow through the channel would not have provided enough fluid force on an AISI 304 Stainless Steel probe, such used in cryogenic applications, an alternate material was utilized. Low damping PVC was chosen as the replacement for the faux probe whose material and geometric properties can be found in Table 3.1. Figure 3.1(a) shows the probe.

To mount the PVC tube in the test section, it was fitted with an aluminum bushing attached with silicone. Then, a brass Swagelok fitting with nylon inserts was used to secure the bushing inside of the bossing. This configuration produced a secure, undamaged PVC probe when mounted in the test section (see Figure 3.1(b) - not to scale).

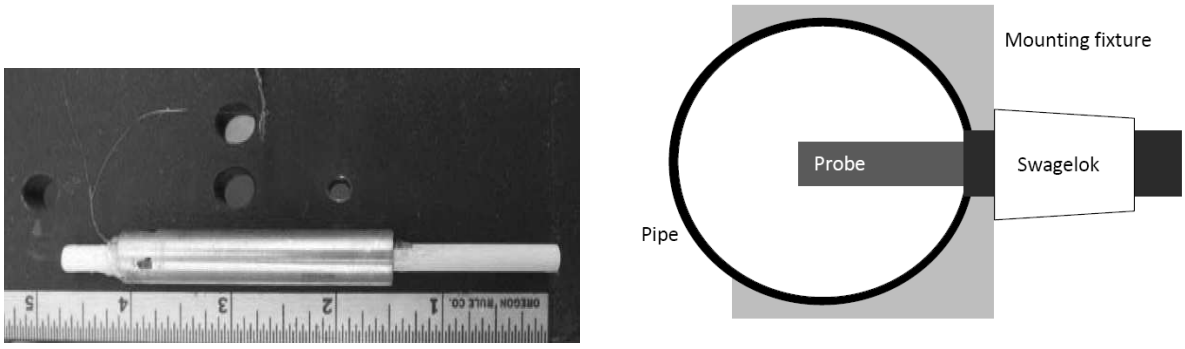

(a) (b)

Figure 3.1: PVC probe in aluminum bushing (a) and illustration of installation (b)

3.4.3 Measurement and Data Capture

Strain data was recorded using foil Vishay strain gages mounted at the fixed end of the beam that is the PVC probe, where the strain is a maximum. A single gage was used with wiring in a quarter Wheatstone bridge circuit. Data was collected for both lift and drag direction response by changing rotating the mounted probe to the appropriate orientation. A sample probe is shown in Figure 3.1(a). Analog voltage data was amplified using a Micromeasurements 2310 Signal Conditioning Amplifier. A Tektronix TDS 2014 digital oscilloscope was then used to collect and store all data. Data processing and analysis was performed using MATLAB version 2008b. To reduce noise recorded, all electronic measurement equipment was connected to a ground isolating transformer. In addition, both channel vibrations interfering with data collection of probe vibration, as well as water temperature fluctuation effect on strain gage readings were considered. However, both were found to have minimal effect on the recorded data.

Flow data was captured using the water channel's attached mercury and water manometers. Manometer measurements were related to pump frequency, a calibration which is required prior to each test due to variations in head in the water tank.

3.4.4 Probe Experimental Frequency Behavior

The frequency response of the probe is a factor in verification of a key assumption of strain response prediction. In addition, it may prove to be essential to fatigue life calculation as well. The added mass effect of water displaced by the probe is expected to decrease the natural frequency of the probe from the free response frequency of the probe in air. This reduction can be estimated by theory. Experimental analysis of the probe's strain response in the frequency domain shows a modal peak near 475 Hz. This peak is shown in an example of the drag response in Fig. 3.2(a) and in an example of the lift response in Fig. 3.2(b).

These frequencies were obtained through a Fourier transform of the time variant vibration response. This closely matches the natural frequency predicted by analysis of 499Hz, a difference of under 5%. Observations during the course of experimentation have resulted in a progressive cycle of experimentation, analysis, and refinement of experimental procedures and equipment.

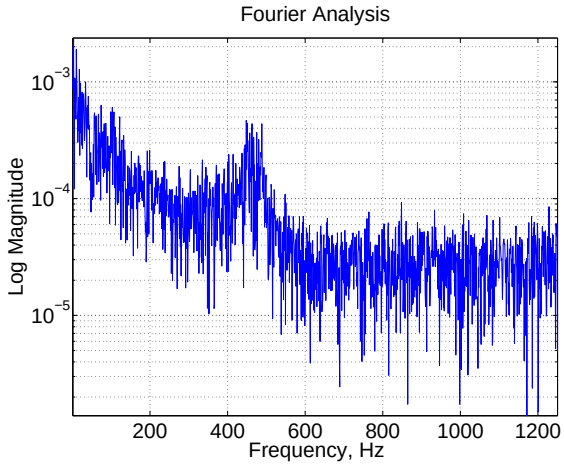

(a) FDR drag direction

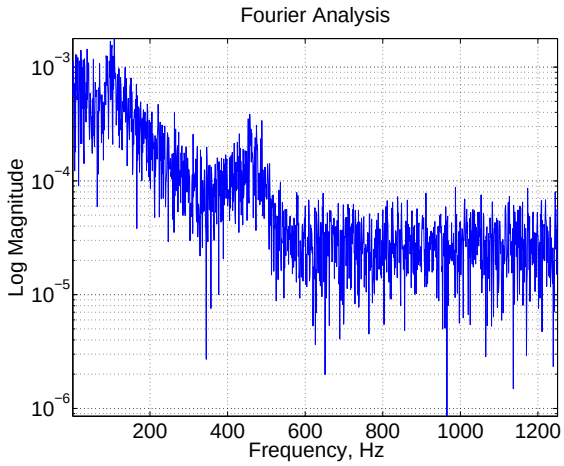

(b) FDR lift direction

Figure 3.2: Example of frequency domain response (FDR)

3.4.5 Comparison with Experimental Strain Data

Observations during the course of experimentation have resulted in a progressive cycle of experimentation, analysis, and refinement of experimental procedures and equipment. Experimental results have shown successful data capture and seem to fit the analytical model quite well for mean and RMS strains as shown in Figures 3.3(a), 3.3(b) and 3.4. The largest

discrepancies are seen for the lower velocities. Since we are dealing with such low velocities and much lower strains, experimental errors in this region are amplified. In addition, the prediction model used is known to have problems for low amplitudes of vibration seen at these lower velocities [11].

The same analysis predicts the shear stresses experienced by the probe (Figures 3.5(a) and 3.5(b)). In these plots, the experimental values obtained by experiment for bending strains have been treated by the method described in Eqs. (3.20-3.24) to give so called, extracted shear strains to aid comparison in the plot.

To ensure the analysis method is still compatible with longer, slender probes a comparison case with Kawamura's results was generated for displacement amplitudes [79]. As before, results show good agreement, except at lower reduced velocities which is again a known weakness of the model. Shear strains are also predicted (not shown) which are at maximum $100\mu\epsilon$.

3.4.6 Potential of Elliptical Sensor Sections

It was noted earlier that substantial benefit may be obtained from having sensors using elliptical sections (with major diameter aligned with flow direction) in preference to circular sections. Figure 3.7 illustrates the reduced frontal area when considering an elliptical section with a major/minor axis ratio of two, keeping characteristic length constant. Not only should mean drag coefficient be reduced, but the fluctuating lift and drag coefficients also. It follows

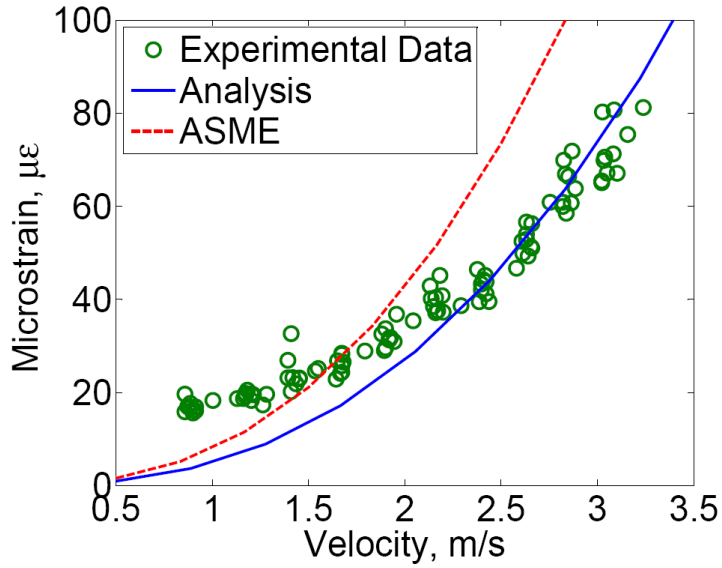

(a) Normal strains in drag direction

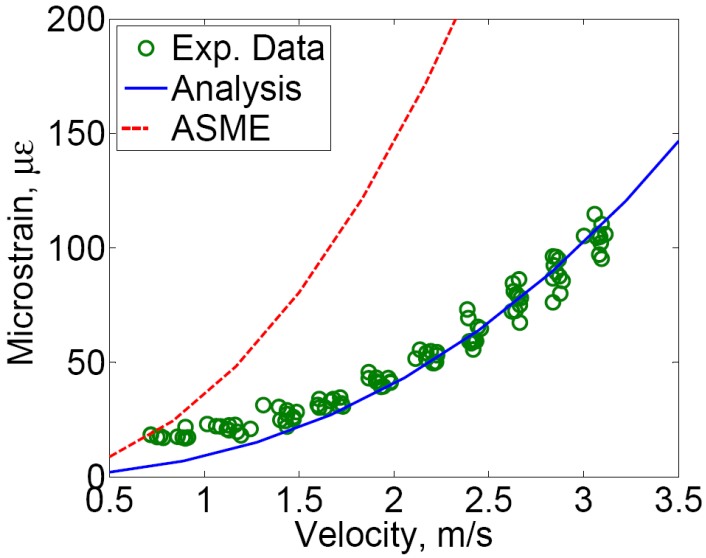

(b) Normal strains in lift direction

Figure 3.3: Comparison of variation of RMS strains with tests in water flume for circular cross section

that the overall response in the drag direction should be substantially reduced. However, response amplitude in the lift direction may in fact increase due to the slender nature of the sensor in this direction. Delany and Sorensen [12] indicate that the mean drag coefficient for

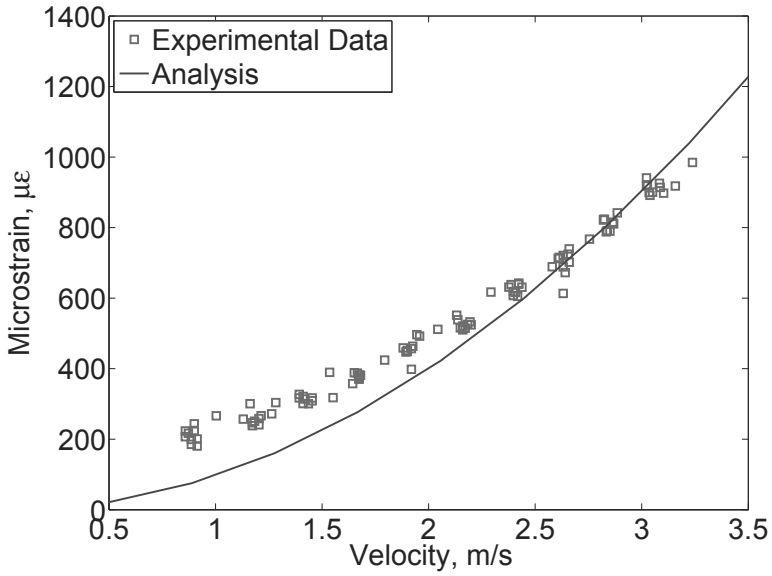

Figure 3.4: Comparison of variation of mean strains with tests in water flume for circular cross section

an ellipse with a major to minor axis ratio of 2 is approximately 60% of that for a circular cylinder. This approximation is later used in Li, Davidson and Mantell [80] and confirmed during their numerical study. Investigations by Modi [81] and Kim [82] suggest that the fluctuating coefficients also reduce to less than 60% of circular cylinder values. However, 60% will be used in order to be conservative. Using these approximations, a simulation was performed for an elliptic cylinder with major/minor axis ratio of 2 with the same flow conditions and material properties as for the circular cylinder described in the previous section.

A significant reduction in both mean and RMS drag strains is shown by Figures 3.8(a), 3.9, 3.10 and 3.11(a). However, lift RMS strains are increased significantly as shown in Figures 3.8(b) and 3.11(b). This shows that elliptical cross sections, despite their more streamlined shape, are particularly unsuitable for this problem.

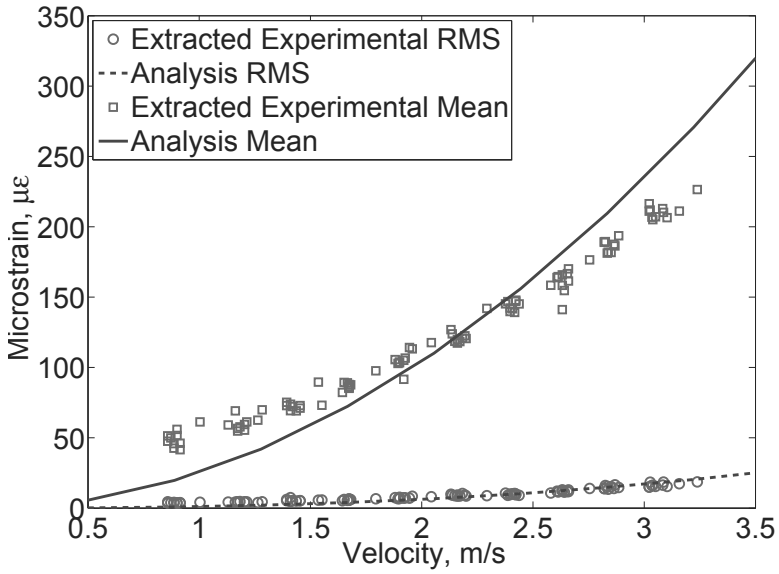

(a) Mean and RMS shear strains in drag direction σ_{12}

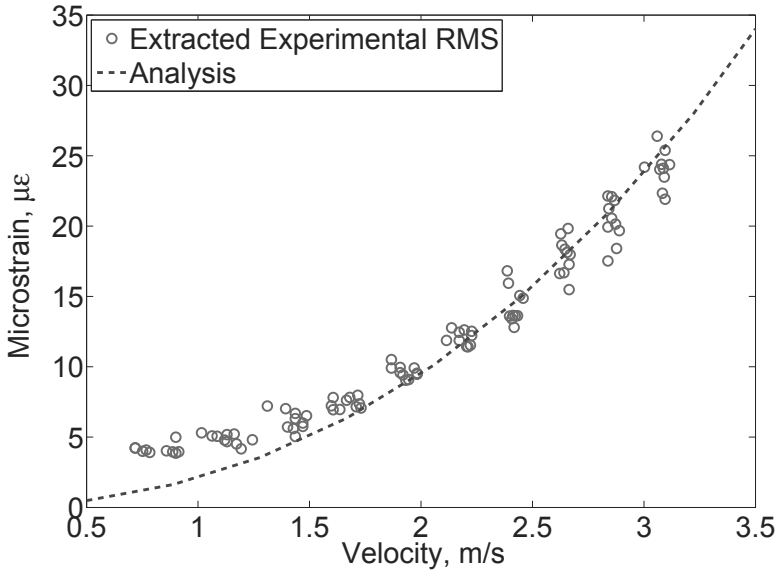

(b) RMS shear strains in lift direction σ_{13}

Figure 3.5: Predicted shear strains for circular cross section

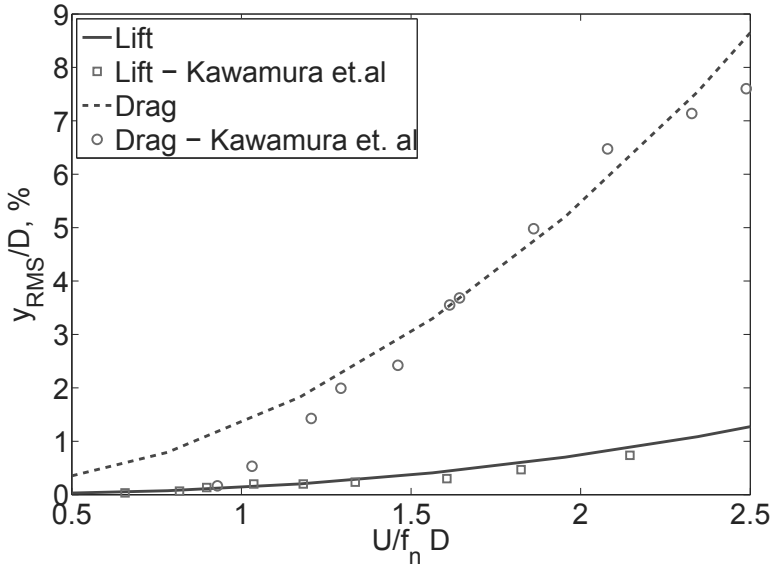

Figure 3.6: Comparison of predicted amplitudes with Kawamura results for Length:Diameter ratio $\approx$ 10

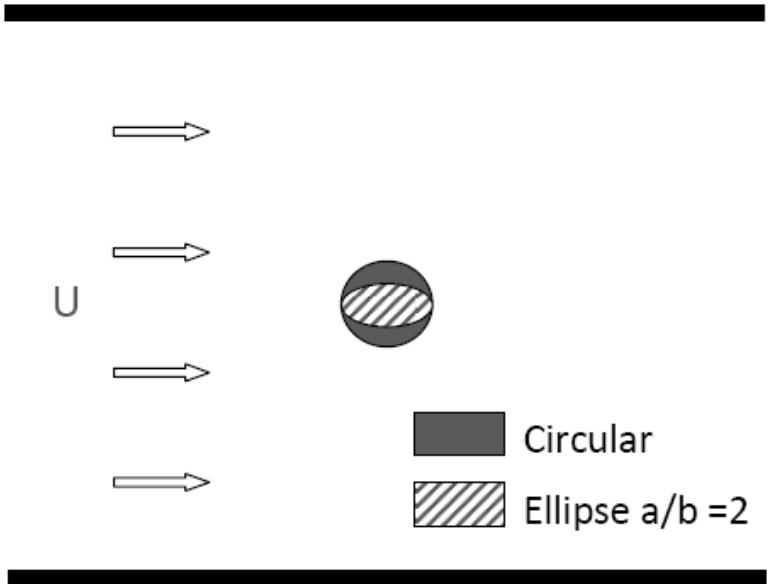

Figure 3.7: Illustrating the reduced frontal area of an elliptical cross-section

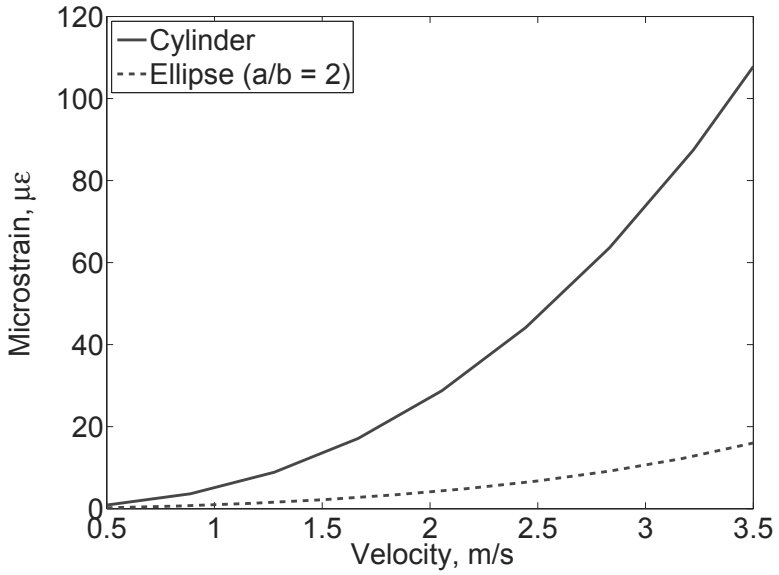

(a) RMS strains in drag direction σ_{12}

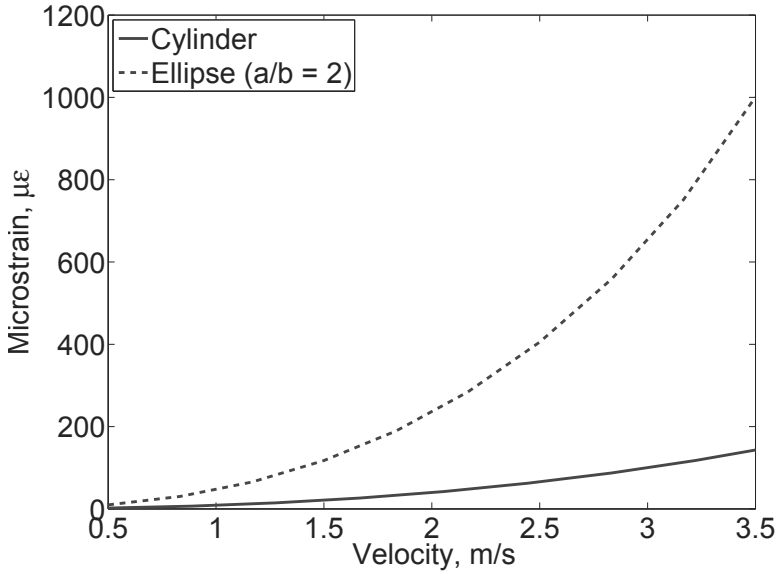

(b) RMS strains in lift direction σ_{13}

Figure 3.8: Comparison of fluctuating response of elliptical and circular sections for experimental conditions

3.5 LOX, LH2 and LMH Results

Upon experimental confirmation of model suitability for sensor vibration problems, predictive results for a range of velocities up to operating maximum for Liquid Oxygen (LOX), Liquid

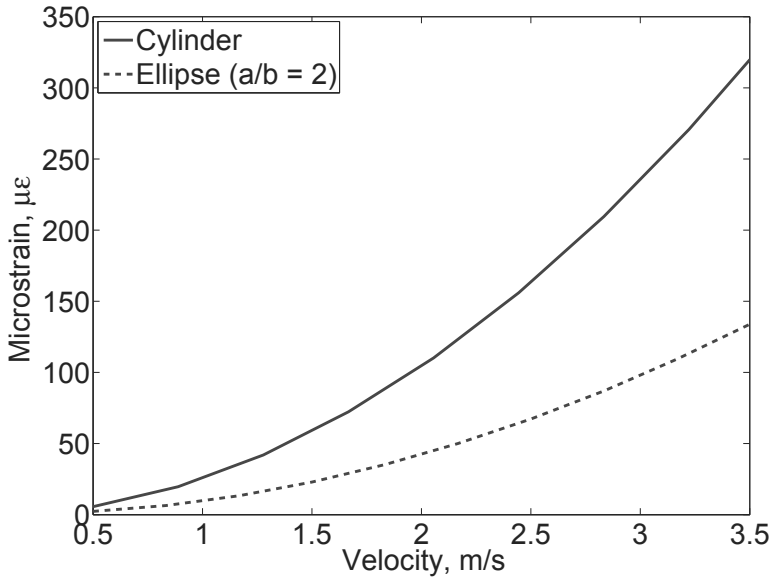

Figure 3.9: Comparison of mean shear response of elliptical and circular sections for experimental conditions

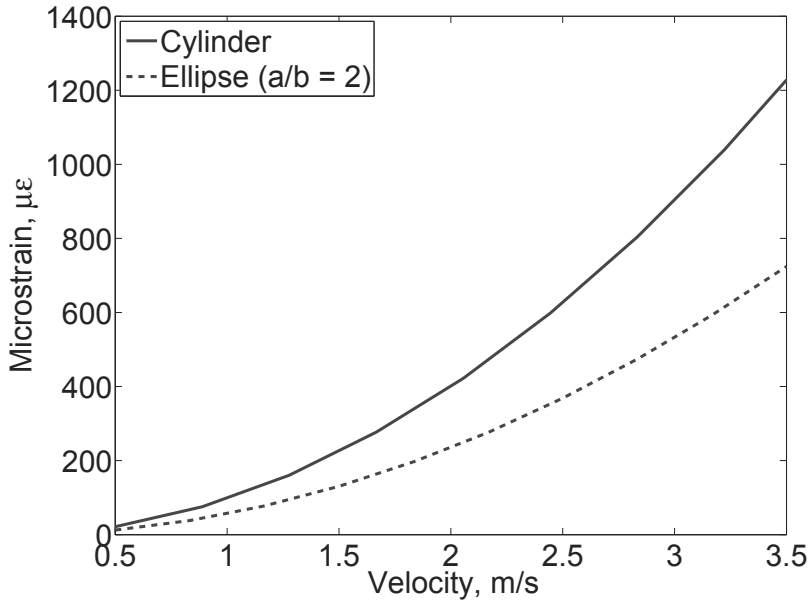

Figure 3.10: Comparison of mean response of elliptical and circular sections for experimental conditions

Hydrogen (LH2) and Liquid Methane (LMH) have been generated. The probe material is assumed to be SS304 (supplied by Luna Innovations) whose properties are listed below. For

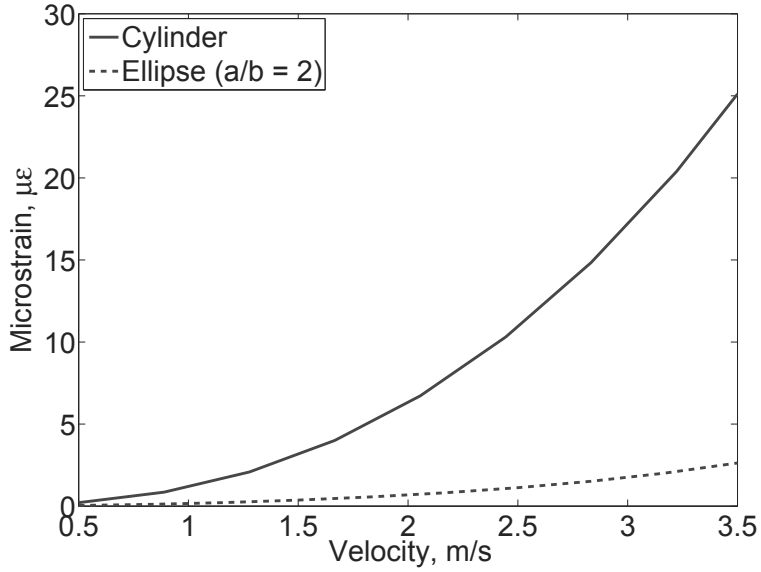

(a) RMS shear strains in drag direction

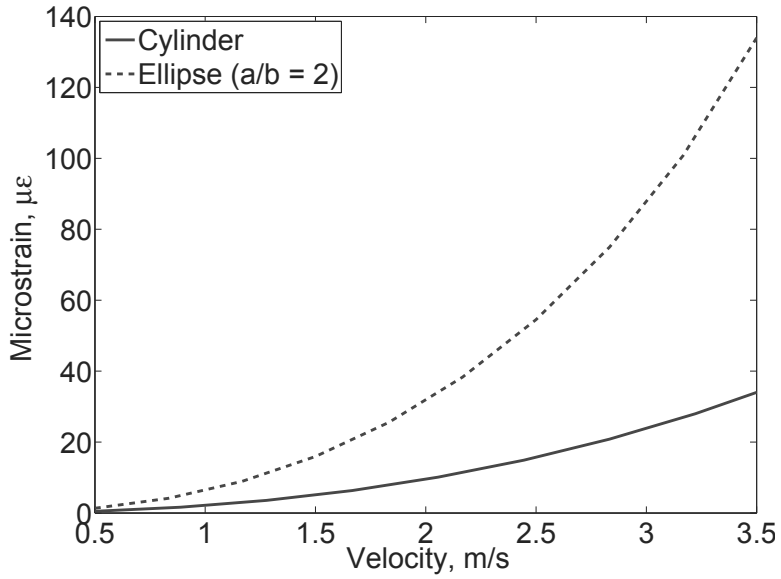

(b) RMS shear strains in lift direction

Figure 3.11: Comparison of fluctuating shear response of elliptical and circular sections for experimental conditions

the first case, the length and diameter of the probe are assumed to be 2 and 0.25 inches respectively. In the second case, length remains unchanged but diameter is halved to 0.125 inches. For both cases, wall thickness is assumed to be approximately 1mm. Additionally,

Property	Symbol	Value	Unit
Elastic modulus	E	192	GPa
Density	ρ_p	8000	kg/m^3
Poisson ratio	ν	0.29	kg/m

Table 3.2: Properties of SS304

Property	Symbol	Value	Unit
Density	ρ	1141	kg/m^3
Dynamic Viscosity	μ	2.30 x 10^{-4}	Pa-s
Maximum Flow Velocity	U	25	m/s

Table 3.3: Properties of LOX

structural damping (ξ) is assumed to be equal to 0.05 to take into account both material damping and the slight passive damping provided through adhesives etc. in the mounting mechanism. Please note that the material properties used assume room temperature as material data for cryogenic temperatures was not available.

3.5.1 LOX

During analysis, LOX is assumed to have properties as shown in Table 3.3 (provided by Luna Innovations).

3.5.1.1 LOX with 1/4 inch probe diameter

These results can be seen in Fig. 3.12. Here shear stresses can be seen to be a significant percentage of the bending stresses. When running analysis for this case we note that for certain velocities lock-in in the lift direction is not avoided but is suppressed. A warning dialog box (generated by the code) such as that shown in Figure 3.13 will alert the user to potential issues with a proposed design. In addition, further detail is output in the MATLAB command window, providing further feedback to the user, also seen in Figure 3.13. For this case, the information presented is visible in Figure 3.12. It is evident that for this industrial case, lock-in is only just encountered which means a significant redesign would not be required, rather only slight modification.

3.5.1.2 LOX with 1/8 inch probe diameter

These results can be seen in Fig. 3.14. In this case lift direction lock-in is neither avoided nor suppressed for the full operating velocity range. A warning dialog box shown in Fig. 3.15 is displayed alerting the user to this issue, as well as the corresponding text output.

These initial results suggest that probe redesign is necessary which may simply be a case of alternate material selection or reducing probe length. Here it is important to note that the lift direction results contain a numerical instability due to being in the lock-in region and hence are not valid. However, since the code produces results in seconds many design iterations are possible in a short period of time, allowing the user to see which designs are

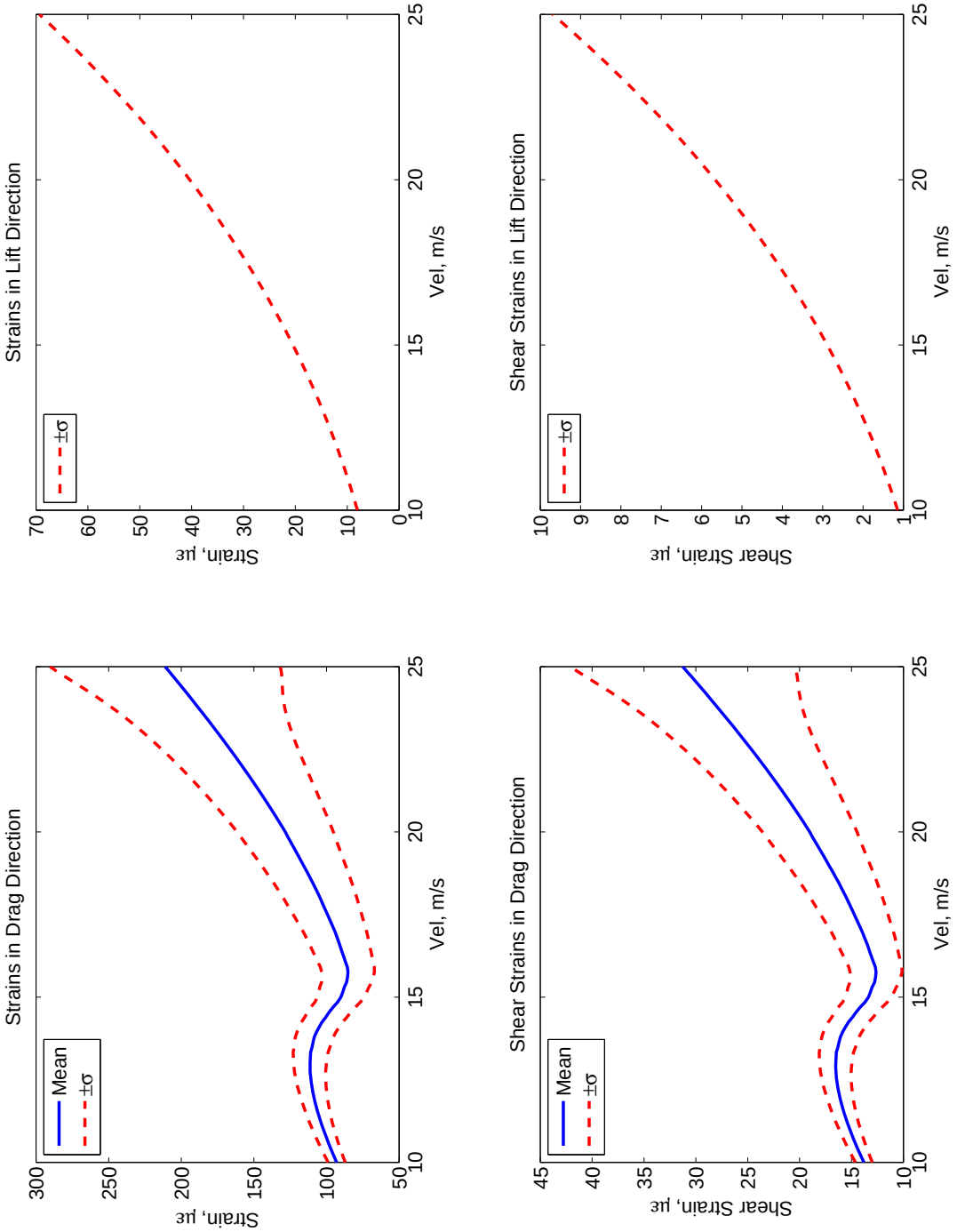

Figure 3.12: Full analysis results for LOX and 1/4 inch probe

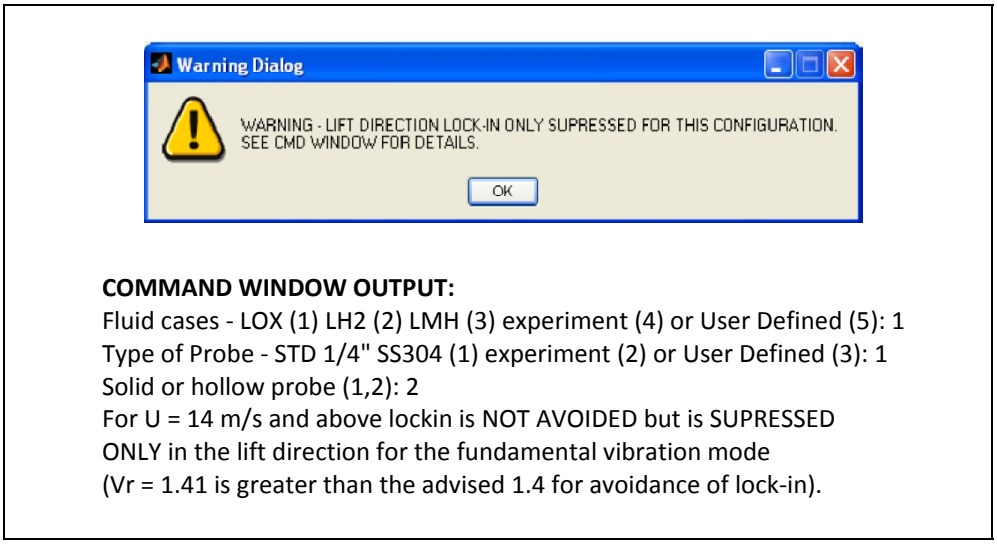

Figure 3.13: Warning dialog box alerting user of no lift direction lock-in avoidance but suppression only

Property	Symbol	Value	Unit
Density	ρ	71	kg/m^3
Dynamic Viscosity	μ	1.75 x 10^{-5}	Pa-s
Maximum Flow Velocity	U	101.5	m/s

Table 3.4: Properties of LH2

not subject to lock-in.

3.5.2 LH2

During analysis, LH2 is assumed to have properties as listed in Table 3.4.

A similar analysis was performed for the LH2 flow parameters at a 1/4 inch probe diameter. This analysis produced a double warning as displayed in Figure 3.17 and the analysis plots can be seen in Fig. 3.16.

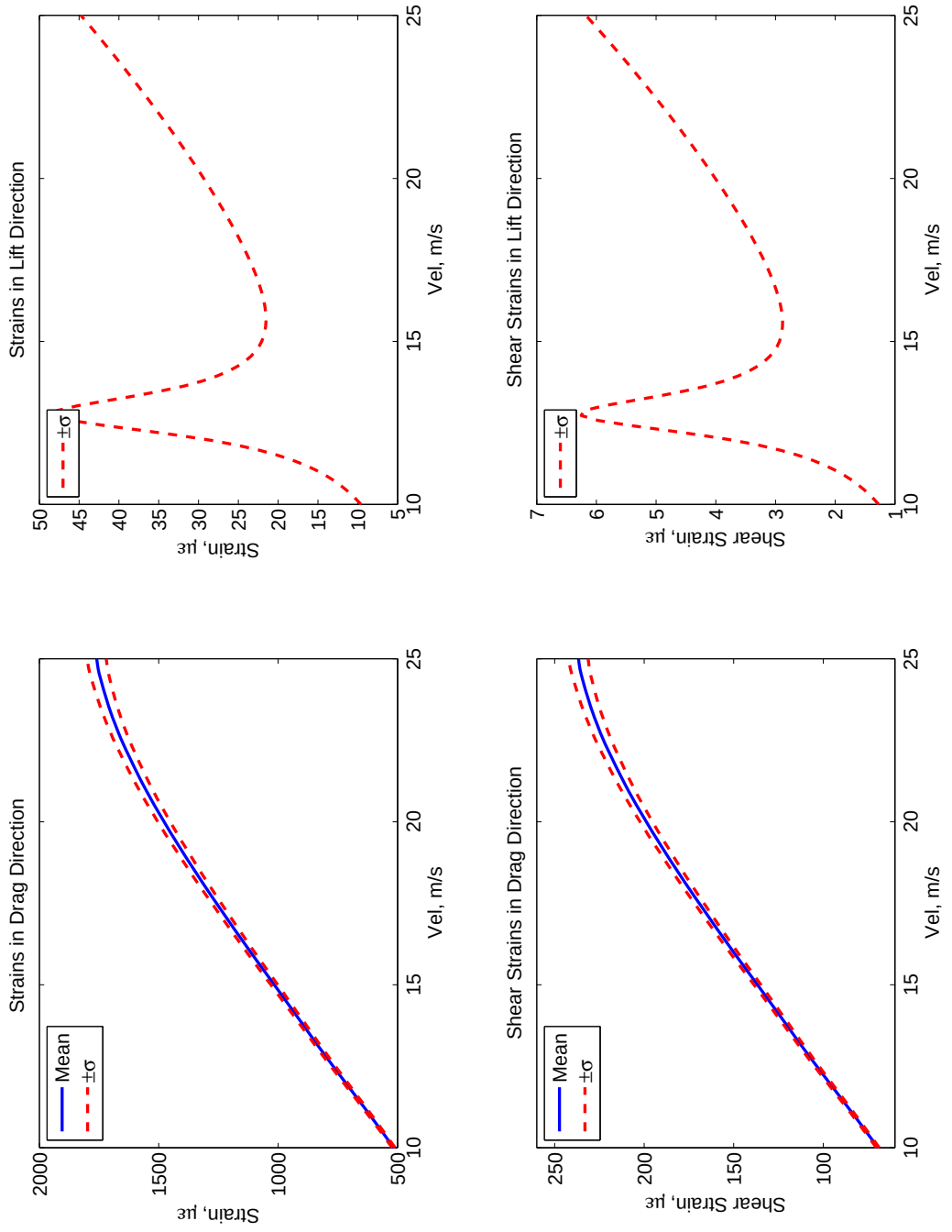

Figure 3.14: Full analysis results for LOX and 1/8 inch probe

This result means that for some of the operating range, lock-in is suppressed only, but at higher velocities (in this case greater than 36 m/s) lock-in is not avoided or suppressed and

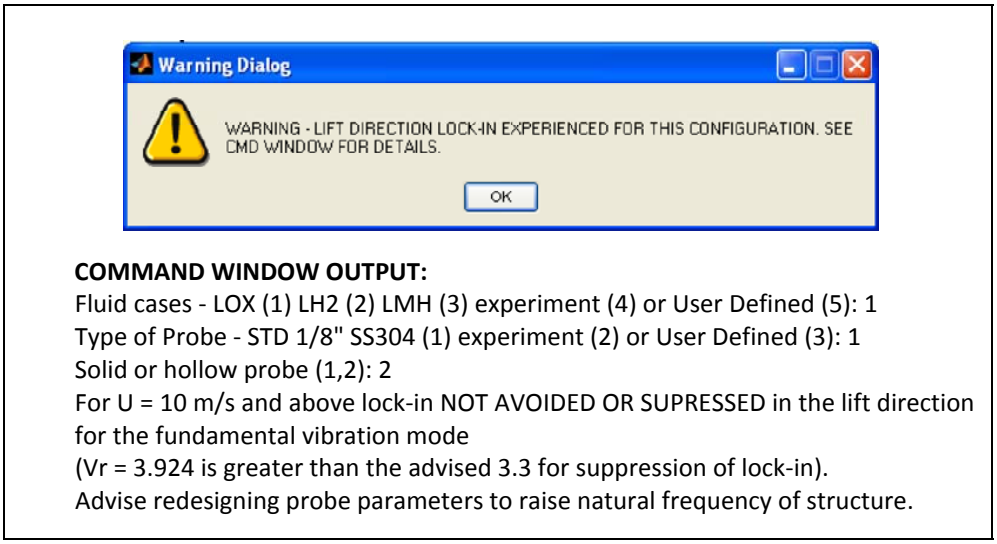

Figure 3.15: Warning dialog box alerting user of lift direction lock-in

Property	Symbol	Value	Unit
Density	ρ	423	kg/m^3
Dynamic Viscosity	μ	1.84 x 10^{-4}	Pa-s
Maximum Flow Velocity	U	80.25	m/s

Table 3.5: Properties of LMH

probe redesign is advised. Since this occurs for the 1/4 inch case, a 1/8 inch diameter case was not performed.

3.5.3 LMH

During analysis, LMH is assumed to have properties as listed in Table 3.5. As for the LH2 analysis, a double warning was produced, seen in Figure 3.19. Figure 3.18 shows the analysis results.

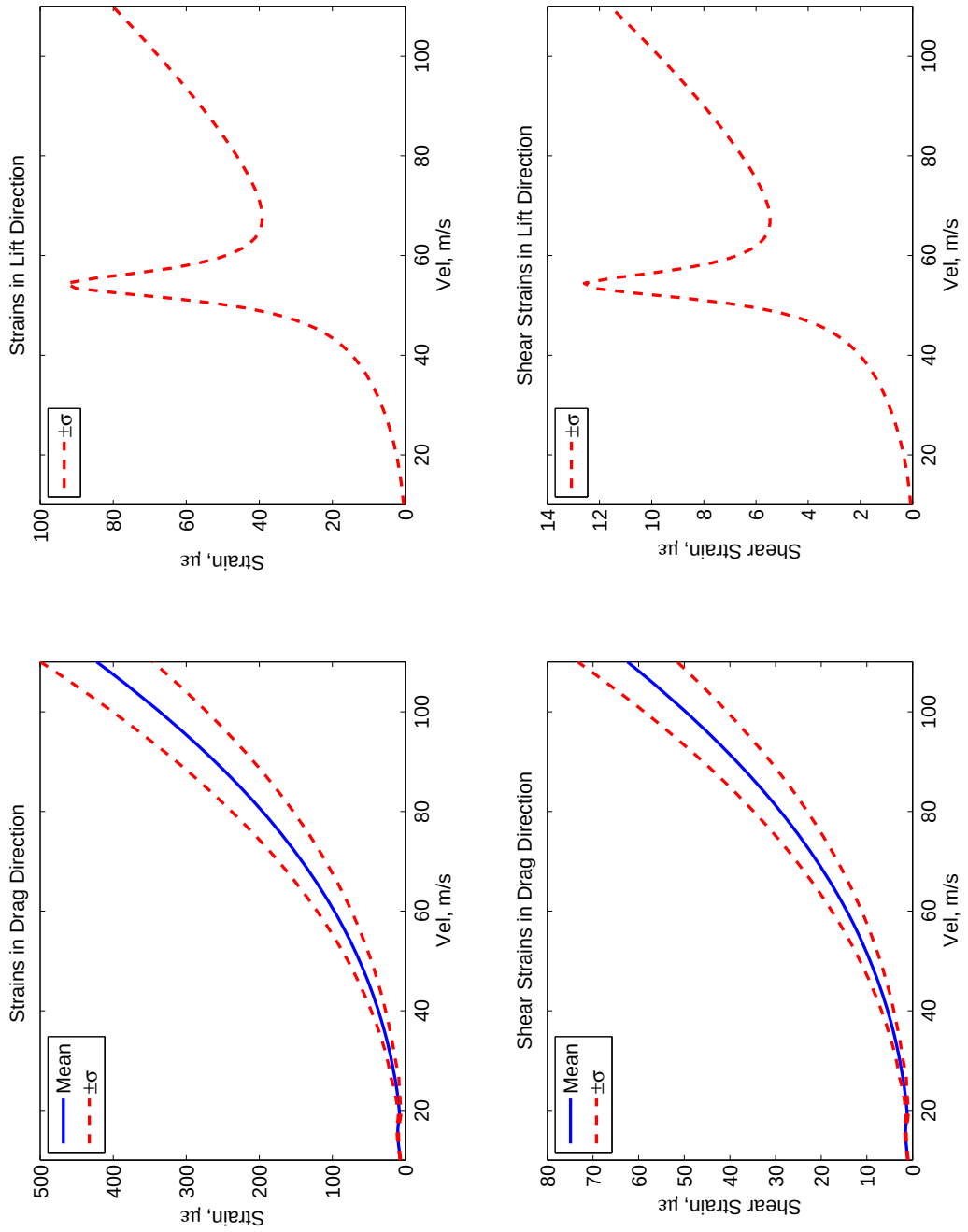

Figure 3.16: Full analysis results for LH2 and 1/4 inch probe

COMMAND WINDOW OUTPUT:
Fluid cases - LOX (1) LH2 (2) LMH (3) experiment (4) or User Defined (5): 2
Type of Probe - STD 1/4" SS304 (1) experiment (2) or User Defined (3): 1
Solid or hollow probe (1,2): 2
For U = 16 m/s and above lock-in is NOT AVOIDED but is SUPRESSED ONLY in the lift direction for the fundamental vibration mode
(Vr = 1.487 is greater than the advised 1.4 for avoidance of lock-in).
For U = 36 m/s and above lock-in NOT AVOIDED OR SUPRESSED in the lift direction for the fundamental vibration mode
(Vr = 3.357 is greater than the advised 3.3 for suppression of lock-in).
Advise redesigning probe parameters to raise natural frequency of structure.

Figure 3.17: MATLAB output for LH2 case

Again, a 1/8 inch analysis was not performed since lock-in is experienced below full operating velocity for this fluid flow.

3.6 Conclusions

The ASME recommendations for sensor design are updated to include shear deformation of the sensor. Bending strains in the lift and drag directions were experimentally validated using water flow at a range of velocities. The elliptical cross section studied clearly shows little benefit over a circular cross section, however a better solution may exist for other major/minor axis ratios but have not been explored here. Currently mean drag coefficient, fluctuating drag coefficient and fluctuating lift coefficient for an elliptical section are taken from literature. To explore further major/minor axis ratios, a return to literature followed

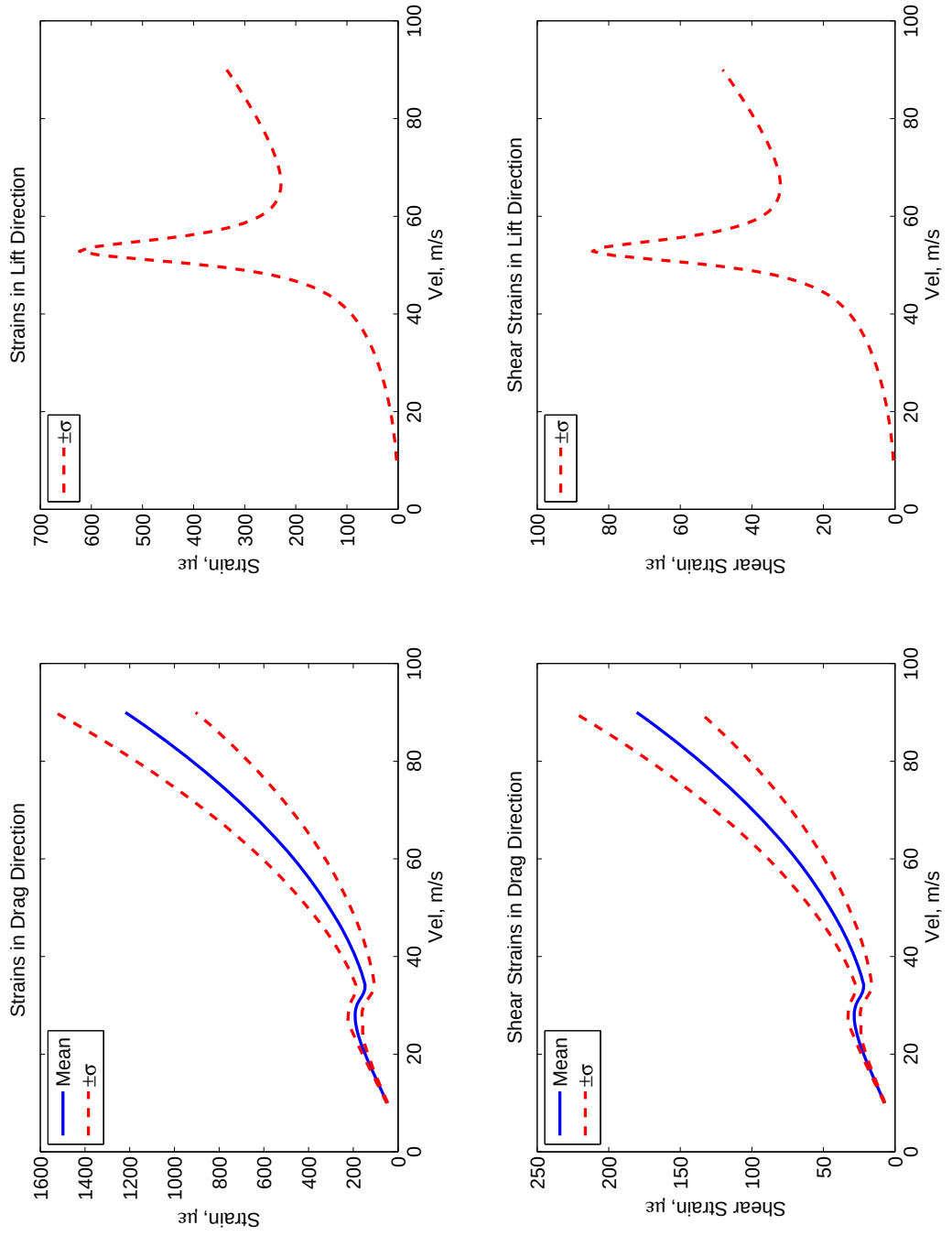

Figure 3.18: Full analysis results for LMH and 1/4 inch probe

by a switch to numerical computations will be required. Reducing the principal stresses which inherently lead to fatigue failure of such sensors is an optimization problem where

COMMAND WINDOW OUTPUT:
Fluid cases - LOX (1) LH2 (2) LMH (3) experiment (4) or User Defined (5): 3
Type of Probe - STD 1/4" SS304 (1) experiment (2) or User Defined (3): 1
Solid or hollow probe (1,2): 2
For U = 15 m/s and above lock-in is NOT AVOIDED but is SUPRESSED ONLY in the lift direction for the fundamental vibration mode
(Vr = 1.406 is greater than the advised 1.4 for avoidance of lock-in).
For U = 35 m/s and above lock-in NOT AVOIDED OR SUPRESSED in the lift direction for the fundamental vibration mode
(Vr = 3.319 is greater than the advised 3.3 for suppression of lock-in).
Advise redesigning probe parameters to raise natural frequency of structure.

Figure 3.19: MATLAB output for LMH case

the major/minor axis ratio could be optimized for a given flow condition. Regardless of sensor cross section, it is more than often the case that the sensors are manufactured from solid stock. The central hole placement for wires etc. as well as the size of the hole are uncertainties as a discrepancy between flexural and shear axis may exist. Including these uncertainties is an important next step for elliptical cross sections as small uncertainty in angle of attack (from mounting) can lead to major changes in the principal stresses.

From an industrial viewpoint, the initial designs for the operating conditions presented served a purpose to show the various warnings generated during user evaluation. However, these designs are clearly not suitable for their flow environment and will have to be redesigned. Additionally, it is not known what manufacturing restrictions exist and thus potentially infeasible designs can be studied using this method. The onus is thus on the engineer to weed out these designs independent of this analysis.

Chapter 4

Non-Stationary Response Using Karhunen Loeve Expansion

4.1 Introduction

Until now, work centered on developing a design tool for FIV of sensors has been discussed. A significant portion of this work depends on stochastic modeling. Through development of the tool described in the previous chapter, interest in stochastic systems prompted investigation of their analysis methods. Focusing on the stationarity property of the turbulence modeling from the previous chapter, the author became interested in the restrictions of such an assumption and how non-stationary processes can be modeled. For a stationary process, the mean and standard deviation are time invariant, however for a non-stationary

process, the mean and standard deviation now vary with time. Investigation showed a field which is very dense with a variety of analysis methods but one factor remained constant throughout the literature - modeling non-stationary processes in large systems is difficult and expensive since complex analytic expressions often must be developed for each problem (e.g. [64, 65, 62, 7]). Techniques which rely upon expansion and summation techniques have been largely avoided until the advent of increased computational power. The advantage of such a method (e.g. polynomial chaos) is that it is applicable to almost any structure and any form of excitation. This is a key advantage over the few simple closed form solutions which exist. Therefore, work was undertaken to find a method by which structures subject to a non-stationary force could be analyzed efficiently.

Ideally, this work could be brought full circle such that the models developed could feed back into the FSI work, however, modification of a turbulence model is another dissertation in itself and thus beyond what will be discussed here. Rather, this work aims to explore if a method can be developed to allow a non-expert engineer to run stochastic analyses on a structure and obtain meaningful results. The key to this work is that the engineer need not have detailed knowledge of the random force, but only its covariance function which is obtained through experimentation or from the literature for similar applications.

Such a method should have application to further detailed design studies where complex structures are analyzed through commercial finite element software. Here, the method developed could form a "wrapper" around commercial codes thus allowing for non-intrusive non-stationary vibration analysis in house, without the need to ask the commercial vendor

for bespoke software additions which are often very expensive.

4.2 Karhunen-Loeve Expansion

Non-stationary random vibration is characterized by time-dependent statistical moments. As this work focuses on Gaussian cases, the mean (1st moment) and auto-covariance (2nd moment) completely describe the probability distribution [83]. Mean and auto-covariance are described through the following integral equations:

$$\mu_X(t) = E[X(t)] = \int_{-\infty}^{\infty} X(t).p(X(t))dx(t) \tag{4.1}$$

The mean, μ_X, depends upon the random vibration set X and the probability function p. The covariance of random variables X and Y with mean values μ_X and μ_Y is:

$$C_{XY}(t_1, t_2) = E[(X(t_1) - \mu_X)(Y(t_2) - \mu_Y)] \tag{4.2}$$

If a process X^* is substituted for Y in Eq. (4.2) where X^* is simply a time-shifted version of X, then Eq. (4.2) is known as auto-covariance. This auto-covariance differs to that in the stationary case as it is a function of two instants of time [5].

In many engineering problems, a random process may have statistical dependence on more than one random variable. In this case, it is necessary to consider joint probability density

functions. This step becomes cumbersome when calculating using the joint distribution of many random variables, hence, in practice, it is advantageous to study the simple interaction of two random variables and extract as much information as possible from that relationship [5]. This is achieved through covariance and correlation analyses [5].

The Karhunen-Loeve (KL) expansion provides a way to discretize the auto-covariance function such that it may be used in the calculation of system response [46]. Using KL expansion, the forcing function of a system may be written as a combination of the mean forcing component, μ_F, and the summation component:

$$f(t) = \mu_F(t) + \sum_{i=1}^{n} \sqrt{\lambda_i}\xi_i\phi_i(t) \tag{4.3}$$

Here, ξ_i are sets of independent identically distributed (i.i.d.) random variables (zero mean and standard deviation of 1), λ_i are the eigenvalues of the auto-covariance and $\phi_i(\mathbf{t})$ are the eigenvectors of the auto-covariance. The eigenvectors can be further expanded as:

$$\phi_i(t) = \sum_{j=1}^{m} d_{ji}h_j(\mathbf{t}) \tag{4.4}$$

where d_{ji} are unknown constants and h_j are user-defined basis functions. The eigenvalues and eigenvectors of the auto-covariance function ($C_{XX}(t_1, t_2)$) are found by solving a Fredholm

equation of the second kind [46].

$$\int_{t_{min}}^{t_{max}} C_{XX}(t_1, t_2)\phi_i(t_1)dt_1 = \lambda_i\phi_i(t_2) \tag{4.5}$$

The procedure for solving these problems numerically is outlined in Ghanem and Spanos [46]. This results in an eigenvalue problem, Eq. (4.6), using user-defined basis functions and the auto-covariance of the system. Construction of the **N** matrix is very similar to that for axial bar type of FEM problems.

$$\mathbf{CD} = \mathbf{\Lambda ND} \tag{4.6}$$

where

$$C_{ij} = \int_{t_{min}}^{t_{max}} \int_{t_{min}}^{t_{max}} C(t_1, t_2)h_i(t_2)h_j(t_1)dt_1dt_2 \tag{4.7}$$

$$N_{ij} = \int_{t_{min}}^{t_{max}} h_i(t)h_j(t)dt \tag{4.8}$$

and

$$\Lambda_{ij} = \delta_{ij}\lambda_i \tag{4.9}$$

Once the eigensystem is solved, the eigenvectors must be scaled appropriately. The MAT-

LAB eigensystem solver typically scales the eigenvectors such that the Euclidean norm is equal to one. While this is appropriate in many fields, it is not so in this case as the magnitude of the eigenvector plays an integral role in the calculation of the response using KL expansion. An appropriate way of scaling is making use of the Fredholm equation (4.5) once again. The eigenvectors $\phi_i(t)$ and eigenvalues λ_i are first calculated using the MATLAB eigenvalue solver then these values are used to calculate the right hand side of the Fredholm equation. The left and right hand side values are compared and a scaling factor for the eigenvector computed such that the equation is balanced. The left and right hand side of the Fredholm equation are once again computed using these scaled eigenvectors to be sure a correct scaling factor has been used.

The response of the system is also represented by a KL expansion process [46]. The i.i.d. random variables used have a useful property when constructing the variance of the response. These variables ξ are orthogonal such that their expectation is given by ($E[\xi_i, \xi_j] = \delta_{ij}$). This means the standard deviation of the response is represented as:

$$\sigma_X(t) = \sqrt{\sum_{i=1}^{n} \lambda_i \left(\sum_{j=1}^{n} d_{ji} m_j(t) \right)^2} \tag{4.10}$$

m_j are the deterministic response of the system due to the input basis functions h_j. In the author's previous work, h_j were continuous global trigonometric functions [84]. These functions were chosen based on the author's knowledge of system response, both transient and steady state. This requires an appreciation for the particular physics involved in the

system which is not so easy when considering a MDOF system. Therefore, it is appropriate to use more generalized functions. It is easiest to represent the eigenvectors in discretized form, using piecewise linear or higher order polynomial Lagrange interpolation functions in the same manner as in a time Finite Element Method. As a first step for simplicity, discretized h_j were chosen to be simple piecewise constants which makes the calculation of both $\mathbf{C}$ and $\mathbf{N}$ very easy and computationally inexpensive. Once discretized, the covariance eigenvectors are used as before [84] as deterministic forcing functions to the SDOF system. The response due to these forcing functions are p and hence (4.10) can be rewritten as:

$$\sigma_X(t) = \sqrt{\sum_{i=1}^{n} \lambda_i p_i(t)^2} \tag{4.11}$$

By the same logic, the auto-covariance of the displacement for a SDOF system can be calculated by:

$$R_{XX}(t_1, t_2) = \sum_{i=1}^{n} \lambda_i p_i(t_1) p_i(t_2) \tag{4.12}$$

Discretizing the basis functions, rather than following the example in [84] allows for a more generic algorithm where a system can be solved when the effects of the covariance are not known. The price paid for the generic nature of this algorithm is the greater number of terms required for the convergence of the solution. However, significant computational time is saved when constructing the $\mathbf{C}$ and $\mathbf{N}$ matrices through numerical integration which completely offsets a few extra simple summation steps.

4.3 Application To A Simple SDOF System

The SDOF system to be solved can be found in Mulani, Kapania and Scott [84] (some details are available in an excerpt of this text in the Appendix). Here spring stiffness k, damping coefficient ζ, mass m and correlation length (time beyond which events are considered uncorrelated) l_c are $300N/m$, 0.2, $1kg$ and $0.05s$ respectively. The time period considered is from 0 to 1 second. Two different covariance functions are considered. The first is exponential auto-covariance (4.13) and the second is a modulated exponential covariance (4.14). Graphical representation of these functions are found in Figures 4.1 and 4.2 respectively.

$$C_{FF}(t_1, t_2) = e^{-|t_1 - t_2|/l_c} \tag{4.13}$$

$$C_{FF}(t_1, t_2) = e^{-(t_1+t_2)} e^{-|t_1 - t_2|/l_c} \tag{4.14}$$

Upon implementation of the temporal discretization, results for the standard deviation of the system are obtained and compared to both the analytical solution and numerical solution provided in Mulani, Kapania and Scott[84] as seen in Figures 4.3 and 4.4. The corresponding auto-covariance of the displacements are presented in Figures 4.5 and 4.6.

It is clear that for 6 KL terms the continuous basis functions used previously, is closer to the analytic solution than the discretized basis functions used in this study. This efficiency was achieved by prior knowledge of the physical nature of the problem. However, when

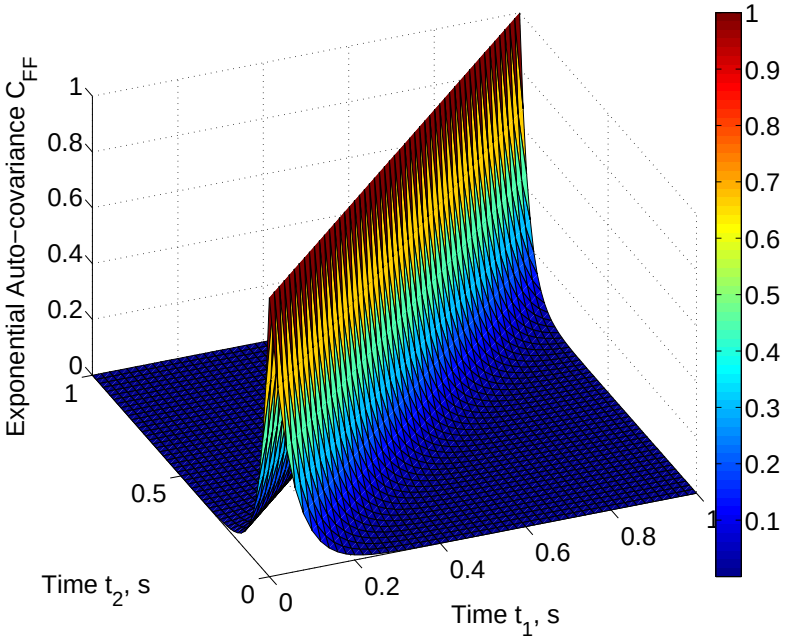

Figure 4.1: Exponential auto-covariance function

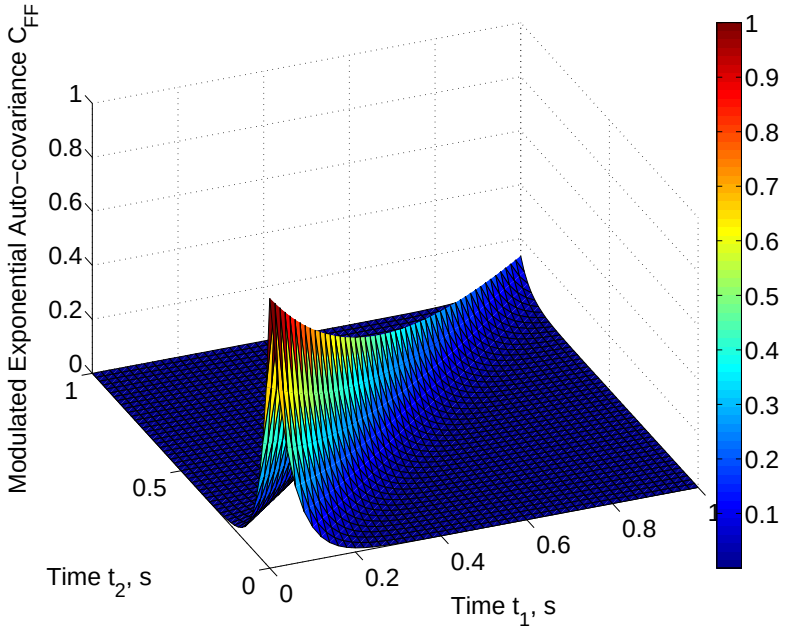

Figure 4.2: Modulated exponential auto-covariance function

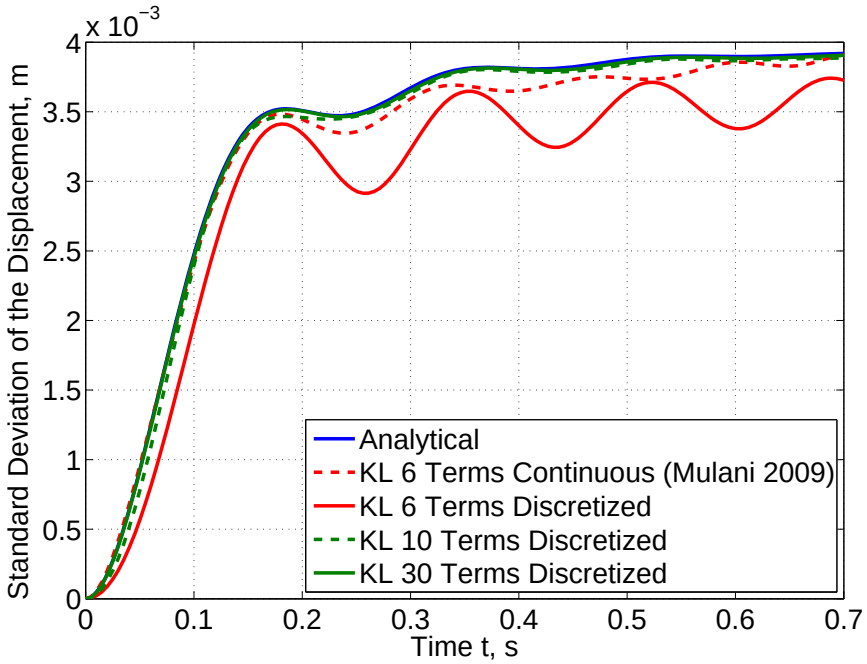

Figure 4.3: Standard deviation of displacement for exponential covariance using continuous and discretized basis functions

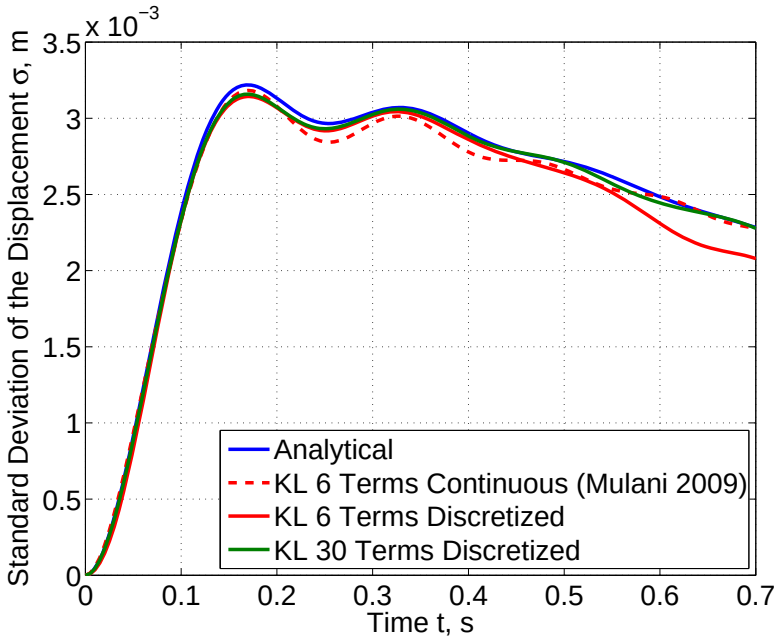

Figure 4.4: Standard deviation of displacement for modulated exponential covariance using continuous and discretized basis functions

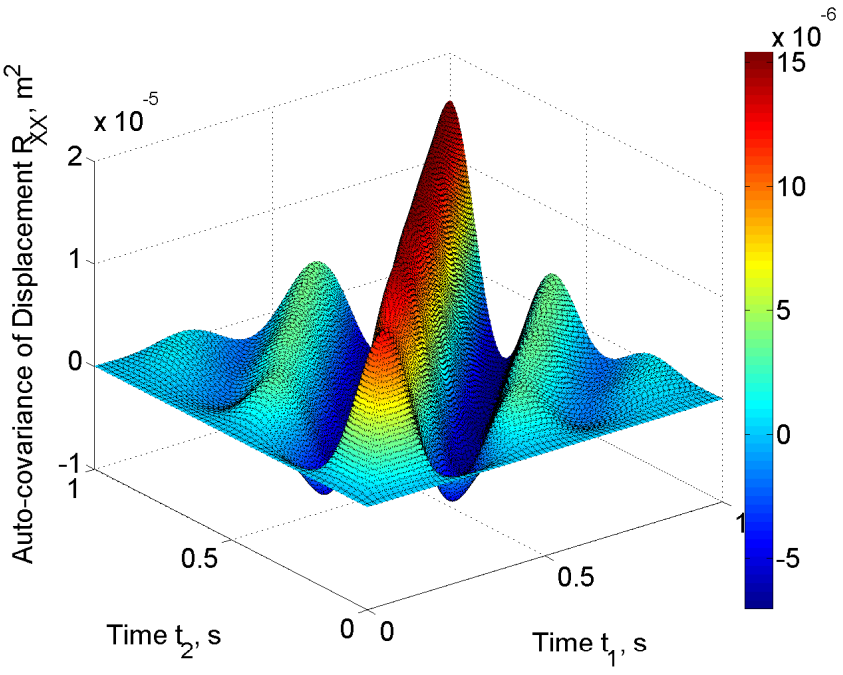

Figure 4.5: Auto-covariance of displacement for exponential covariance using discretized basis functions

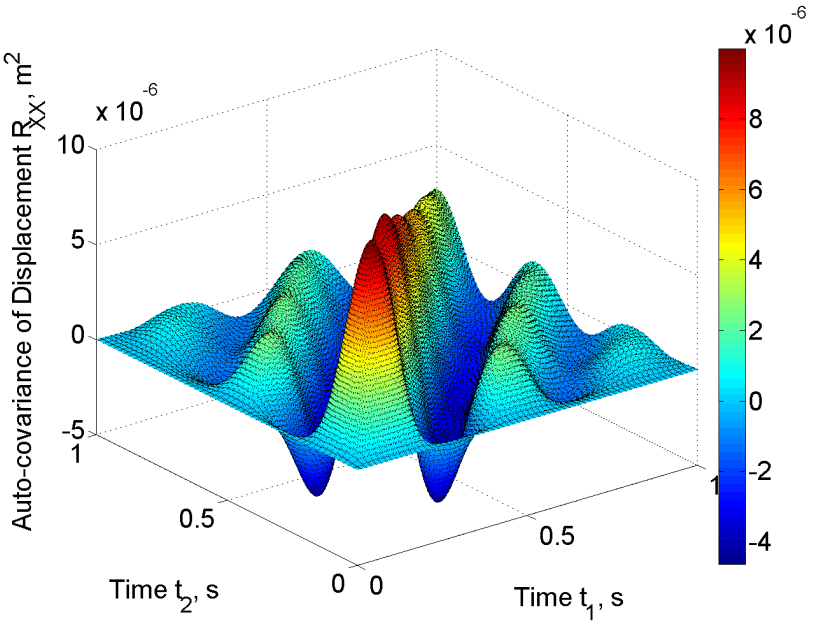

Figure 4.6: Auto-covariance of displacement for modulated exponential covariance using discretized basis functions

dealing with a more complex system such prior knowledge will most likely not exist thus demonstrating the need for a generic treatment of the basis functions as presented here. To fall within 95% of the analytic solution, 30 KL terms are required for the discretized basis functions. While this may seem a large number, the runtime of the algorithm is still significantly less than that required of the method presented previously by the authors [84].

Since KL is a truncated series, an error is introduced which is clearly highly dependent on the number of KL expansion variables used. The error in the calculated covariance functions relative to the analytic expressions presented earlier are shown in Figures 4.7(a) to 4.8(b).

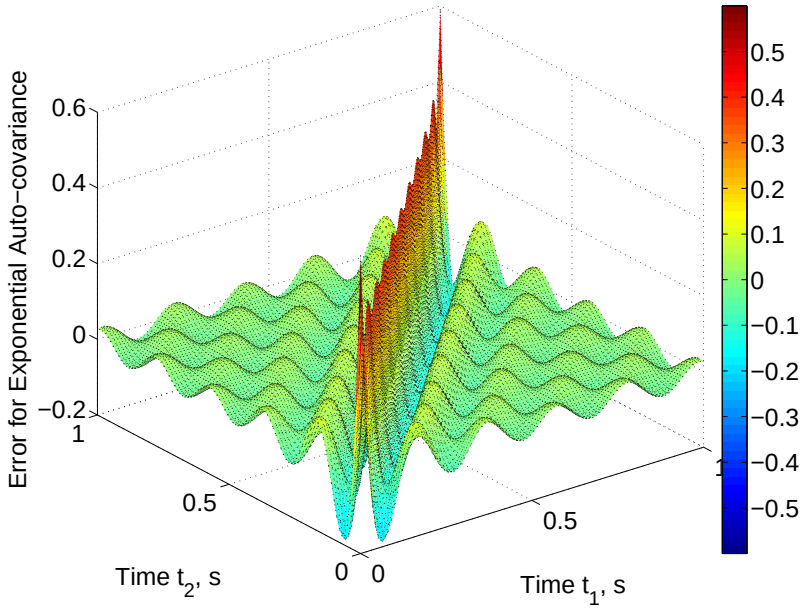

(a) 10 terms

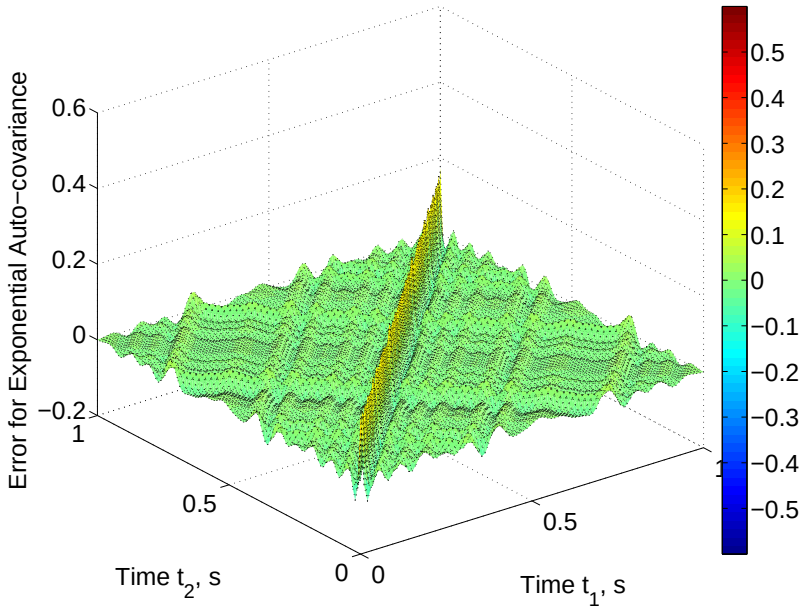

(b) 30 terms

Figure 4.7: Error introduced in calculated exponential auto-covariance using 10 and 30 KL expansion terms

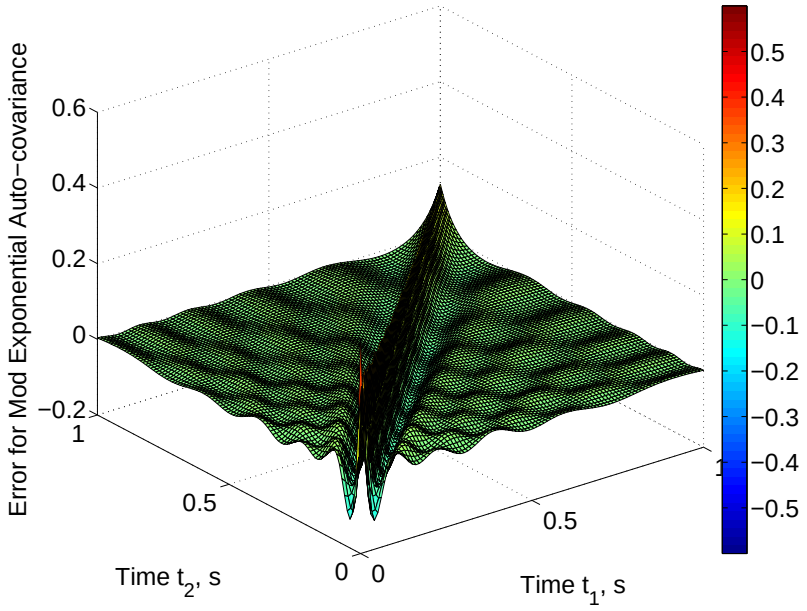

(a) 10 terms

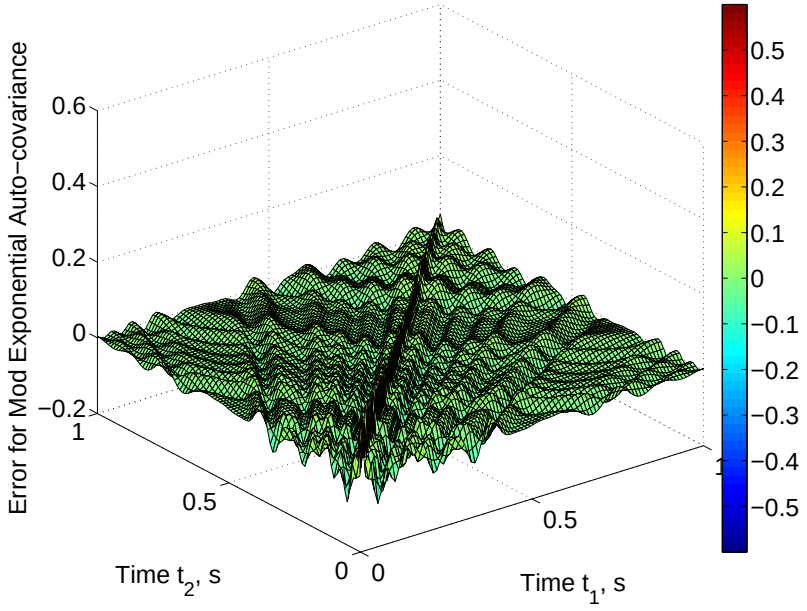

(b) 30 terms

Figure 4.8: Error introduced in calculated modulated exponential auto-covariance using 10 and 30 KL expansion terms

4.4 Application To A MDOF System

4.4.1 Derivation for 2DOF System

To demonstrate how the KL expansion can be used in multi degree of freedom systems, a simple two degree of freedom system is considered.

$$\left[M\right]\begin{Bmatrix}\ddot{x}_1\\ \\ \ddot{x}_2\end{Bmatrix}+\left[C\right]\begin{Bmatrix}\dot{x}_1\\ \\ \dot{x}_2\end{Bmatrix}+\left[K\right]\begin{Bmatrix}x_1\\ \\ x_2\end{Bmatrix}=\begin{Bmatrix}F_1\\ \\ F_2\end{Bmatrix} \tag{4.15}$$

The forces applied at each degree of freedom may be correlated to one another or they may not be correlated to one another. The response due to forcing functions uncorrelated to one another will be developed. In the case of non-stationary excitations, the standard deviation and mean value of the forcing functions vary with time.

For the 2DOF system presented, the forcing functions are assumed to take the same form as that presented in Eq. (4.3). In order to keep track of the contribution to the system by forcing at each DOF, a left superscript is added in the form (i) representing the force applied at the i^{th} DOF. As before the eigenvectors of the individual covariance functions $C_{X_iX_i}$ are ${}^{(i)}\phi$. The system to be solved is a 2DOF system as shown in Eq. (4.15). As before the forcing functions are represented through a KL expansion and in this case are considered to

be zero mean processes.

$$\begin{Bmatrix} f_1(t) \\ f_2(t) \end{Bmatrix} = \begin{Bmatrix} \sum_{i=1}^{n} \sqrt{{}^{(1)}\lambda_i}\,{}^{(1)}\xi_i\,{}^{(1)}\phi_i \\ \sum_{j=1}^{n} \sqrt{{}^{(2)}\lambda_j}\,{}^{(2)}\xi_j\,{}^{(2)}\phi_j \end{Bmatrix} \tag{4.16}$$

The response at each degree of freedom is found through a modal analysis. The goal is to keep the response due to each covariance function separate in order to keep track of their contributions easily. If the matrix ψ represents the mass normalized eigenvectors of the dynamic system, then the EOM becomes:

$$\begin{Bmatrix} \ddot{q}_1 \\ \ddot{q}_2 \end{Bmatrix} + \begin{bmatrix} 2\zeta_1\omega_1 & 0 \\ 0 & 2\zeta_2\omega_2 \end{bmatrix} \begin{Bmatrix} \dot{q}_1 \\ \dot{q}_2 \end{Bmatrix} + \begin{bmatrix} \omega_1^2 & 0 \\ 0 & \omega_2^2 \end{bmatrix} \begin{Bmatrix} q_1 \\ q_2 \end{Bmatrix} = \begin{bmatrix} \psi \end{bmatrix}^T \begin{Bmatrix} \sum_{i=1}^{n} \sqrt{{}^{(1)}\lambda_i}\,{}^{(1)}\xi_i\,{}^{(1)}\phi_i \\ \sum_{j=1}^{n} \sqrt{{}^{(2)}\lambda_j}\,{}^{(2)}\xi_j\,{}^{(2)}\phi_j \end{Bmatrix} \tag{4.17}$$

The system can now be solved as SDOF expressions. For example:

$$\ddot{q}_1 + 2\xi_1\omega_1\dot{q}_1 + \omega_1^2 q_1 = \psi_{11} \sum_{i=1}^{n} \sqrt{{}^{(1)}\lambda_i}\,{}^{(1)}\xi_i\,{}^{(1)}\phi_i + \psi_{21} \sum_{j=1}^{n} \sqrt{{}^{(2)}\lambda_j}\,{}^{(2)}\xi_j\,{}^{(2)}\phi_j \tag{4.18}$$

We want to keep the response due to ${}^{(1)}\phi_i$ and ${}^{(2)}\phi_j$ separate for the purposes of this expansion. To do this, we will evaluate the response with the ${}^{(1)}\phi_i$ with the prescribed initial conditions and designate this q_{k1}, where k represents the DOF being considered. Next the response will be evaluated for ${}^{(2)}\phi_j$ with zero initial conditions and designated q_{k2} where k

is referring to the degree of freedom. Therefore, q_k is simply the sum of the responses q_{k1} and q_{k2}. Looking at the response at the k DOF, the response q_k will be:

$$q_{k1}(t) = \sum_{i=1}^{n} \sqrt{{}^{(1)}\lambda_i}^{(1)} \xi_i{}^{(1)} p_{ik}(t) \tag{4.19}$$

$$q_{k2}(t) = \sum_{j=1}^{n} \sqrt{{}^{(2)}\lambda_j}^{(2)} \xi_j{}^{(2)} p_{jk}(t) \tag{4.20}$$

Bringing the response back into the original coordinate system by $\mathbf{x} = \psi\mathbf{q}$, x_1 is:

$$x_1(t) = \sum_{i=1}^{n} \left[\psi_{11} \left(\sqrt{{}^{(1)}\lambda_i}^{(1)} \xi_i{}^{(1)} p_{i1}(t) + \sqrt{{}^{(2)}\lambda_i}^{(2)} \xi_i{}^{(2)} p_{i1}(t) \right) + \right. \tag{4.21}$$
$$\left. \psi_{12} \left(\sqrt{{}^{(1)}\lambda_i}^{(1)} \xi_i{}^{(1)} p_{i2}(t) + \sqrt{{}^{(2)}\lambda_i}^{(2)} \xi_i{}^{(2)} p_{i2}(t) \right) \right]$$

Grouping the terms together:

$$x_1(t) = \sum_{i=1}^{n} \left[\sqrt{{}^{(1)}\lambda_i}^{(1)} \xi_i \left(\psi_{11}{}^{(1)} p_{i1}(t) + \psi_{12}{}^{(1)} p_{i2}(t) \right) + \right. \tag{4.22}$$
$$\left. \sqrt{{}^{(2)}\lambda_i}^{(2)} \xi_i \left(\psi_{11}{}^{(2)} p_{i1}(t) + \psi_{12}{}^{(2)} p_{i2}(t) \right) \right]$$

$$x_1(t) = \sum_{i=1}^{n} \left[\sqrt{{}^{(1)}\lambda_i}^{(1)} \xi_i{}^{(1)} m_{i1}(t) + \sqrt{{}^{(2)}\lambda_i}^{(2)} \xi_i{}^{(2)} m_{i1}(t) \right] \tag{4.23}$$

The response at x_2 is developed in a similar fashion and becomes:

$$x_2(t) = \sum_{i=1}^{n} \left[\sqrt{{}^{(1)}\lambda_i}\,{}^{(1)}\xi_i\, {}^{(1)}m_{i2}(t) + \sqrt{{}^{(2)}\lambda_i}\,{}^{(2)}\xi_i\, {}^{(2)}m_{i2}(t) \right] \tag{4.24}$$

These expressions are now used to obtain the equations for standard deviation and auto-covariance of the displacement. Considering the first degree of freedom only once again:

$$\begin{aligned} R_{X_1X_1}(t_1,t_2) =& E[x_1(t_1), x_1(t_2)] \\ =& \sum_{i=1}^{n}\sum_{j=1}^{n} E\left[{}^{(1)}\xi_i, {}^{(1)}\xi_j \right] \sqrt{{}^{(1)}\lambda_i}\sqrt{{}^{(1)}\lambda_j}\, {}^{(1)}m_{i1}(t_1)\, {}^{(1)}m_{j1}(t_2) \\ &+ E\left[{}^{(2)}\xi_i, {}^{(2)}\xi_j \right] \sqrt{{}^{(2)}\lambda_i}\sqrt{{}^{(2)}\lambda_j}\, {}^{(2)}m_{i1}(t_1)\, {}^{(2)}m_{j1}(t_2) \\ &+ E\left[{}^{(1)}\xi_i, {}^{(2)}\xi_j \right] \sqrt{{}^{(1)}\lambda_i}\sqrt{{}^{(2)}\lambda_j}\, {}^{(1)}m_{i1}(t_1)\, {}^{(2)}m_{j1}(t_2) \\ &+ E\left[{}^{(2)}\xi_i, {}^{(1)}\xi_j \right] \sqrt{{}^{(2)}\lambda_i}\sqrt{{}^{(1)}\lambda_j}\, {}^{(2)}m_{i1}(t_1)\, {}^{(1)}m_{j1}(t_2) \end{aligned} \tag{4.25}$$

Using the orthogonality property of independent identically distributed variables (i.i.d):

$$\begin{aligned} E\left[{}^{(1)}\xi_i, {}^{(1)}\xi_j \right] &= \delta_{ij} \\ E\left[{}^{(2)}\xi_i, {}^{(2)}\xi_j \right] &= \delta_{ij} \end{aligned} \tag{4.26}$$

For zero correlation of the forcing functions, the cross-correlation of the i.i.d. random vari-

ables must be zero:

$$E\left[{}^{(1)}\xi_i, {}^{(2)}\xi_j\right] = 0 \tag{4.27}$$
$$E\left[{}^{(1)}\xi_i, {}^{(2)}\xi_j\right] = 0$$

Hence, for the uncorrelated random variables the auto-covariance and variance become:

$$R_{X_1X_1}(t_1,t_2) = \sum_{i=1}^{n}\left({}^{(1)}\lambda_i{}^{(1)}m_{i1}(t_1){}^{(1)}m_{i1}(t_2) + {}^{(2)}\lambda_i{}^{(2)}m_{i1}(t_1){}^{(2)}m_{i1}(t_2)\right) \tag{4.28}$$
$$R_{X_2X_2}(t_1,t_2) = \sum_{i=1}^{n}\left({}^{(1)}\lambda_i{}^{(1)}m_{i2}(t_1){}^{(1)}m_{i2}(t_2) + {}^{(2)}\lambda_i{}^{(2)}m_{i2}(t_1){}^{(2)}m_{i2}(t_2)\right)$$

$$\sigma^2_{X_1}(t) = \sum_{i=1}^{n}\left({}^{(1)}\lambda_i{}^{(1)}m_{i1}{}^2(t) + {}^{(2)}\lambda_i{}^{(2)}m_{i1}{}^2(t)\right) \tag{4.29}$$
$$\sigma^2_{X_2}(t) = \sum_{i=1}^{n}\left({}^{(1)}\lambda_i{}^{(1)}m_{i2}{}^2(t) + {}^{(2)}\lambda_i{}^{(2)}m_{i2}{}^2(t)\right)$$

Although no correlation exists between the forcing functions, cross-correlation terms exist for the response and are given by the following expression:

$$R_{X_1X_2}(t_1,t_2) = \sum_{i=1}^{n}\left({}^{(1)}\lambda_i{}^{(1)}m_{i1}(t_1){}^{(1)}m_{i2}(t_2) + {}^{(2)}\lambda_i{}^{(2)}m_{i1}(t_1){}^{(2)}m_{i2}(t_2)\right) \tag{4.30}$$

and

$$\sigma^2_{X_1X_2}(t) = \sum_{i=1}^{n} \left({}^{(1)}\lambda_i{}^{(1)}m_{i1}(t){}^{(1)}m_{i2}(t) + {}^{(2)}\lambda_i{}^{(2)}m_{i1}(t){}^{(2)}m_{i2}(t) \right) \tag{4.31}$$

This derivation is easily extended to larger systems, hence 2DOF and 10DOF examples will be shown in the next subsection, confirming this derivation.

4.4.2 Validation of Derivation

To validate this portion of the derivation, covariance functions are chosen such that an analytic calculation for the auto covariance of the response can be formed. The solution of an MDOF system under random loading is given by [5]:

$$R_{X_iX_j}(t_1, t_2) = \sum_m \sum_k \int_0^{t_1} \int_0^{t_2} h_{ik}(u) h_{jm}(v) C_{F_kF_m}(t_1 - u, t_2 - v) dv du \tag{4.32}$$

Here h_{ik} are the impulse response functions of the dynamic system at the i^{th} degree of freedom.

4.4.2.1 2DOF Case

The first dynamic system studied for the 2DOF case is assumed to be a spring damper system with proportional damping with zero correlation between the forcing functions (hence $C_{F_kF_m} = 0 \, if \, k \neq m$). The masses are assumed to be 1 kg each and spring stiffnesses are 300

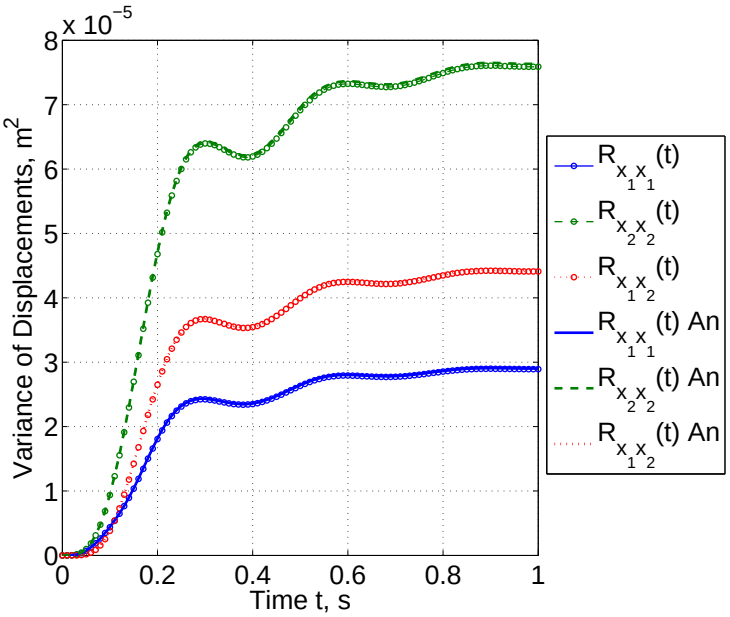

Figure 4.9: Comparison of KL with Analytic (An) results for Exp-Exp Forcing

N/m each. A range of excitation cases exist; the first applies exponential forcing functions with different correlation lengths to each degree of freedom of the form of Eq. (4.13), the second is a mix of exponential and modulated exponential functions (Eqs. (4.13) and (4.14)) and the third are two modulated exponential covariance functions. The variance for each case can be found in Figures 4.9 to 4.11.

Excellent agreement with the analytical solution is found here and on average, 30 KL terms were required to achieve these results. At this point it should be noted these functions were chosen such that the analytical expression Eq. (4.32) could be used to check the computations. In general, solving this double integral equation for large systems with complex covariance functions is very computationally expensive and requires a switch to Monte Carlo simulations which should be avoided for this design tool application. Other combinations

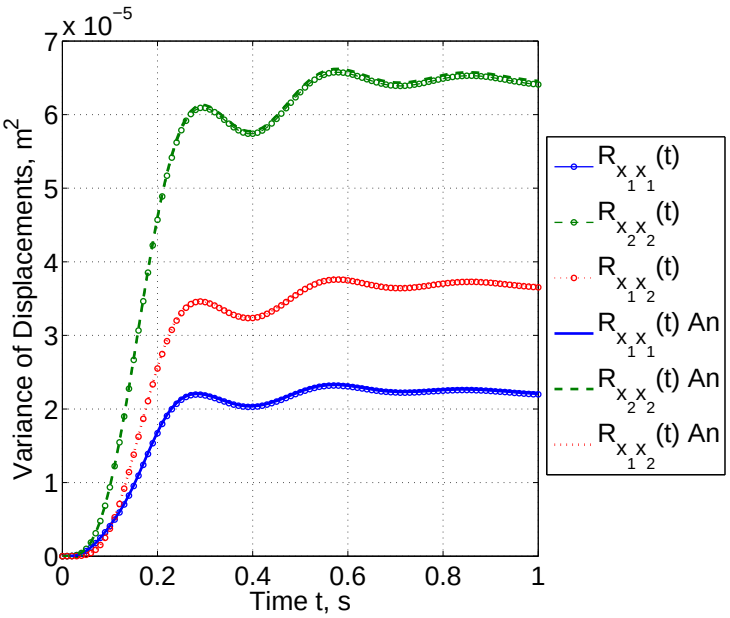

Figure 4.10: Comparison of KL with Analytic (An) results for Mod Exp-Exp Forcing

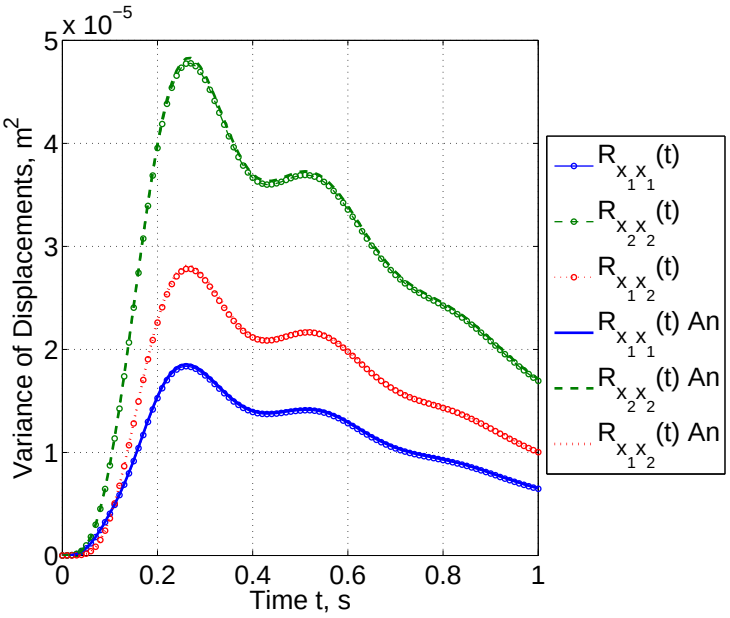

Figure 4.11: Comparison of KL with Analytic (An) results for Mod-Mod Forcing

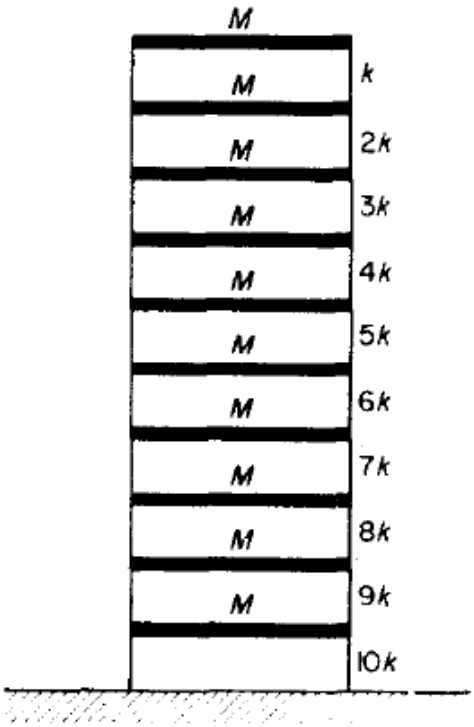

Figure 4.12: Roberts simplified building model [3]

of forcing functions are possible and of most interest are those which form non-symmetric covariance plots.

4.4.2.2 10 DOF Case

For developments in stochastic analysis of MDOF systems, a 10 DOF building vibration example presented by Roberts is often used as a test case [3]. Figure 4.12 shows the simplified building model which is represented by the equations of motion below where M represent each mass , k represents stiffness, i represents DOF 2 to 9 and $Y(t)$ represents base forcing.

$$M\ddot{x_1} + 19kx_1 - 9kx_2 = -Y(t) \tag{4.33}$$

$$M\ddot{x_i} + (21 - 2i)kx_i - (11 - i)kx_{i-1} - (10 - i)kx_{i+1} = -Y(t)$$

$$M\ddot{x_{10}} + kx_{10} - kx_9 = -Y(t)$$

In this case the base excitation is represented by a non-stationary function. This non-stationary function is defined using the well defined modulation method where a stationary function $Z(t)$ is operated on by a modulating function $A(t)$ such as pulses or sine waves. Simply put:

$$Y(t) = A(t)Z(t) \tag{4.34}$$

Following Roberts, A is assumed to be a train of half-sine pulses. $A(t)$ is expressed as:

$$A(t) = \sum_{n=-\infty}^{\infty} c_n e^{inpt} \tag{4.35}$$

where

$$c_n = \frac{2}{\pi r} \frac{\pi n/r}{1 - 4n^2/r^2} \tag{4.36}$$

Function $Z(t)$ is obtained through inverse Fourier transform of its spectrum $S_z(\omega)$:

$$S_z(\omega) = \frac{1}{2\pi} \frac{4}{\omega^2 + 4} \tag{4.37}$$

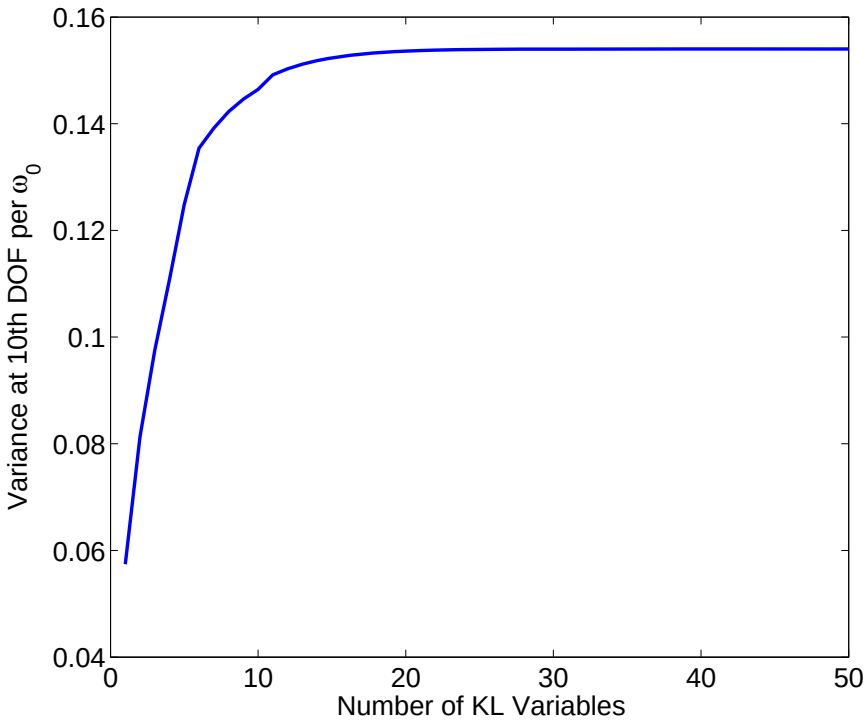

Figure 4.13: Peak variance at 10DOF for varying numbers of KL expansion terms

Using these relationships the auto-covariance function for $Y(t)$ can be constructed as follows:

$$R_{YY}(t_1,t_2) = \frac{4}{\pi^2 r^2} \sum_{n_1=-m}^{m} \sum_{n_2=-m}^{m} \frac{cos(\pi n_1/r)cos(\pi n_2/r)}{(1-4n_1^2/r^2)(1-4n_2^2/r^2)} e^{ip(n_1t_1+n_2t_2)} \tag{4.38}$$

As in Roberts, $r = 2$, $p = 2$, $m = 6$ and modal damping of 0.1 per mode is assumed [3]. Using R_{YY} and (4.32) a solution can be obtained using Mathematica, without using the additional approximations present in Roberts paper. Due to the more complex nature of a 10 DOF system over the previously considered 2 DOF, a convergence study was performed to check the appropriate number of KL expansion terms were being utilized. The convergence plot is shown in Figure 4.13. At this point an error was found in the algorithm causing the summation over the desired KL terms to stop prematurely. Upon fixing this issue, much

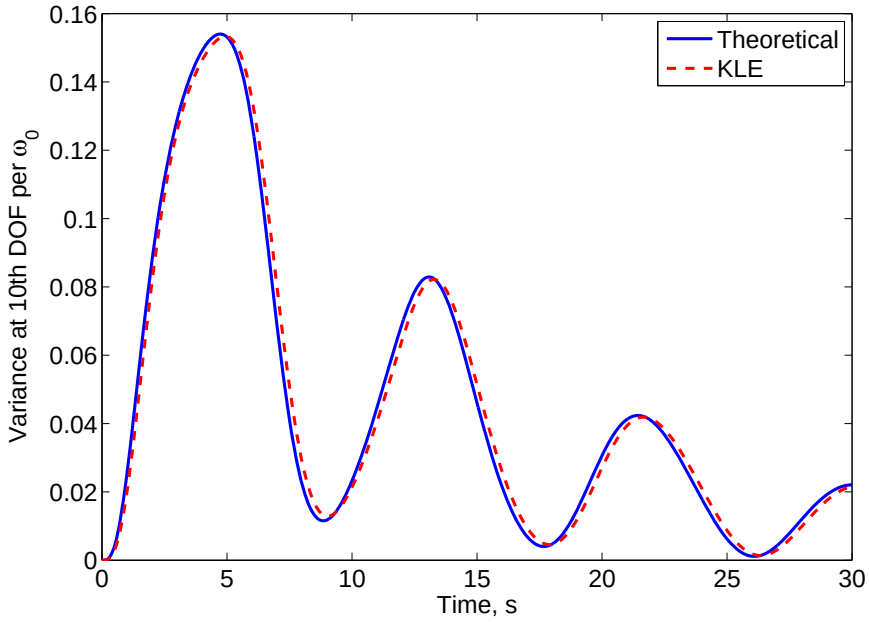

Figure 4.14: Comparison of KL results and theoretical solution for Roberts example [3]

improved results were found for the variance at the 10th DOF. These results and their comparison to theory are shown in Figure 4.14. The results shown here show very good agreement and at a fraction of computational cost compared to the exact solution (less than 1 minute solve time versus several minutes for the analytic solution). The slight difference in the plot curves can be attributed to truncation and the known slight numerical damping existing in the KL expansion method [46].

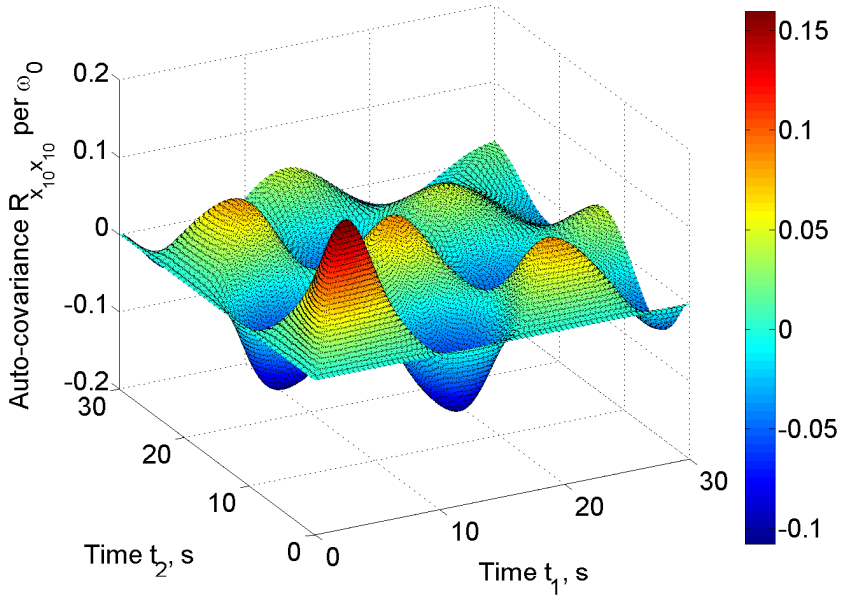

Figure 4.15: Auto-covariance of displacement at 10th floor

4.5 Application To A Continuous System

4.5.1 Derivation for Beam

Following qualification of the method for MDOF systems, a logical progression is application to a continuous system. For this dissertation, the case of a cantilevered beam is chosen, which aids in bringing steering this and future work back into the fluid-structure interaction area discussed earlier in this dissertation. Since the example chosen for validation of the results produced by this method considers a long slender cooling tower, Euler-Bernoulli beam theory is sufficient. As a reminder, the governing equation for an Euler-Bernoulli beam in transverse

vibration is given as:

$$\frac{\partial^2}{\partial x^2}\left(EI\frac{\partial^2 w}{\partial x^2}\right)+\rho_s A\frac{\partial^2 w}{\partial t^2}=0 \tag{4.39}$$

The free vibration response of a constant cross-section beam is well known and can be found in any standard structural dynamics text. The natural frequency of such a beam is given as:

$$\omega_r=\beta_r^2\sqrt{\frac{EI}{m}} \tag{4.40}$$

where βL, for the first four modes, are found to be 1.8751,4.6941,7.8548 and 10.996. A typical representation of the mode shapes is:

$$Y_r(x)=A_r\left[\sin(\beta_r x)-\sinh(\beta_r x)-\frac{\sin(\beta_r L)+\sinh(\beta_r L)}{\cos(\beta_r L)+\cosh(\beta_r L)}(\cos(\beta_r x)-\cosh(\beta_r x))\right] \tag{4.41}$$

These modes are normalized such that:

$$\int_0^L m(x)Y_r(x)^2dx=1 \tag{4.42}$$

The response of a beam to excitation is assumed to take the form:

$$y(x,t)=\sum_r^\infty Y_r(x)\eta_r(t) \tag{4.43}$$

where the modal equation of motion, for a truncated number of mode shapes s, becomes:

$$\ddot{\eta}_s(t) + 2\xi_s\omega_s\dot{\eta}_s + \omega_s^2\eta_s(t) = N_s(t) \tag{4.44}$$

$$N_s(t) = \int_0^L Y_s f(x,t)dx \tag{4.45}$$

To introduce a non-stationary forcing function in the form of a KL expansion, $f(x,t)$ must be formed. Here, the forcing function is formed by the product of two parts, one dependent on position x and the other on time t. Hence for KL expansion:

$$f(x,t) = a(x)\sum_i^n \sqrt{\lambda_i}\xi_i\phi_i \tag{4.46}$$

therefore

$$N_s(t) = \sum_i^n \sqrt{\lambda_i}\xi_i\phi_i \int_0^L Y_s a(x)dx \tag{4.47}$$

It therefore follows that the response is obtained for each mode in a similar manner to the MDOF system in the previous section.

4.5.2 Validation of Derivation

To investigate the validity of the KL representation of the forcing function described in the previous section, a suitable example was sought for comparison. A common real structure used for stochastic studies of continuous systems is that of a chimney [85, 9]. Though some

Table 4.1: Properties of chimney

Property	Value	Unit
Distributed mass	10686	kg/m
Fundamental frequency	0.26	Hz
Modal damping	0.005	
Height	180	m

details of the analysis are missing, the important physical properties of the structure are available and can be found in Table 4.1: The mean forcing in this type of example is usually represented through a log wind profile [85] which is a semi-empirical representation of the wind velocity distribution above the ground, but it is the random component of forcing that is of most interest here. Assuming self-weight is not included and also assuming a log wind profile for the spanwise force distribution, a sudden increase in velocity over the span is applied, representing a gust. A gust can be represented through use of a non-stationary modulated exponential function. This type of function has already been presented in Eq. (4.14). As seen in Figure 4.2, this function reduces in magnitude over a period of time to zero. Upon application of this forcing function to the chimney, variance and auto-covariance of the response at the tip can be computed and then plotted (Figures 4.16 and 4.17 respectively). The variance obtained is compared to that offered through a theoretical solution, solved in Mathematica. For these results, 201 terms were used in the KL expansion and required 1 minute or less to run on a MacBook Pro with 2.4Ghz Intel Core i5 processor and 4GB of 1067Mhz DDR3 RAM. In comparison, the theoretical solution takes 15 minutes or more to run.

Excellent agreement is found between these curves where significant oscillation in the variance

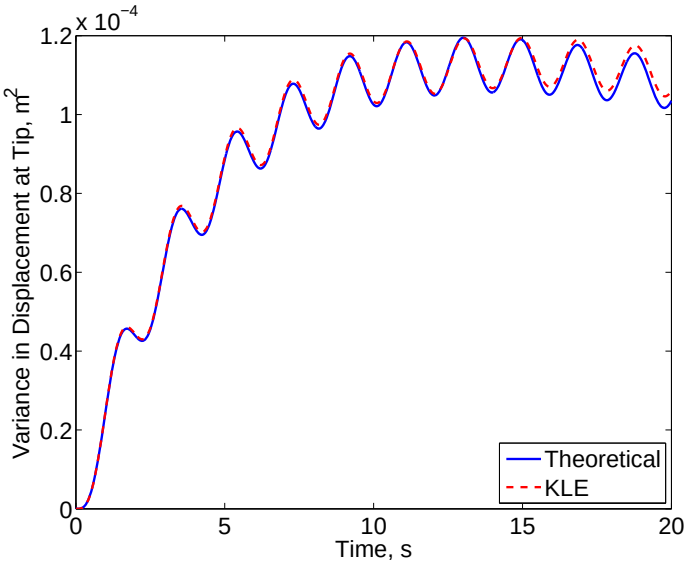

Figure 4.16: Variance of tip displacement for chimney

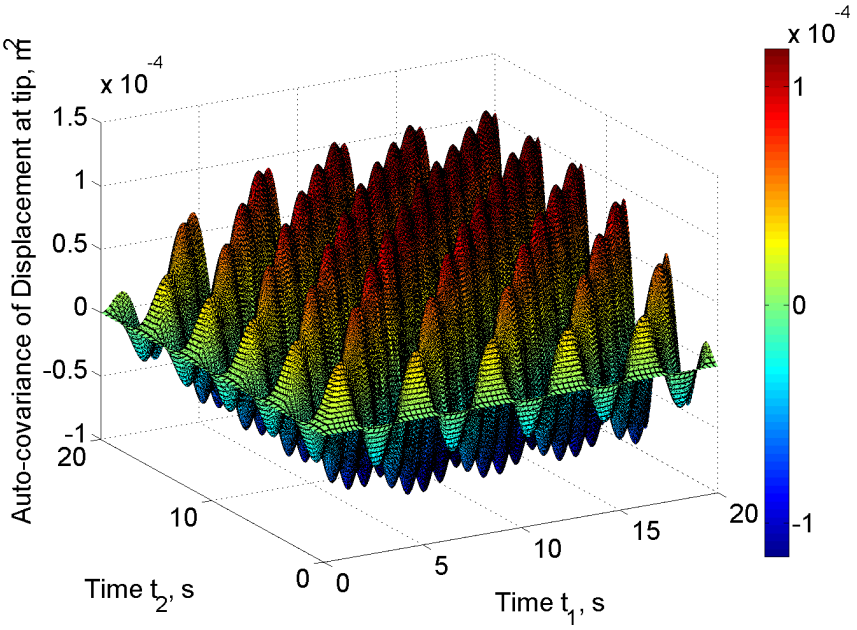

Figure 4.17: Auto-covariance of tip displacement for chimney

is observed. Looking at the auto-covariance plot in Figure 4.17 these oscillations are observed throughout the domain and the peaks reduce little when moving away from the $t_1 = t_2$ diagonal (variance). This is indicative of narrow band frequency response and indicates that the response is dominated by the first one or two modes only. The highly oscillatory nature of the solution did cause some problems when computing the theoretical solution within Mathematica. Inappropriate time steps led to errors in the solution and no response results being produced. Few issues were faced when implementing the KLE method for this example as it shares many common features with the algorithms developed for the MDOF systems, which cut debugging time significantly. However, the highly oscillatory nature of the solution required a great number (201) of KLE variables to converge on a solution, much greater than the 30 KLE terms that have been seen previously.

4.6 Conclusions

An extension of the application of KL expansion from SDOF to MDOF systems has been presented. Previously, knowledge of appropriate global basis functions for a particular covariance excitation function were needed, thus requiring the user to have an *a priori* knowledge of system response. While this is known for small systems, such knowledge is most likely unknown for large MDOF systems. Temporal discretization, allows for generic treatment of almost any covariance function and reduces the complexity of the integrations necessary in the KL expansion method. Results presented for the 2DOF system considered cases were the

forcing functions were not correlated which is a valid assumption as non-stationary forces are typically only correlated for a very short period of time. These results showed excellent agreement with theory. Further demonstration of the method for the well defined 10DOF model given by Roberts, showed very good agreement with theory and proved the method to work on a larger scale. Finally, application of the method to a continuous system also showed good agreement with theory and increases confidence that this method can be applied in many different settings.

The proposed method here is now ready for the analysis of more complex structures (applicable later in the design process) since the mode shapes and natural frequencies of these structures are readily obtained through commercial finite element software. Here the method could be implemented as a wrapper (and hence be non-intrusive), where the commercial FEM solver is called to generate the mode shapes and frequencies and this method generates the non-stationary response functions.

Chapter 5

Conclusions and Future Work

5.1 Conclusions

In order to measure the success of this study, the results presented should be considered in parallel with the objectives of these studies. Work began with the need to investigate current sensor design guides for fluid-structure interaction environments in the context of a real industrial problem. It was thought that a design tool could be produced for the case presented which would aid engineers in the design process. Investigation of the problem showed areas in the fluid-structure interaction guidelines which were lacking and required further modeling. While movement into full fluid-structure interaction numerical methods is attractive for result accuracy, such a step is not appropriate in design so care was taken to ensure the resulting tool was simple to use yet captured the physics of the problem adequately

such that invalid designs could be weeded out early before further detailed investigation. An improved model was developed and tested through simple experimentation. It was seen that the model performed very well for sensors subject to pipe flow. Following testing of the tool's predictive accuracy, designs provided by an industrial partner were investigated. It was found that the designs supplied were mostly inadequate in stiffness for the proposed pipe flow environment and would require redesign. This was noted as a significant success for the tool, saving the industrial partner much time in their design process. The key results from this study were presented at AIAA Conference and later presented in the AIAA Journal. The latter portion of this work, containing non-stationary response of MDOF and continuous systems, will now be submitted to the same journal.

Through investigation of fluid-structure interaction problems, much emphasis on stochastic modeling was found. During investigation, it was discovered that significant and often invalid assumption of stationarity of a process was often used, where non-stationarity would in fact be appropriate. The primary driver for such simplification is the non-availability of simple closed form solutions for non-stationary processes and often complicated and expensive numerical solutions. It was therefore sought to close this gap by development of a tool to analyze structures subject to non-stationary forcing using a method requiring minimal set up by an engineer and minimal computational cost. A method utilizing the Karhunen-Loeve expansion was developed including improvements to permit utilization of the method without *a priori* knowledge of the system response. The numeric method produced was developed from SDOF through MDOF and finally extended to continuous systems. Results

produced by the method compared favorably to exact theoretical results and took minimal computation time (seconds versus minutes) on the same CPU/memory combination. While exact solutions exist for the cases tested and can be solved analytically, it is not feasible to use this method for more complex systems to calculate their response. Utilization of the method as developed in this work is therefore appropriate in cases where large systems need to be studied. The key results from this study were presented in two papers at AIAA conference and one has since been published in the AIAA Journal.

5.2 Future Work

While significant results were found during this work, there is always room for improvement in the models developed. Ideally, the work presented herein would come full circle allowing the stochastic model developments to feed back into the fluid-structure interaction tools. In reality, there are several areas in the Karhunen Loeve models which must be explored first. One such area is inclusion of spatial-temporal coupling of the non-stationary forcing functions in continuous systems for the Karhunen Loeve method developed. Such an improvement will allow for existing coupled turbulence models to be applied through the KL expansion to a variety of structures, fully utilizing the efficiency of this method. This introduces a significant complication of correlation between forcing location and time. Cross-correlation within the KL expansion is a difficult and tricky step to take and one which requires much investigation. Once developed, such an improvement to the proposed method in this dissertation could

allow for non-stationary response analysis of structures in the "Future Aircraft" programs at Virginia Tech, such as the Truss-Based Wing and SensorCraft.

Systems such as the 2 DOF model presented experience different forces at each DOF. However, in this work these forces were uncorrelated with respect to one another. A substantial amount of time was spent exploring partial-correlation between these forcing functions and how to represent this relationship through the KL expansion method developed. The most simple representation of partial-correlation is made through presentation in the correlation matrix (seen in [45]). Often, the system is uncorrelated through principal orthogonal decomposition and the response reassembled in a similar manner to modal analysis of a structure. However, implementation of this idea in KLE form proved to be unsuccessful due to the i.i.d. variables and the value they should take on computing their "expectation" (previously 0 when indices i and j are not equal, see Eq. (4.27)). Of the studies exploring partial-correlation, the most useful of which was that by Vorechovsky [86] who developed a method to allow an engineer to start with two uncorrelated processes (in expansion form like the KLE) and define the correlation between them. It was thought that this would solve the problem of the expectation between the two i.i.d. random variables. Unfortunately, a satisfactory solution was not obtained in this case when applying the method to the KLE formulation described herein. This is obviously an important problem which warrants further study.

Bibliography

[1] Farell, C., "Closure to: Flow around fixed circular cylinders: Fluctuating loads," *Journal of Engineering Mechanics*, Vol. 109, 1981, pp. 1153.

[2] Shin, Y. and Wambsganss, M., "Flow-induced vibration in LMFBR steam generators: A state-of-the-art review," *Nuclear Engineering and Design*, Vol. 40, No. 2, 1977, pp. 235 – 284.

[3] Roberts, J. B., "The covariance response of linear systems to non-stationary random excitation," *Journal of Sound and Vibration*, Vol. 14, No. 3, 1971, pp. 385–400.

[4] Newland, D. E., *An introduction to random vibrations, spectral & wavelet analysis*, Dover Publications Inc., 2005.

[5] Wirsching, P. H., Paez, T. L., and Ortiz, K., *Random vibrations: Theory and practice*, Dover Publications Inc., 1995.

[6] Benaroya, H. and Han, S. M., *Probability models in engineering and science*, CRC Press, Taylor & Francis Group, 2005.

BIBLIOGRAPHY

[7] Paez, T. L., "Random vibrations: Assesment of the state of the art," Tech. rep., Experimental Structural Dynamics Department, Sandia National Laboratories, Albuquerque, New Mexico, 1999.

[8] Lin, Y. K., *Probabilistic theory of structural dynamics*, Robert E. Krieger Publishing Company, 1976.

[9] Muller, F. and Nieser, H., "Measurements of wind-induced vibrations on a concrete chimney," *Journal of Industrial Aerodynamics*, Vol. 1, 1976, pp. 239–48.

[10] Kawamura, T., Nakao, T., Hayashi, M., and Gotoh, N., "Experimental studies on vibrations of a circular cylinder in cross flow at supercritical Reynolds numbers," *American Society of Mechanical Engineers, Pressure Vessels and Piping Division (Publication) PVP*, Vol. 363, 1998, pp. 35 – 44.

[11] Blevins, R. D., *Flow-induced vibration*, R. E. Krieger, 1986.

[12] Delany, N. and Sorensen, N., "Low-speed drag of cylinders of various shapes," *National Advisory Committee for Aeronautics – Technical Notes*, 1953.

[13] Roshko, A., "On the drag and shedding frequency of two dimensional bluff bodies," Tech. Rep. TN 31169, NACA, 1954.

[14] Fung, Y. C., "Fluctuating lift and drag acting on a cylinder in a flow at supercritical Reynolds numbers," *Journal of the Applied Sciences*, Vol. 27, No. 11, 1960, pp. 801–814.

[15] Weaver, D. S., Ziada, S., Au-Yang, M. K., Chen, S. S., Paidoussis, M. P., and Pettigrew, M. J., "Flow-induced vibrations in power and process plant components: Progress and prospects," *Journal of Pressure Vessel Technology*, Vol. 122, No. 3, 2000, pp. 339–348.

[16] Bearman, P. W., "Vortex shedding from oscillating bluff bodies," *Annual Review of Fluid Mechanics of Materials*, Vol. 16, 1984, pp. 195–222.

[17] Gerrard, J. H., "The mechanics of the formation region of vortices behind bluff bodies," *Journal of Fluid Mechanics*, Vol. 25, 1966, pp. 401–413.

[18] Sarpkaya, T., "An inviscid model of two dimensional vortex shedding for transient and asymptotically steady separated flow over an inclined plate," *Journal of Fluid Mechanics*, Vol. 68, 1975, pp. 109–128.

[19] Sarpkaya, T., "Fluid forces on oscillating cylinders," *Journal of the Waterway Port, Coastal and Ocean Division*, Vol. 104, 1978, pp. 275–290.

[20] Sarpkaya, T., "Vortex-induced oscillations," *Journal of Applied Mechanics*, Vol. 46, 1979, pp. 241–258.

[21] Sarpkaya, T. and Schoaff, R. L., "Inviscid model of two dimensional vortex shedding by a circular cylinder," *AIAA Journal*, Vol. 17, 1979, pp. 1193–1200.

[22] Sarpkaya, T. and Schoaff, R. L., "A discrete vortex analysis of flow about stationary and transversely oscillating circular cylinders," Tech. Rep. NPS-69SL7901, Naval Postgraduate School, Monterey, CA, 1979.

[23] Gabbai, R. and Benaroya, H., "An overview of modeling and experiments of vortex-induced vibration of circular cylinders," *Journal of Sound and Vibration*, Vol. 282, No. 3-5, 2005, pp. 575 – 616.

[24] Wooton, L. R., Warner, M. H., Sainsbury, R. N., and Cooper, D. H., "Oscillations of piles in marine structures: A resume of the full-scale experiments at Immingham," Tech. Rep. Tech. Rep. 41, CIRIA, 1972.

[25] King, R., "Vortex-excited oscillations of a circular cylinder in steady currents," *Offshore Technical Conference*, OTC, 1974.

[26] Zdravkovich, M. M., "Modification of vortex shedding in the synchronization range," *Journal of Fluids Engineering*, Vol. 104, 1982, pp. 513–517.

[27] Bishop, R. E. D. and Hassan, A. Y., "The lift and drag forces on a circular cylinder in a flowing fluid," *Proceedings of the Royal Society*, Vol. Series A277, 1963, pp. 32–50.

[28] Iwan, W. D. and Blevins, R. D., "A model for vortex induced oscillation of structures," *Journal of Applied Mechanics*, Vol. 41, No. 3, 1974, pp. 581–586.

[29] Iwan, W. D., "The vortex induced oscillation of elastic structures," *Journal of Engineering for Industry*, Vol. 97, 1975, pp. 1378–1382.

[30] Keefe, R. T., "An investigation of the fluctuating forces acting on a stationary circular cylinder in a subsonic stream and of the associated sound field," Report no. 76, 112, University of Toronto, 1961.

[31] Various, "Section III Division I," *ASME Boiler and Pressure Vessel Code*, Vol. 1, Oct. 1998, pp. 219–240.

[32] Corcos, G. M., "Resolution of pressure in turbulence," *The Journal of the Acoustical Society of America*, Vol. 35, No. 2, 1963, pp. 192–199.

[33] Corcos, G. M., "The resolution of turbulent pressures at the wall of a boundary layer," *Journal of Sound and Vibration*, Vol. 6, No. 1, July 1967, pp. 59–70.

[34] Au-Yang, M. and Jordan, K., "Dynamic pressure inside a PWR – A study based on laboratory and field test data," *Nuclear Engineering and Design*, Vol. 58, No. 1, 1980, pp. 113 – 125.

[35] Powell, A., "On the fatigue failure of structures due to vibrations excited by random pressure fields," *The Journal of the Acoustical Society of America*, Vol. 30, No. 12, 1958, pp. 1130–1135.

[36] Au-Yang, M. K., "Response of reactor internals to fluctuating pressure forces," *Nuclear Engineering and Design*, Vol. 35, No. 3, 1975, pp. 361 – 375.

[37] Chen, S. S. and Wambsganss, M. W., "Response of a flexible rod to near field flow noise," Tech. Rep. Report ANL-7685, Argonne National Laboratory, 1970.

[38] Pettigrew, M. J. and Gorman, D. J., "Vibration of heat exchanger tube bundles in liquid and two-phas cross-flow," *Flow-Induced Vibration Design Guidelines*, June 1981, pp. 89–110.

[39] Axisa, F., Antunes, J., and Villard, B., "Random excitation of heat exchanger tubes by cross-flows," *Journal of Fluids and Structures*, Vol. 4, No. 3, 1990, pp. 321 – 341.

[40] Au-Yang, M. K., "Joint and cross acceptances for cross-flow-induced vibration—Part I: Theoretical and finite element formulations," *Journal of Pressure Vessel Technology*, Vol. 122, No. 3, 2000, pp. 349–354.

[41] Okajima, A., Kosugi, T., and Nakamura, A., "Experiments on flow-induced in-line oscillation of a circular cylinder in a water tunnel. (1st-report, the difference of the response characteristics when a cylinder is elastically supported at both ends and cantilevered)," *JSME International Journal, Series B (Fluids and Thermal Engineering)*, Vol. 44, No. 4, 2001, pp. 695 – 704.

[42] Nakamura, A., Okajima, A., and Kosugi, T., "Experiments on flow-induced in-line oscillation of a circular cylinder in a water tunnel. (2nd report, influence of the aspect ratio of a cantilevered circular cylinder)," *JSME International Journal, Series B (Fluids and Thermal Engineering)*, Vol. 44, No. 4, 2001, pp. 705 – 11.

[43] Sakai, T., Iwata, K., Morishita, M., and Kitamura, S., "Vortex-induced vibration of a cantilever circular cylinder in super-critical Reynolds number flow and its suppression by structure damping," *JSME International Journal, Series B: Fluids and Thermal Engineering*, Vol. 44, No. 4, 2001, pp. 712 – 720.

[44] Iwata, K., Morishita, M., Sakai, T., Yamaguchi, A., and Ogura, K., "Evaluation of turbulence-induced vibration of a circular cylinder in supercritical Reynolds number

flow," *JSME International Journal, Series B: Fluids and Thermal Engineering*, Vol. 44, No. 4, 2001, pp. 721 – 728.

[45] Haldar, A. and Mahadevan, S., *Probability, reliability and statistical methods in engineering design*, Wiley, 2000.

[46] Ghanem, R. G. and Spanos, P. D., *Stochastic finite elements: A spectral approach*, Dover Publications Inc., revised ed., 1991.

[47] Hammond, J. K., "On the response of single and multidegree of freedom systems to non-stationary random excitations," *Journal of Sound and Vibration*, Vol. 7, No. 3, 1968, pp. 393–416.

[48] Stefanou, G., "The stochastic finite element method: Past, present and future," *Computer Methods in Applied Mechanics and Engineering*, Vol. 198, No. 9-12, 2009, pp. 1031 – 1051.

[49] Spanos, P. D. and Zeldin, B. A., "Monte Carlo treatment of random fields: A broad perspective," *Applied Mehanics Reviews*, Vol. 51, No. 3, 1998, pp. 219.

[50] Brenner, C. E. and Bucher, C., "A contribution to the SFE-based reliability assessment of nonlinear structures under dynamic loading," *Probabilistic Engineering Mechanics*, Vol. 10, No. 4, 1995, pp. 265 – 273.

[51] Charmpis, D. C. and Papadrakakis, M., "Improving the computational efficiency in finite element analysis of shells with uncertain properties," *Computer Methods in Applied*

Mechanics and Engineering, Vol. 194, No. 12-16, 2005, pp. 1447 – 1478, Special Issue on Computational Methods in Stochastic Mechanics and Reliability Analysis.

[52] Graham, L. L., Gurley, K., and Masters, F., "Non-Gaussian simulation of local material properties based on a moving-window technique," *Probabilistic Engineering Mechanics*, Vol. 18, No. 3, 2003, pp. 223 – 234.

[53] Graham, L. L. and Deodatis, G., "Response and eigenvalue analysis of stochastic finite element systems with multiple correlated material and geometric properties," *Probabilistic Engineering Mechanics*, Vol. 16, No. 1, 2001, pp. 11 – 29.

[54] Huyse, L. and Maes, M. A., "Random field modeling of elastic properties using homogenization," *Journal of Engineering Mechanics*, Vol. 127, No. 1, 2001, pp. 27–36.

[55] Cai, G. Q. and Lin, Y. K., "Generation of non-Gaussian stationary stochastic processes," *Physical Review E*, Vol. 54, 1996, pp. 299–303.

[56] Deheuvels, P. and Martynov, G. V., "A Karhunen-Loeve decomposition of a Gaussian process generated by independent pairs of exponential random variables," *Journal of Functional Analysis*, Vol. 255, No. 9, 2008, pp. 2363 – 2394, Special issue dedicated to Paul Malliavin.

[57] Grigoriu, M., "Spectral representation for a class of non-Gaussian processes," *Journal of Engineering Mechanics*, Vol. 130, No. 5, 2004, pp. 541–546.

[58] Pradlwarter, H. J., Schuëller, G. I., and Schenk, C. A., "A computational procedure to estimate the stochastic dynamic response of large non-linear FE-models," *Computer Methods in Applied Mechanics and Engineering*, Vol. 192, No. 7-8, 2003, pp. 777 – 801.

[59] Priestley, M. B., "Evolutionary spectra and non-stationary processes," *Journal of the Royal Statistical Society, Series B*, Vol. 27, 1965, pp. 204–237.

[60] Priestley, M. B., "Power spectral analysis of non-stationary random processes," *Journal of Sound and VIbration*, Vol. 6, No. 1, 1967.

[61] Rouillard, V. and Sek, M. A., "Simulation of non-stationary vehicle vibrations," *Journal of Automobile Engineering*, Vol. 215, 2001, pp. 1069–1075.

[62] Shihab, S. and Preumont, A., "Non-stationary random vibrations of linear multi-degree-of-freedom systems," *Journal of Sound and Vibration*, Vol. 132, No. 2, 1989, pp. 457–471.

[63] DiPaola, M., "Moments of non-linear systems: Probabilistic methods in civil engineering," *Proceedings of Fifth ASCE Special Conference*, 1988.

[64] Ibrahim, Y., "Covariance function of non-stationary response of linear systems," *Journal of Sound and Vibration*, Vol. 149, No. 3, 1991, pp. 504–508.

[65] Gasparini, D. A., "Response of MDOF systems to non-stationary random excitation," *Journal of the Engineering Mechanics Division*, Vol. 105, No. 1, 1979, pp. 13–27.

[66] Schuëller, G. I., Pradlwarter, H. J., and Schenk, C. A., "Non-stationary response of large linear FE models under stochastic loading," *Computers & Structures*, Vol. 81, No. 8-11, 2003, pp. 937 – 947, K.J Bathe 60th Anniversary Issue.

[67] Masri, S. F., Smyth, A. W., and Traina, M.-I., "Probabilistic representation and transmission of non-stationary processes in multi-degree-of-freedom systems," *Journal of Applied Mechanics*, Vol. 65, 1998, pp. 398–410.

[68] Schevenels, M., Lombaert, G., and Degrande, G., "Application of the stochastic finite element method for Gaussian and non-Gaussian systems," *Proceedings of ISMA Conference*, 2004, pp. 3299–3313.

[69] Phoon, K., Huang, S., and Quek, S., "Implementation of Karhunen-Loeve expansion for simulation using a wavelet-Galerkin scheme," *Probabilistic Engineering Mechanics*, Vol. 17, No. 3, 2002, pp. 293 – 303.

[70] Phoon, K. K., Huang, H. W., and Quek, S. T., "Simulation of strongly non-Guassian processes using Karhunen-Loeve expansion," *Probabilistic Engineering Mechanics*, Vol. 20, 2005, pp. 188–198.

[71] Bland, S. M., "Progress on cryogenic temperature sensor SBIR," 2005.

[72] Han, S. M., Benaroya, H., and Wei, T., "Dynamics of transversely vibrating beams using four engineering theories," *Journal of Sound and Vibration*, Vol. 225, No. 5, 1999, pp. 935 – 988.

BIBLIOGRAPHY

[73] Craig, R., R. and Kurdila, A., J., *Fundamentals of structural dynamics*, John Wiley, second edition ed., 2006.

[74] Meirovitch, L., *Fundamentals of vibrations*, McGraw-Hill, international ed., 2001.

[75] Bercin, A. N. and Tanaka, M., "Coupled flexural-torsional vibrations of Timoshenko beams," *Journal of Sound and Vibration*, Vol. 207, No. 1, 1997, pp. 47 – 59.

[76] Dozaki, K., Morishita, M., and Iwata, K., "Modification and design guide of thermowell for FBR," *American Society of Mechanical Engineers, Pressure Vessels and Piping Division (Publication) PVP*, Vol. 363, 1998, pp. 125 – 133.

[77] Au-Yang, M. K., "Joint and cross acceptances for cross-flow-induced vibration—Part II: Charts and applications," *Journal of Pressure Vessel Technology*, Vol. 122, No. 3, 2000, pp. 355–361.

[78] Fox, R. W., McDonald, A. T., and Pritchard, Philip, J., *Introduction to fluid mechanics*, Wiley, 6th ed., 2003.

[79] Kawamura, T., Nakao, T., Hayashi, M., and Murayama, K., "Strouhal number effect on synchronized vibration range of a circular cylinder in cross flow," *JSME International Journal, Series B (Fluids and Thermal Engineering)*, Vol. 44, No. 4, 2001, pp. 729 – 37.

[80] Li, Z., Davidson, J., and Mantell, S., "Numerical simulation of flow field and heat transfer of streamlined cylinders in cross flow," *Transactions of the ASME. Journal of Heat Transfer*, Vol. 128, No. 6, 2006, pp. 564 – 70.

[81] Modi, V. J. and Wiland, E., "Unsteady aerodynamics of stationary elliptic cylinders in subcritical flow," *AIAA Journal*, Vol. 8, No. 10, 1970, pp. 1814 – 1821.

[82] Kim, M.-S., "Unsteady viscous flow over elliptic cylinders at various thickness with different Reynolds numbers," *17th AIAA Computational Fluid Dynamics Conference*, June 6-9 2005.

[83] Poulimenos, A. G. and Fassois, S. D., "Parametric time-domain methods for non-stationary random vibration modelling and analysis A critical survey and comparison," *Journal of Mechanical Systems and Signal Processing*, Vol. 20, 2006, pp. 763–816.

[84] Mulani, S. B., Kapania, R. K., and Scott, K. M. L., "Generalized linear random vibration analysis using auto-covariance orthogonal decomposition," *AIAA Journal*, Vol. 48, No. 8, 2010, pp. 1652–1661.

[85] Torrielli, A., Tubinco, F., and Solari, G., "Effective wind actions on ideal and real structures," *Journal of Wind Engineering and Industrial Aerodynamics*, Vol. 98, 2010, pp. 417–428.

[86] Vorechovsk, M., "Simulation of simply cross correlated random fields by series expansion methods," *Structural Safety*, Vol. 30, No. 4, 2008, pp. 337 – 363.

Appendix: Exerpts from "Generalized Linear Random Vibration Analysis Using Auto-Covariance Orthogonal Decomposition"

The following includes exerpts from Mulani, Kapania and Scott [84], showing the development of an analytic solution to the KL expansion problem. As before, the KL expansion is defined as in Eq. (4.3) and the eigenvalues and eigenvectors obtained through solving solved through use of the Fredholm equation, Eq. (4.5).

Again, the eigenfunctions of the auto-covariance are represented as :

$$\phi_k(t) = \sum_{j=1}^{m} d_{jk} h_j(t) \tag{A.1}$$

where d_{jk} are constants and h_j are user-defined basis functions.

Therefore for such a time domain, the components of h_j should be chosen such that they form a complete basis of the system, but it is not a necessary condition. The d_{jk} can be viewed as the h_j basis function participation factors of the eigenfunction, ϕ_k of the excitation auto-covariance. For the steady state response of the dynamic system, h are chosen such that they represent complete cosine and sine functions over the selected time domain and are given as :

$$h = \left\{1, \cos\frac{\pi}{L}t, \sin\frac{\pi}{L}t, \ldots, \cos\frac{\pi\,(n-1)}{L}t, \sin\frac{\pi\,(n-1)}{L}t\right\} \tag{A.2}$$

Here h_j are represented in each position of the complete vector h. For the transient analysis of the dynamic systems, each h_j is chosen such that the basis function vector h includes multiples of both half cosine and half sine functions to represent the response components corresponding to basis functions with lower frequencies as the system response starts with a frequency of zero. It is important to choose such functions to represent transient response with refined basis functions as compared to basis functions given in Eq. (A.2) and therefore the vector of basis functions h is given as :

$$h = \left\{1, \cos\frac{\pi}{2L}t, \sin\frac{\pi}{2L}t, \ldots, \cos\frac{\pi\,(n-1)}{2L}t, \sin\frac{\pi\,(n-1)}{2L}t\right\} \tag{A.3}$$

Using the definition of the KL expansion of the forcing function as given earlier, a SDOF

system is written as :

$$m\,\ddot{x} + c\,\dot{x} + k\,x = \mu_F\,(t) + \sum_{i=1}^{n} \xi_i \sqrt{\lambda_i} \left(\sum_{j=1}^{n} d_{ji} h_j\,(t) \right) \tag{A.4}$$

For convenience during the derivation, it is assumed that the mean value of the forcing function, $\mu_F(t)$ is zero, the initial displacement and the velocity are deterministic, and assumed to be zero. Even if the initial displacement and the velocity are non-zero, they can be associated with the mean component of the forcing function; if the mean component of the forcing function is zero, then they can be associated with the major component of the KL expansion. If the mean value of the forcing function, $\mu_F(t)$ is a non-zero function of time, then the mean of the non-stationary response will be non-zero and $\mu_F(t)$ will not affect the calculation of the standard deviation of the response. The displacement response of the SDOF is given as :

$$x\,(t) = \sum_{i=1}^{n} \xi_i \sqrt{\lambda_i} \left(\sum_{j=1}^{n} d_{ji} m_j\,(t) \right) \tag{A.5}$$

The response functions, m_j, corresponding to the basis functions, h_j of the excitation are obtained. Ω_i for the steady-state and the transient analysis are defined by Eq. (A.6) and Eq. (A.7), respectively.

$$\Omega = \left\{ 0, \frac{\pi}{L}, \frac{\pi}{L}, \ldots, \frac{(n-1)\,\pi}{L}, \frac{(n-1)\,\pi}{L} \right\} \tag{A.6}$$

$$\Omega = \left\{ 0, \frac{\pi}{2L}, \frac{\pi}{2L}, \ldots, \frac{(n-1)\,\pi}{2L}, \frac{(n-1)\,\pi}{2L} \right\} \tag{A.7}$$

By comparing Eqs. (A.4) and (A.5), it is seen that for complex, multi-degree-of-freedom structures, the statistics of the response when excited by the stochastic forcing function can be easily obtained. The user can choose the basis functions, h_j given by either Eq. (A.2) or Eq. (A.3). Then, the user has to obtain the eigenvalues, λ_i and d_{ji}, the h_j basis function participation factors of the eigenfunctions, ϕ_i of the excitation auto-covariance, outside of commercial FEM softwares. The response functions, m_j, corresponding to the basis functions, h_j of the excitation should be obtained to construct the PDF or statistics of the response of the system.

Using the orthogonality of iid basis random variables, ξ, which is given as :

$$< \xi_i, \xi_j >= \quad \delta_{ij} \tag{A.8}$$

where $\langle\ \rangle$ is the mathematical expectation operator, the covariance, ${\sigma^2}_x\,(t)$ and auto-covariance, $R_{XX}\,(t_1, t_2)$ of the response are given as [46] :

$${\sigma^2}_x\,(t) = \sum_{i=1}^{n} \lambda_i \left(\sum_{j=1}^{n} d_{ji} m_j\,(t) \right)^2 \tag{A.9}$$

$$R_{XX}\,(t_1, t_2) = < x\,(t_1)\,, x\,(t_2) > \tag{A.10}$$

$$= \sum_{i=1}^{n} \lambda_i \left(\sum_{j=1}^{n} d_{ji} m_j\,(t_1) \right) \left(\sum_{k=1}^{n} d_{ki} m_k\,(t_2) \right) \tag{A.11}$$

From Eq. (A.9), it can be seen that the standard deviation of the response depends upon the eigenvalues of the forcing auto-covariance function, participation factors of the chosen basis

functions and the deterministic system response of the basis functions. Equation (A.11) indicates that the auto-covariance of the response depends upon the deterministic responses at two different times of the chosen basis functions. The exponential auto-covariance described by Eq. (4.13) is a particular type of the auto-covariance whose eigenfunctions and eigenvalues can be obtained using analytical methods. The obtained eigenfunctions of this auto-covariance are defined by analytical functions which would be accurate as compared to the obtained by the weighted residual method while solving the Fredholm Eq. (4.5) of the 2^{nd} kind. By differentiating Eq. (4.5) twice with respect to time and applying appropriate boundary conditions at $t = t_{min}$ and $t = t_{max}$, transcendental Eq. (A.12) and Eq. (A.15) are obtained. Solutions of Eq. (A.12) along with Eqs. (A.13, A.14) define symmetric eigenvalues and eigenfunctions. In the same way, solutions of Eq. (A.15) along with Eqs. (A.16, A.17) define anti-symmetric eigenvalues and eigenfunctions. Additional information on analytical method used to obtain eigenfunctions and eigenvalues is given [46].

For symmetric eigenfunctions of an exponential auto-covariance :

$$C - \kappa \tan(\kappa a) = 0 \tag{A.12}$$

$$\phi_i(t) = \frac{\cos(\kappa_i t)}{\sqrt{a + \frac{\sin(2\kappa_i a)}{2\kappa_i}}} \tag{A.13}$$

$$\lambda_i = \frac{2C}{\kappa_i^2 + C^2} \tag{A.14}$$

For anti-symmetric eigenfunctions of an exponential auto-covariance :

$$\kappa^* + C\tan\left(\kappa^* a\right) = 0 \tag{A.15}$$

$$\phi_i^*\left(t\right) = \frac{\sin\left(\kappa_i^* t\right)}{\sqrt{a - \frac{\sin\left(2\kappa_i^* a\right)}{2\kappa_i^*}}} \tag{A.16}$$

$$\lambda_i^* = \frac{2C}{\kappa_i^{*^2} + C^2} \tag{A.17}$$

where C is the correlation length parameter of the forcing auto-covariance, a is equal to the half of the time domain considered in the KL expansion, and κ_i and κ_i^* are the solutions of the transcendental Eq. (A.12) and Eq. (A.15). The ϕ_i and ϕ_i^* are symmetric and antisymmetric eigenfunctions of the exponential auto-covariance, respectively. The λ_i and λ_i^* are the eigenvalues of the same auto-covariance function. Hence, the forcing function and the displacement can be written as summation of orthogonal components obtained using the KL expansion and are given in Eq. (A.18) and Eq. (A.19):

$$F\left(t\right) = \sum_{i=1}^{n} \xi_i \sqrt{\lambda_i}\phi_i\left(t\right) \tag{A.18}$$

$$x\left(t\right) = \sum_{i=1}^{n} \xi_i \sqrt{\lambda_i} S_i\left(t\right) \tag{A.19}$$

where ϕ_i and S_i are defined in Eqs. (A.20-A.23).

$$\phi_{1,3,5,\ldots,n} = c_i \cos(\eta_i t) \tag{A.20}$$

$$\phi_{2,4,6,\ldots,n} = e_i \sin(\eta_i t) \tag{A.21}$$

$$S_{1,3,5,\ldots,n} = \frac{c_i \cos(\eta_i t + \nu_i)}{k\sqrt{(1-\sigma_i^2)^2 + (2\zeta\sigma_i)^2}} \tag{A.22}$$

$$S_{2,4,6,\ldots,n} = \frac{e_i \sin(\eta_i t + \nu_i)}{k\sqrt{(1-\sigma_i^2)^2 + (2\zeta\sigma_i)^2}} \tag{A.23}$$

Therefore, the covariance, ${\sigma^2}_x(t)$ and the auto-covariance, $R_{XX}(t_1, t_2)$ of the response are given as

$$\sigma_X^2(t) = \sum_{i=1}^{n} \lambda_i S_i^2(t) \tag{A.24}$$

$$R_{XX}(t_1, t_2) = \sum_{i=1}^{n} \lambda_i S_i(t_1) S_i(t_2) \tag{A.25}$$

The variance of SDOF system, $\sigma_x^2(t)$, when excited by stationary auto-covariance with zero initial displacement and velocity is given as [6] :

$$\begin{aligned}\sigma_x^2(t) = \int_{-\infty}^{\infty} \frac{S_{FF(\omega)} d\omega}{(\omega_n^2 - \omega^2)^2 + (2\zeta\omega_n\omega)^2} \Bigg[1 + e^{-2\zeta\omega_n t} \Bigg\{1 + \frac{\omega_n}{\omega_d}\zeta \sin 2\omega_d t \\ - e^{\zeta\omega_n t}\left(2\cos\omega_d t + \frac{2\omega_n}{\omega_d}\zeta\sin\omega_d t\right) cos\omega t - e^{\zeta\omega_n t}\frac{2\omega}{\omega_d}\zeta\sin\omega_d t \sin\omega t \\ + \frac{(\zeta\omega_n)^2 - \omega_d^2 + \omega^2}{\omega_d^2}\sin^2\omega_d t\Bigg\}\Bigg]\end{aligned} \tag{A.26}$$

Equation (A.26) requires the definition of power spectral density function of the auto-covariance. The PSD of exponential auto-covariance function can be defined :

$$S_{FF}(\omega) = \frac{C_1}{\alpha^2 + \omega^2} \tag{A.27}$$

where C_1 and α are constants, which define exponential auto-covariance's distribution. The transient displacement variance of the SDOF system when excited by an exponential auto-covariance is given as :

$$\begin{aligned}\sigma_x^2(t) = &\left[1 + e^{-2\zeta\omega_n t}\left(1 + \frac{\omega_n}{\omega_d}\zeta\sin(2\omega_d t)\right)\right] I_1 - 2\left[e^{-2\zeta\omega_n t}\left(\cos\omega_d t + \frac{\omega_n}{\omega_d}\zeta\sin\omega_d t\right)\right] I_2 \\ &- 2\left[\frac{e^{-2\zeta\omega_n t}}{\omega_d}\sin\omega_d t\right] I_3 + \frac{e^{-2\zeta\omega_n t}}{\omega_d^2}\sin^2\omega_d t\left[\left((\zeta\omega_n)^2 - \omega_d^2\right) I_1 + I_4\right]\end{aligned} \tag{A.28}$$

where I_1, I_2, A, I_3, and I_4 are given as :

$$I_1 = \frac{\pi(\alpha + 2\zeta\omega_n) C_1}{2\zeta\omega_n^3\alpha(\alpha^2 + \omega_n^2 + 2\zeta\omega_n\alpha)}$$

$$\begin{aligned}I_2 = \pi A C_1 \Bigg[&\frac{e^{-\alpha t}}{\alpha} - \frac{e^{-\zeta\omega_n t}}{\zeta\sqrt{1-\zeta^2}}\left(\sqrt{1-\zeta^2}\cos\omega_d t - \zeta\sin\omega_d t\right) \\ &+ \frac{(\alpha^2 + 2\omega_n^2(1-2\zeta^2))\left(\sqrt{1-\zeta^2}\cos\omega_d t + \zeta\sin\omega_d t\right)}{2\omega_n^3\zeta\sqrt{1-\zeta^2}}\Bigg]\end{aligned}$$

$$A = \frac{1}{\left(\alpha^2+\omega_n^2\right)^2-\left(2\alpha\zeta\omega_n\right)^2}$$

$$I_3 = \pi A C_1\left[e^{-\alpha t}-\frac{e^{-\zeta\omega_n t}}{2\zeta\sqrt{1-\zeta^2}}\left(\left(2\zeta\sqrt{1-\zeta^2}\right)\cos\omega_d t-\left(2\zeta^2-1+\frac{\alpha^2+2\omega_n^2\left(1-2\zeta^2\right)}{\omega_n^2}\right)\sin\omega_d t\right)\right]$$

$$I_4 = \frac{\pi C_1}{2\zeta\omega_n\left(\alpha^2+2\alpha\zeta\omega_n+\omega_n^2\right)} \tag{A.29}$$